Universidade de Lisboa

Faculdade de Ciências

Departamento de Biologia Vegetal

Electrophysiologic and Molecular Characterization of Membrane Anionic Transporters in Pollen Tubes

Doutoramento em Biologia

Especialidade em Biologia do Desenvolvimento

Pedro Nuno Resende Dias

Tese orientada pelo Prof. Doutor José A. Feijó e Prof. Doutor Jorge Marques da Silva

2015

Documento especialmente elaborada para a obtenção do grau de doutor

RESUMO

O tubo polínico é uma célula com propriedades únicas, e um papel crucial no ciclo de vida das plantas superiores. Algumas das suas características mais notáveis fizeram do tubo polínico um sistema modelo em plantas para o estudo de certos fenómenos, que incluem polarização e o crescimento apical. A polarização e o crescimento apical estão interrelacionados no tubo polínico, que por sua vez estão interligados com os diversos fluxos iónicos extracelulares e os seus gradientes intracelulares. Ao longo dos anos tem sido demonstrado a importante relação entre os diferentes iões, os seus gradientes e fluxos, com a polarização e crescimento apical do tubo polínico evidenciando a sua importância e o quão intimamente estes fenómenos estão relacionados. Qualquer perturbação nos fluxos iónicos invariavelmente causa perturbações no crescimento do tubo polínico, em casos mais extremos levando mesmo ao rebentamento do tubo ou à incapacidade de fertilizar os óvulos.

No entanto, apesar do vasto conhecimento adquirido, ainda há muito por descobrir relativamente aos genes envolvidos no transporte iónico na membrana plasmática do tubo polínico. Vários canais e bombas de catiões já foram identificados ao longo dos anos. No entanto, até ao momento, a identidade molecular dos transportadores aniónicos ainda está por determinar.

Através da análise transcriptomica foram identificados diversos genes candidatos para canais aniónicos expressos em pólen. Alguns deles, como é o caso do CLC-c, altamente expresso em pólen, já foram testados mas não foi possível obter nenhum resultado conclusivo, deixando em aberto a questão sobre quais o genes responsáveis pelos fluxos aniónicos já conhecidos. Alguns dos outros genes candidates incluem genes promissores, como o caso dos homólogos do SLAC1, responsáveis pelos fluxos aniónicos nas células guarda.

Outro candidato promissor, é o gene recentemente identificado homologo do TMEM16A, um canal de Cl^- activado por Ca^{2+} (CaCC), com apenas uma cópia no genoma de *Arabidopsis*. Particularmente interessante é o perfil electrofisiológico destes canais, que espelham boa parte das propriedades já previamente observadas das correntes aniónicas em protoplastos de pólen por meio de experiências de patch clamp. Ainda assim, persiste a questão sobre a natureza molecular dos transportadores aniónicos na membrana plasmática do tubo polínico.

Para tentar responder a esta questão, um mutante por inserção de T-DNA para este gene em particular foi obtido e caracterizado extensivamente nesta tese. Trabalho realizado previamente no nosso laboratório já tinha identificado pela primeira vez a presença de correntes aniónicas em protoplastos de pólen de *Arabidopsis thaliana* e de *Lilium longiflorum*, mostrando a sua regulação por $[Ca^{2+}]_{in}$. No entanto, uma serie de diferenças dos valores esperados nessas correntes levaram à postulação da ideia que outro ião deveria estar a ser transportado conjuntamente com os aniões. A hipótese centra-se na possibilidade dessas diferenças poderem ser causadas por pH e H^+. Para testar esta hipótese e expandir o nosso conhecimento sobre a natureza das correntes aniónicas, uma caracterização extensiva destas for realizada. Resultados preliminares obtidos com *Lilium longiflorum* providenciaram suporte inicial, demonstrando uma forte regulação por pH extracelular.

O trabalho focou-se então no pólen de *Arabidopsis thaliana*, para usufruir das diferentes linhas mutantes disponíveis, onde um forte efeito regulatório por pH extracelular também foi observado, apesar de ter características distintas com *Lilium*. Com o aumento do pH externo as correntes aniónicas aumentam dramaticamente, as suas conductâncias mudam, perdem a sua forte rectificação e os potencias de inversão movem-se na direcção do potencial de equilibro esperado para Cl^- e H^+. Este resultados dão suporte à hipótese de que os H^+ são de facto transportados conjuntamente com os aniões, explicando as discrepâncias previamente observadas nas correntes aniónicas, e sugerindo a presença de um sistema de co-transporte para H^+ e Cl^-.

Ao realizar esta experiência na linha mutante *cacc* uma diferença substancial é observada. No mutante não há resposta ao pH externo. As correntes aniónicas não são fortemente afectadas, as conductâncias alteram-se ligeiramente mas a rectificação mantém-se, e o potencial de inversão não se desvia na direcção das alterações do gradiente de H^+. Estes resultados denotam o facto de que o gene CaCC não só está envolvido no transporte de aniões através da membrana plasmática do tubo polínico, mas que será especificamente um co-transportador de aniões por H^+.

Este resultado é, tanto quando sabemos, a primeira identificação molecular positiva para um transportador aniónico na membrana plasmática de pólen de *Arabidopsis*.

No entanto, esta linha mutante não evidencia nenhum fenótipo macroscópico, e grande parte do seu fenótipo está relacionado com pH. Uma excepção é o efeito desta mutação ao processo de rundown. No mutante a duração do rundown é maior, comparado com o tipo silvestre, ainda que ambos subsequentemente percam percentagens de corrente idêntica. Isto é um indicio de que o CaCC tambem estará a

competir pela mesma molécula desconhecida responsável pelo efeito de rundown das correntes.

Ao se alterar a concentração aniónica tanto o tipo silvestre como a linha mutante respondem de maneira idêntica, o que sugere que a população total de canais aniónicos não é significativamente afectada pela ausência do co-transportador CaCC. Isto não é inesperado, visto estes processos serem altamente regulados, é de esperar que exista um certo nível de redundância e compensação capazes de suprir a falta de um único transportador. Esta é talvez a razão principal para até agora ter sido tão difícil identificar a sua identidade molecular. Estas experiências ainda servem para validar a hipótese de que de facto o Cl^- não é o único ião a ser transportado nas nossas condições experimentais, como se pode observar pelos desvios do potencial de inversão com diferentes concentrações externas de Cl^-. Conjuntamente, estes resultados com os obtidos aquando a variação do pH externo, apontam para uma possível estequiometria de 2:1 para o co-transportador CaCC.

Para além disto, ao se substituir o Cl^- extracelular da solução de banho por NO_3^-, outro resultado importante é observado. Enquanto em tipo silvestre não existe diferença, confirmando o que já havia sido publicado anteriormente, de que os canais aniónicos na membrana plasmática de pólen são igualmente permeáveis a Cl^- e NO_3^-. No mutante *cacc* existe uma diferença clara entre ambas as condições. Estes resultados sugerem de que o gene CaCC é particularmente selectivo para Cl^-, e muito pouco para NO_3^-. Isto fará do CaCC um co-transportador especifico para Cl^-/H^+.

Estes resultados fazem do CaCC presente no pólen de *Arabidopsis* bastante diferente dos seus homólogos. Isto não é necessariamente invulgar, outros canais aniónicos em plantas têm vindo a ser descritos como tendo actividade de co-transporte e não de canal como previamente pensado. De facto, o nosso conhecimento sobre a estrutura e funcionamento dos canais aniónicos ainda está em aberto, com diversas descobertas que evidenciam inúmeras diferenças entre os canais aniónicos e os mais bem estudados canais catiónicos.

Para complementar estes resultado o pH interno também foi alterado, para um pH mais acidico, em linha com o pH esperado para o interior do tubo polínico na região apical. Estas experiências mostram vários resultados intrigantes, revelando uma regulação complexa por pH interno nas correntes aniónicas e uma falha na resposta no mutante *cacc* comparativamente à resposta em tipo silvestre.

Com a identificação molecular e caracterização electrofisiológica de um transportador aniónico da membrana plasmática em pólen, procuramos mais evidências para o papel

deste gene no desenvolvimento da planta. Um ensaio de competição foi realizado e apesar dos resultados mostrarem um aparente desvio à proporção fenótipica esperada, estes não têm significância estatística suficiente. O papel do gene CaCC no desenvolvimento vegetal parece ser limitado, e é de esperar que o seu impacto possa ser camuflado pela actividade de transportadores na maioria das situações.

Uma prova de principio foi também realizada, de modo a integrar outra técnica electrofisiológica, a sonda vibrátil, com as vantagens da técnica de patch clamp. Esta abordagem permitirá no futuro um abordagem mais ampla aquando a caracterização de potenciais novos canais. Com este propósito, uma nova caracterização da eficiência dinâmica da sonda foi realizada e uma nova espécie foi testada.

Os fluxos iónicos de *Nicotiana tabacum* foram caracterizados e comparados com os de *Lilium longiflorum*. Ambos mostram a mesma distribuição especial dos diferentes fluxos iónicos ao longa da membrana plasmático em tubos polínicos em crescimentos, no entanto com amplitudes e padrões temporais distintos. Usando um protocolo de aquisição modificado foi também possível determinar que os componentes temporais das oscilações observadas nos fluxos apicais também têm uma distribuição espacial distinta, que poderá ser usado no futuro para em mais detalhe determinar a posição ou zona de influência de diferentes genes.

Em suma, as correntes aniónicas do polen de *Arabidopsis thaliana* foram extensivamente caracterizadas. Esta caracterização permitiu estudar o efeito regulador do pH nestas correntes, identificar um gene, uma co-transportador Cl^-/H^+, e caracterizar de igual modo o seu mutante, que denota uma ausência de resposta das correntes aniónicas ao pH. Foi a primeira vez que um gene foi positivamente identificado com sendo um transportador aniónico na membrana plasmática em pólen.

Palavras chave:

Arabidopsis thaliana, pólen, transporte aniónico, regulação por pH, patch clamp

ABSTRACT

The pollen tube is a remarkable cell, playing a fundamental role in the life cycle of higher plants. Some of its characteristics have made it a preferred choice as a model plant system to study apical cell growth and polarization. Apical cell growth and polarization are entangled in pollen tube, and this has been shown to be linked to many extracellular fluxes and internal gradients. Over the years, evidence linking each of these ions, either by their extracellular fluxes or by internal gradients to the polarization and apical growth processes have highlighted their importance and how closely related these phenomena are. Disrupting any of these ionic fluxes invariably leads to pollen tube growth arrest, burst or failure to fertilize the ovules.

Still, despite the wealth of knowledge acquired, there is still a large gap in identifying all the genes involved in the ion transport in pollen plasma membrane. A number of channels and pumps have been positively identified over the years, including several cation channels and a number of pumps as well. However, all attempts to identify the molecules responsible for the anion transport have been, so far, unsuccessful.

Transcriptomic studies have identified several candidate anionic channels genes that are presented in pollen. Some of them, as the case of the CLC-c, that is highly expressed in pollen, were checked but failed to provide any conclusive result, leaving open the question as to which genes mediate the observed anionic fluxes and gradients. Some of the other candidate genes include promising genes, as the SLAC1 homologues, responsible for the anion fluxes in the guard cell.

Another promising candidate is the recently identified TMEM16A homologue, a Ca^{2+}-activated Cl^- channel (CaCC) with only one copy in the *Arabidopsis* genome. Of particular interest is the electrophysiological profile of this channel, that mimic most of the properties that had been previously observed in plant pollen anion currents by means of patch clamp experiments. The question remains about the molecular nature of the anionic transporters in pollen plasma membrane.

To answer this, a T-DNA insertion mutant for this particular gene was genotyped and extensively characterized in this thesis. Previous work done in our lab had identified anionic currents in both *Arabidopsis thaliana* and *Lilium longiflorum* pollen protoplasts, and linked them to $[Ca^{2+}]_{in}$ regulation. Still, a number of differences from some of the expected values on those currents led to the idea that some other ion could be transported alongside anions under the experimental conditions. The hypothesis is that the observed discrepancies in expected behavior would be caused by pH and H^+. To

address this and extend our understanding on the nature of the anionic currents, an extensive characterization of the anionic currents was performed. Preliminary results obtained with *Lilium longiflorum* supported this hypothesis, evidencing a strong regulation by extracellular pH.

Focusing on *Arabidopsis thaliana* pollen to take advantage of the mutant lines available, a strong regulatory effect of extracellular pH was also observed, although with different properties then in *Lilium*. Under increasing extracellular pH the anionic currents increased dramatically, their conductances changed, the strong outward rectification that characterized them was lost and the current reversal potentials moves toward the expected values for Cl^- and H^+. These results strongly support the hypothesis that H^+ are also being transported along with Cl^-, explaining the previously observed discrepancies of the anionic currents, and suggesting the presence of a co-transport system transporting H^+ and Cl^-.

While performing the same experiences in the *cacc* mutant line a remarkable difference was observed. In the *cacc*, there is no response to external pH: currents were not largely affected, conductances had slight changes but rectification was unaffected, and the reversal potential did not follow the changing H^+ gradient. These results point out to the fact that the CaCC gene is not only a transporter responsible for anion transport in pollen plasma membrane, but specifically an anion/H^+ co-transporter.

This result is, to our knowledge, the first positive molecular identification of an anion transporter in the plasma membrane of pollen.

Even so, the fact remains, that this mutant line shows no obvious phenotypes in terms of reproduction, and most of the differences found were linked to pH. One notable exception is the impact of this mutation on the rundown of the currents. In the mutant the length of rundown is extended, compared to wild type, despite both having a similar percentual loss in current amplitude. This is an indication that the CaCC is also competing for whatever molecule or process is regulating the rundown of the currents.

When the anionic concentration was modified both wild type and mutant line evidenced similar behaviors, suggesting that the overall population of anionic channel still conducted anions in a similar way, even in the absence of the CaCC co-transporter. This is not unexpected, given the tight control these processes are subject to, a certain level of redundancy and compensation to overcome the lack of just one transporter is expected. This is perhaps the main reason why it has been so challenging to identify them in the first place. Still, these experiments further validated the fact that Cl^- is not the only ion being transported under our experimental conditions, as evidenced by the reversal potential

shifts with changing external [Cl^-]. Taken together these results with the reversal shifts when pH was changed, we can propose a stoichiometry of 2:1 for the CaCC co-transporter.

Furthermore, by substituting the extracellular bath solution [Cl^-] for [NO_3^-] another important result emerged. In wild type, there is no difference, confirming what had been published before, that the anionic channels in the plasma membrane of pollen are equally permeable to Cl^- and NO_3^-, while in the *cacc* mutant there is a clear difference between the anionic currents under high [Cl^-] or high [NO_3^-]. These results suggest that the CaCC gene should be highly selective for Cl^-, and not for NO_3^-. This would make the CaCC a specific Cl^-/H^+ co-transporter.

These results would make the CaCC present in *Arabidopsis* pollen to function rather differently than its orthologues in animals. This would not be entirely novel, as many other putative anion channels in plants have recently been show to function not as anion channels, but as co-transporters instead. In fact, our knowledge of anion channels structure and function is still evolving, as many discoveries have highlighted that anion channels to be substantially different from the better studied cation channels, possessing unique properties and behaviors.

To further compliment these results the internal pH was also changed, to a more acidic pH, similar to what would be found in the tip of the growing pollen tube. These experiments evidenced quite a few interesting results, revealing a complex regulation by internal pH on the anionic channels and a lack of response in the *cacc* mutant comparable to that of wild type.

With the identification and electrophysiological characterization of an anionic transporter in pollen plasma membrane, we tried to find further evidences of the role of this gene in plant development. A competition assay was performed and while the results indicated a potentially seed set phenotype for the *cacc* mutant when selfed or reciprocally crossed for the antibiotic resistance, the sample size so far analyzed did not show statistically significant differences. Still, the expected role of the CaCC gene in the overall pollen tube development appears to be limited in scope, as its impact may be masked and compensated by other channels or transporters in circumstances to be determined.

As a proof of principle approach, we integrated another electrophysiological technique, the vibrating probe, with the power of the patch clamp technique. This approach would allow us in the future to have a more overarching scope on the characterization of potential new channels. For this, a *de novo* characterization of the probes dynamic efficiency was made, and a novel species was used to test it.

Nicotiana tabacum ionic fluxes were characterized and compared to the well studied *Lilium longiflorum*. They both evidenced the same spatial pattern in terms of each ion flux spatial distribution across the pollen tube plasma membrane, but with altered amplitudes and temporal patterns. Furthermore, using an altered protocol for data acquisition it was possible to determine that the temporal components of the oscillations observed at the tip also have a spatial distribution that could be used to fine tune the precise location or role of specific genes in future approach.

Overall, the anionic currents of *Arabidopsis thaliana* were extensively characterized. This allowed us to characterize the regulatory effect of pH in these currents, to identify one gene, as an anion/H^+ co-transporter, and extensively characterize its mutant and its absence of pH response. This was the first time a gene was positively identified as a plasma membrane anion transporter in pollen.

Keywords:

Arabidopsis thaliana, pollen, anion transport, pH regulation, patch clamp

Index

FIGURES INDEX

TABLES INDEX

ACKNOWLEDGMENTS

Dedicated to my son,

who was not even born when I started this journey, but ever since has changed my life for the better.

And to Ana Bicho,

without whom I would never have started this journey, and whom was taken away far too young.

To my parents, for all the encouragement and always loving me every single day.

To Carla, for having changed my life.

To my PhD Advisors, Ana Bicho, José Feijó and Jorge Marques da Silva, for all the invaluable support, expertise and guidance.

To my "patch buddies" Barbara Tavares and Patricia Gonçalves, for countless hours working together, cracking skulls, squeezing ideas, and for their genuine friendship.

To my many lab colleagues over these past years - Ana Maria, Erwan, Nuno, Ricardo, Sofia, Micha, Maitê, Michael, Daniel, Claudia, Pedro Lima, Carlos, Nicole, Custódio, Abid, Joana, and many others for their friendship and knowledge and love of science.

To Faculdade de Ciências da Universidade de Lisboa, for having me as a PhD Student, to Departamento de Quimica/REQUIMTE da FCT-UNL, to the Gulbenkian Institute of Science and to the Department of Cell Biology, Molecular and Genetics of the University of Maryland, USA for having me along.

And to the FCT for the fellowship, FCUL for the PhD extension scholarship and UMD for the extra support when abroad.

"*I may not have gone where I intended to go, but I think I have ended up where I needed to be.*" – Douglas Adams

DEFINITIONS

Positive Current – the flow of positive ions out of the headstage into the microelectrode and out of the microelectrode tip into the preparation is termed positive current.

Negative Current – the opposite flow of positive ions from the preparation in to the microelectrode tip and in to the headstage.

Outward Current – Current that flows across the membrane, from the inside surface to the outside surface, is termed outward current.

Inward Current – Current that flows across the membrane, from the outside surface to the inside surface, is termed inward current.

Positive Potential – The term positive potential means a positive voltage at the headstage input with respect to ground.

Negative Potential – The opposite of positive potential, a negative voltage at the headstage input with respect to ground.

Transmembrane Potential – The transmembrane potential (V_m) is the potential at the inside of the cell minus the potential at the outside. This term is applied equally to the whole-cell membrane and to membrane patches.

Depolarizing/Hyperpolarizing – The resting V_m value of most cells is negative. If a positive current flows into the cell, V_m initially becomes less negative. For example, V_m might shift from an initial resting value of -70 mV to a new value of -20 mV. Since the absolute magnitude of V_m is smaller, the current is said to depolarize the cell (i.e., it reduces the "polarizing" voltage across the membrane). This convention is adhered to even if the current is so large that the absolute magnitude of V_m becomes larger. For example, a current that causes V_m to shift from -70 mV to +90 mV is still said to depolarize the cell. Stated simply, depolarization is a positive shift in V_m. Conversely, hyperpolarization is a negative shift in V_m.

INTRODUCTION

Flowering plants are the most diverse group of land plants, with an estimated 250.000 different species or more. Evolutionarily, the most important developments that enabled them to become so widespread was the ability to reach reproductive maturity more quickly, fertilization taking place without water, adaptability to animal pollination and seed dispersal, as first described by Darwin back in 1862 (Boavida, Becker, et al., 2005).

The life cycle of higher plants includes several distinct stages, namely: seed germination, vegetative growth, flowering, fertilization, embryo development and seed maturation. Of interest for this work, is the development of the male gametophyte – the pollen grain. Its function is to transport two sperm cells into the plant female tissues, fertilizing both the egg and the central cells inside the ovule, the double fertilization. Their development starts in the stamens, the male reproductive organs. The pollen grains develop within the pollen sac and, after maturation, are released from the anthers. Upon release pollen grains are in a dehydrated state, a metabolic quiescent state that, together with a remarkably tough external wall, help them survive environmental stress during dispersion, and it is also commonly assumed that they already possess all the biochemical components and transcripts needed to germinate prior to rehydration (Taylor & Hepler, 1997; Boavida, Vieira, et al., 2005).

When a pollen grain lands on a receptive and compatible stigma – the female sexual organ – it adheres and quickly rehydrates. The stored RNA, proteins and bioactive small molecules allow for a rapid germination and outgrowth of a tube that penetrates and grows within the style. This tube - the pollen tube - develops from the pollen grain as a cytoplasmic extension that carries the sperm cells within. By interacting with the various tissues of the female organs, the pollen tube grows and finds its way to an ovule, fertilizing it by bursting its contents inside the embryo sac releasing the sperm cells. The two sperm cells then fuse, one with the egg cell, that will produce the zygote, and the other with the central cell, that gives rise to the endosperm, thus leading to the embryo development and a new life cycle (Taylor & Hepler, 1997; Boavida, Vieira, et al., 2005; Michard et al., 2009).

The Pollen Tube

Pollen is the male gametophyte of higher plants and upon germination produces the pollen tube that plays a crucial role in the life cycle of these plants. Besides its obvious role in fertilization, this highly specialized cell is also well known for never dividing during its strictly apical growth, being able to reach lengths of over 40 cm and growth rates up to 4 $\mu m.s^{-1}$ (Michard et al., 2009). This, alongside with the nearly complete description of the *Arabidopsis* pollen transcriptome, makes this cell system well suited for studies regarding apical growth, morphogenesis, cell polarity and development (Pina et al., 2005; Becker & Feijó, 2007).

As intrinsically polarized cells, pollen tubes anatomy reflects that very same concept, with specific and distinct intracellular regions. Namely, a tip domain which is rich in Golgi secretory vesicles outlining an inverted cone; a sub-apical domain which is enriched with a large population of metabolically active organelles, such as mitochondria, dictyosomes, endoplasmatic reticulum vesicles and other larger organelles; a nuclear domain that contains most of the large organelles, the vegetative nucleus and the two sperm cells; a vacuolar domain that contains essentially the large vacuole of the pollen tube, that keeps expanding in size as the tube grows.

The tip and sub-apical domains are often called the “clear zone”, while the nuclear and vacuolar domains are characterized by a distinct “reverse fountain” streaming pattern with organelles moving through the cytoplasm as fast as 10 $\mu m.s^{-1}$. A callose plug isolates the growing part of the pollen tube from the remainder, which eventually dies. Thus, just the front section of the tube is active, and only the tip is growing (Boavida, Vieira, et al., 2005).

An important feature of any growing pollen tube is the “reverse fountain” cytoplasmic streaming in which an ordered forward movement of organelles through the cortical region of the tube undergoes a turnover in the sub-apical domain moving back centrally, away from the tip of the tube, in what’s proposed to be a scaffold to bring nutrients, energy and building materials to the active growth part of the pollen. Within the tip itself, the motion is chaotic and turbulent, with vesicles appearing to move in a random, diffusive manner from the base of the clear zone to the extreme apex.

As the pollen tube grows, new segments of cell wall are produced and deposited on the apical region of the tube, effectively extending its size. As stated previously, this growth occurs without further differentiation or division of the pollen tube and is restricted to its

tip. It relies only on the secretion of membrane and cell wall materials at the pollen tube tip region.

The polarization of pollen tubes is not restricted to morphological aspects, but it is also evident in the emergent electrical fields that were first measured in the 70's. Pollen tubes act as polarized electric dipoles, with the grain acting as the source and the tube acting as the sink of a large ionic current that transverses the tube cytoplasm (Weisenseel & Jaffe, 1976).

Ionic Fluxes and Gradients

From the early studies by Lionel Jaffe's group, a door was open to study the electrical fields and ionic currents that emerged from growing pollen tubes, which was followed by many other research groups over the past four decades. They applied a new method at the time, the vibrating probe, allowing them to infer total electric current flowing between two different measured points. The probe, which consisted of a simple platinum-black electrode that vibrated between two points in space, allowed to measure the voltage at those two locations (Jaffe & Nuccitelli, 1974; Weisenseel et al., 1975; Weisenseel & Jaffe, 1976).

Further developments of this method paved the way for measuring single ion fluxes (Kühtreiber & Jaffe, 1990), by using ionic selective ionophores, which allowed for each individual ion flux to be mapped independently from each other, further expanding the initial observations from Jaffe's group. It was shown that these ionic fluxes are fundamental for proper pollen tube growth and development, as impairment of any of these individual ionic fluxes leads to an inevitable disruption of normal physiology, often leading to premature pollen tube burst, growth arrest, swelling of pollen tip, cytoplasmic stream disruption and other abnormalities that decrease pollen tube viability and fitness. More recently, with the advances in imaging techniques and fluorescent dyes, it has been possible to observe intracellular ion gradients that are of direct consequence from extracellular ion fluxes, leading to many reports from different groups over the years (Mascarenhas, 1993; Messerli & Robinson, 1997; Holdaway-Clarke et al., 1997; Feijó et al., 1999, 2001, 2004; Hepler et al., 2001; Zonia et al., 2002; Holdaway-Clarke & Hepler, 2003).

Calcium (Ca^{2+}) was one of the first ions to be shown to greatly affect pollen tube growth. Pollen tubes possess a steep "tip focused" gradient of Ca^{2+} in the tube tip cytosol, which is essential for normal tube growth, as disruption of this gradient leads to tube

growth arrest (Jaffe et al., 1975; Holdaway-Clarke et al., 1997; Feijó et al., 2001; Holdaway-Clarke & Hepler, 2003; Michard et al., 2009).

Proton (H^+) intracellular gradients have also been shown to be highly polarized in pollen tubes, where a constitutive alkaline band in the clear zone and a growth-dependent acidic tip were shown to be fundamental for pollen tube elongation, and later found to be a direct result of a differential distribution of a H^+-ATPase that is excluded from the tip and in higher densities in the sub-apical domain, matching perfectly the previously reported effluxes for H^+ (Feijó et al., 1999; Certal et al., 2008).

The global image that emerges after decades of data accumulation is of a polarized distribution of fluxes, mainly from the tip to the rest of the tube, which implies different roles for each specific ion in the pollen tube growth. Most interesting and relevant process of pollen elongation, redirection and ovule targeting also occur at the tip or sub-apical domain, while the rest of the tube shank and the grain are essentially inert.

Anions

The presence and roles of anions fluxes in pollen tube growth and development has been a matter of debate for some decades, despite overwhelming evidence supporting the existence of Cl^- fluxes. It has long been known that pollen tube germination and growth require the presence of extracellular ions such as K^+, Ca^{2+}, boron and a slightly acidic pH (Weisenseel et al., 1975). Early ion substitution experiments with non-permeable anions suggested that they were not required for the growth of the pollen tubes to occur (Weisenseel & Jaffe, 1976). However, these experiments were never repeated nor confirmed over time, being severally limited by technical aspects at the time. Later it was reported that when Cl^- is substituted by NO_3^- in the germination medium, this promotes a preference in growth reorientation under an electric field, suggesting there is some distinct role between these two different anionic species and that each one plays a specific role in pollen development (Malhó et al., 1992).

Nonetheless, anionic fluxes have been shown by different groups to permeate the pollen tube membrane and to play an important role in pollen tube development. Large anionic fluxes permeate the growing pollen tube tip of *Lilium longiflorum* and of *Nicotiana tabacum*, which lead to an accumulation of anions in the extracellular medium. In fact, these anionic fluxes by far exceed in magnitude those reported for all other ionic species, such as H^+, Ca^{2+} or even K^+, reaching current densities of up to 8000 $pmol.cm^{-2}.s^{-1}$ in *Lilium* pollen tube tip, under oscillatory regime. Pharmacological evidence also confirmed the

nature of these ionic fluxes, by the use of Cl^- channel specific blockers such as DIDS, niflumic acid and NPPB, which led to pollen tube growth inhibition and increased apical volume, along with other more specific effects to each inhibitor (Zonia et al., 2001, 2002). It was also shown that use of IP4, a known Ca^{2+}-activated Cl^- conductance blocker (Carew et al., 2000) also inhibited pollen tube growth, increased apical volume and disrupted anionic flux (Zonia et al., 2002).

Much of the controversy that was prevalent in the field during the decade of 2000, resulted from the conflicting interpretations of two papers published in 2002 and 2004 (Zonia et al., 2002; Messerli et al., 2004). While Zonia et al. assumed that the results confirmed the existence of Cl^- fluxes (anionic fluxes actually, since the probe is nonspecific for different anionic species), Messerli et al. suggested that the ion-selective anionic probe used was sensitive to the pH buffer and was indirectly measuring changes in the H^+ gradient instead of the anionic one. However they failed to mimic the exact measurement conditions from the previous group, namely buffer concentrations and pH, and did not take into account the pharmacological evidences provided (Kunkel et al., 2006). To further complicate matters, another paper reported that by applying the patch clamp technique they failed to detect any anionic activity with the protocols they used (Dutta & Robinson, 2004), suggesting that there wouldn't be any anionic transport in pollen tubes. This very same paper also reported the absence of hyperpolarization-activated Ca^{2+} channels, which were subsequently found later on by other groups in pollen protoplasts from different species, including *Arabidopsis thaliana* (Shang et al., 2005; Qu et al., 2007; Wu et al., 2007). Still, further experiments were needed to confirm either side of the story (Hepler et al., 2006; Kunkel et al., 2006; Moreno et al., 2007). Seven years later the question was raised that these authors may have mistakenly assumed the absence of anionic single channel activity due to the fact that they could be witnessing large stable whole-cell like currents instead, under cell-attached configuration (Tavares et al., 2011).

In *Nicotiana tabacum* the pollen grain germination is associated with a Cl^- tip efflux that, if blocked by Cl^- channel or transporter inhibitors (NPPB, NA, DIDS, furosemide, DiBAC3(5), bumetanide), prevents the on-set of germination, either completely (NPPB, NA and DIDS, although DIDS was reported not to affect Cl^- efflux has much as the other two) or just partially (furosemide, DiBAC4(5), bumetanide) (Matveyeva et al., 2003). More recently, it has been shown that cytoplasmic Cl^- is also involved in the polarization of *Nicotiana tabacum* pollen tube during germination, and is in fact affected by external $[Cl^-]$ and by plasma membrane voltage polarization, which has also been linked to the H^+-ATPase (Breygina, Matveeva, et al., 2009). It was also demonstrated that NPPB inhibited Cl^- efflux during hydration from the grain and from the tube tip, leading to cell growth halt; this results were also mimicked by increasing extracellular $[Cl^-]$ (up to 200 mM in

germination or 100 mM in tube growth), which the authors proposed created an equilibrium between [Cl^-] across the pollen plasma membrane. Furthermore, this study also reported a depolarization of the plasma membrane in response to NPPB, with further disruption of functional compartmentalization polarity of the cytoplasm, while DIDS induced pollen tube swelling and bursting (Breygina, Smirnova, et al., 2009; Breygina et al., 2010). It has also been reported that the pollen tube mitochondria treated with DIDS showed hyperpolarized membranes and changes in reactive oxygen species content and excretion, and this and previous results suggest that pollen tube growth is dependent on the activity of multiple anion channels, in both localization and function (Breygina et al., 2010).

High Cl^- levels selectively inhibit 'kiss-and-run' endocytosis–exocytosis or flicker fusion (Smith et al., 2008). The endocytosis rate appears to be linked to the rate of exocytosis, and these are sensitive to levels of Ca^{2+} and Cl^-. High Cl^- levels blocked tobacco pollen tube growth, but did not immediately block smooth vesicle endocytosis at the apex (Breygina et al., 2009a), suggesting that an endosomal pathway differs from the 'kiss-and-run' exocytosis–endocytosis pathway.

Furthermore, transcriptomic studies have highlighted several anion/Cl^- membrane transporters and channels to be specifically and highly expressed in *Arabidopsis* pollen (Pina et al., 2005). Alongside, the cation-chloride co-transporter (CCC) was also found to be highly expressed in pollen (Colmenero-Flores et al., 2007), which further led to the belief that there were in fact anionic fluxes, as in all other living cells. To fully confirm this, patch-clamp studies were performed in pollen grain protoplasts of *Lilium longiflorum* that clearly demonstrated the existence of strong outward rectifying anionic currents regulated by intracellular [Ca^{2+}], which were within range of the previous results obtained with the vibrating probe years before (Tavares et al., 2011).

Thus, there are substantial evidences that demonstrate the importance of Cl^- in pollen germination and pollen tube growth. This has also been shown in countless other cell system, where Cl^- plays important and specific functions, namely the most famous one in plants, the guard cell, where stomatal closure is also mediated by anions. Furthermore, Cl^- has been linked to several different roles such as preservation of electro-neutrality and membrane potential regulation, cytoplasm compartmentalization, and even to mitochondrial regulation as well, but it is most commonly associated with the regulation of osmotic pressure, by driving water movement across the cell. And while there is substantial evidence for the importance of osmotic pressure in apical growth of pollen tubes (Zonia & Munnik, 2004), there is also controversy on the field regarding the validity of these results, and so the link between osmotic pressure and Cl^- remains to be

thoroughly proved. Nonetheless, it has been very well documented that these two phenomena are very important in other plant systems, where K^+ and anionic flow regulate turgor pressure.

Cl^- has also been linked with many cellular process that are in turn linked to Ca^{2+} gradients, which has led to the hypothesis that Cl^- currents could be Ca^{2+} regulated. Many of the cellular process that are affected by changes in Cl^- transport have also been proposed to be physiological effectors of Ca^{2+} gradients (Roy et al., 1999; Parton et al., 2003; Becker et al., 2004; Hwang et al., 2005; Helling et al., 2006). Thus it falls within reason that anions may also play a role in regulating Ca^{2+} gradients, providing for a regulatory feedback loop, since Ca^{2+} also regulates anionic fluxes (Chen et al., 2010; Tavares et al., 2011).

The signaling cascades downstream of Ca^{2+} are multiple (Malhó et al., 2006; Hepler et al., 2012), and may imply phosphorylation through Ca^{2+}-dependent protein kinases (Yoon et al., 2006; Gutermuth et al., 2013), small GTPases (Gu et al., 2005) or calmodulin (Rato et al., 2004; Berkefeld et al., 2010), and could plausibly regulate anionic currents as well, as revealed by the specificity of the IP4 inhibition response (Zonia et al., 2002).

Recently, the relevance of H^+ as a second messenger has come to light (Prolo & Goodman, 2008), paving way for a new regulatory role of H^+. This raises an interesting question as to whether the same could be possible in pollen. The anionic fluxes and H^+ fluxes in pollen plasma membrane seem to be entangled across the pollen tube and grain - whenever there is H^+ efflux there is anion influx, while on the H^+ influx regions anions show an efflux. This does not happen with any other ion combination in pollen, as there are changes across the pollen plasma membrane domains for the fluxes of other ions that are unique to each one of them.

Meanwhile there have been several reports about putative anionic channels in plants and in other systems being proved to actually behave as H^+/Cl^- co-transporters instead (Accardi & Miller, 2004; Jentsch et al., 2005; Scheel et al., 2005; Pusch et al., 2006; De Angeli et al., 2006). These findings have spurred back the discussion about the exact nature of anionic channels that for many decades have been kept in the shadow of the better studied and characterized cation channels, and its functions were limited to simple housekeeping. These latest reports have shaken some of these paradigms surrounding anion channels, revealing much more complex behaviors, regulation and physiological effects of these anion channels/transporters (Miller, 2006; Conde et al., 2010). Besides the recent discoveries in the CLC family, other anionic transporters had already been known and described as anion/H^+ transporters, as was the case of the NO_3^- transporters from the NRT families (Tsay et al., 1993) for instance, and innumerous other solute transporters

found across different membranes and cells all over the plant, showing a huge variety of pH regulation and diverse physiological functions (Carpaneto et al., 2005; Martinoia et al., 2007, 2012; Ortiz-Ramirez et al., 2011).

There is still a long way to go in understanding all the subtleties regarding these duality between anion channels and transporters as is seen, for instances, in the case of the structural architecture of the CFTR protein, a Cl^- channel encoding gene linked to cystic fibrosis in humans, that belongs to the widespread ABC transporters. However, despite maintaining the molecular hallmarks of the ABC family, this protein functions as an ATP-gated Cl^- channel and not as a solute pump (Baukrowitz et al., 1994). Furthermore, it has also been shown that P-type ATPase ion pumps can be degraded to an ion channel under the influence of natural toxins that opens the transport pathway to both sides of the membrane simultaneously (Artigas & Gadsby, 2003).

On the other hand another member of the CLC family was shown to behave as both an anion channel and an anion/H^+ transporter, and this transition is mediated by extracellular acidic pH, uncoupling the two ion transports in CLC-3 (Matsuda et al., 2010), which might provide novel roles for cell regulation under acidic conditions. While many other reports have indicated that pH directly modulates the gating properties of anion channels (Johannes et al., 1998; Colcombet et al., 2005; Picollo et al., 2010; Orhan et al., 2011). Still, the question remains as to what defines the structural difference between the H^+/anion antiporters and H^+ gated anion channels (Miller, 2006; Zdebik et al., 2008; Zifarelli et al., 2008).

Other reports also show a variety of novel links between anion transport and other cation channels or pumps. For instance, members of the glutamate transporter family also contain pore-like ion-permeation pathways to conduct Cl^- ions (Fairman et al., 1995; Slotboom et al., 2001; Ryan & Vandenberg, 2002). While in the Golgi, the CLC-d was shown to co-localize and cooperate with H^+-V-ATPase in the acidification of the endosomal compartments, providing an electric shunt for optimal acidification of the trans-Golgi network. (von der Fecht-Bartenbach et al., 2007).

Finally, there have also been reports pointing out that some co-transporters have sensing functions as well, as is the case of the plant Na^+/H^+ antiporter SOS1 (Silva & Gerós, 2009), which encodes a transmembrane protein with similarities to the plasma membrane Na^+/H^+ antiporters and has been shown to interact with vacuolar calmodulin-like proteins (AtCaM15) in a Ca^{2+} and pH dependent manner (Yamaguchi et al., 2005), leaving open many other possibilities for all other uncharacterized transporters in plants. Furthermore, for instance, the question is still open for the members of the TMEM16 protein family, as despite that some members have been positively identified as de facto Ca^{2+}-activated Cl^-

channels, others do not possess the hallmark of Ca^{2+} activation but still behave as Cl^- channels. Even more surprising is the observation that the remaining members appear to be in fact phospholipid scramblases instead of channels. It is evident that this dual function as transporters and channels, or as transporters and sensors or some other multirole displayed by these proteins involved in the anionic transport phenomena have still much to reveal about the global role of anion transport in cells.

Ion Channels in Pollen

Despite the accumulated knowledge on different ionic species, regarding their fluxes, currents, internal gradients, regulation and relationship with several other fundamental cellular processes, it has been rather challenging to attribute putative genes to functional channels or transporters for each of the currents and fluxes measured by electrophysiology techniques in pollen tubes membrane (Holdaway-Clarke & Hepler, 2003; Michard et al., 2009; Song et al., 2009).

One of the better understood ions in pollen is K^+, with several different passive K^+ currents identified using voltage- or patch-clamp techniques, a few genes cloned and exhibiting distinct characteristics.

The first patch clamp experiments revealed several unitary currents for inward K^+ channels, suggesting an involvement of these in the influx of K^+ during pollen tube growth, while later on the existence of two outward K^+ currents was also reported (Obermeyer & Kolb, 1993; Obermeyer & Blatt, 1995). Similar characteristics were also observed in *Lilium longiflorum* where both inward and outward K^+ currents were detected in the plasma membrane of pollen grains and pollen tubes protoplasts, with slight different activation kinetics and current density from the grain to the tube (Griessner & Obermeyer, 2003). The first evidence of K^+ channels in *Arabidopsis* was linked with pollen growth and germination as well to external pH regulation (Fan et al., 2001), which was also shown for *Brassica chinensis* (Fan et al., 1999, 2003). The first pollen tube membrane channel to be cloned was a pollen-specific K^+ channel of the Shaker family (SPIK), that when disrupted strongly affected the inward rectifying currents of K^+ resulting in impaired pollen tube growth (Mouline et al., 2002).

Further studies evidenced the presence of not only K^+ single-channel currents from outside-out patches but also of Ca^{2+} channels in *Lilium longiflorum* pollen grain and pollen tube tip protoplasts, which were attributed to stretch-activated channels (Dutta & Robinson, 2004), however this was never confirmed by any other group. An

hyperpolarization-activated Ca^{2+} channel that was regulated by actin filaments has also been proposed (Wang et al., 2004). A CNGC was later shown to be localized to the plasma membrane of the growing pollen tube, and was responsible for male sterility by disrupting normal pollen growth (Frietsch et al., 2007), along with the identification of a GLR involved in Ca^{2+} fluxes in pollen tube that was modulated by D-Serine (Michard et al., 2011).

Besides these channels, Ca^{2+}-pumps and P-type H^{+}-pumps have also been identified in pollen and both are fundamental for the homeostasis of ion gradients and normal pollen growth (Schiøtt et al., 2004; Certal et al., 2008), as well as providing means for energizing innumerous other putative co-transporters in the plasma membrane. Furthermore some Ca^{2+}-cation antiporter have also been identified and play an important role in ion flux regulations as well as being crucial for successful plant fertilization (Sze et al., 2004; Lu et al., 2011), pointing out to the importance that a single co-transporter can have in the life cycle of the whole plant.

Despite all this increasing knowledge about cation channels, transporters and pumps in pollen, not much is known about anionic transporters in pollen tubes and their molecular nature.

Analysis of transcriptome data from *Arabidopsis thaliana* has shown a large number of potential transporter genes expressed during pollen germination and tube growth (Pina et al., 2005; Wang et al., 2008), which deeply contrasts with the fact that so little genes have actually been confirmed as such. Of all the expressed genes, only little more than a handful is pollen specific. Even so, the possibility is open to have dozens of different channels and transporters active in pollen membranes. Of all these putative channels, a few were also identified as anion channels, such as two CLC transporters (CLC-c & CLC-d) (Zifarelli & Pusch, 2010), two SLAC1 homologues (SLAH2 & SLAH3) (Geiger et al., 2010, 2011), an ALMT channel (ALMT12) (Meyer et al., 2010), an anion-cation symporter (CCC) (Colmenero-Flores et al., 2007), an anion exchanger and a divalent anion-Na^{+} symporter. Other potential genes have also been proposed to be acting as anion channels, such as the case of the ABC transporters, which are also enriched and pollen specific (Pina et al., 2005; Becker & Feijó, 2007; Song et al., 2009). While these genes are yet to be proven to function as transporters in plants, they do belong to the same family of the CFTR channel in mammals, a Ca^{2+}-activated Cl^{-} transporter that when mutated is responsible for cystic fibrosis.

Some of these genes have in fact been shown to function as anion transporters or channels, but their function in pollen has not been proven so far. The CCC gene for instance, has been shown to act as a cation:Cl^{-} co-transporter and is expressed in multiple plant cell types including the pollen grain. Mutation of this gene induces several

phenotypes all across the plant, some of which might be related to pollen defects or fitness loss (Colmenero-Flores et al., 2007). This transporter is a good candidate for the anionic influx of pollen tubes, although no localization data is available at the moment to confirm this. On the other hand, guard cells anionic efflux is mediated by the well known SLAC1 and ALMT12 channels, since these are also expressed in pollen, they are also two likely candidates to account for the anionic efflux at the tip of the pollen (Gutermuth et al., 2013).

The first anionic currents measured in pollen grain of *Arabidopsis thaliana* and *Lilium longiflorum*, had both inward and outward conductivity and were found to be regulated by $[Ca^{2+}]_{in}$ (Tavares, 2011; Tavares et al., 2011). These anionic currents share a strikingly resemblance with the recently described Ca^{2+}-activated Cl^- channels (CaCC) well known in mammals cell types as the Anoctomin-1 family (TMEM16A) (Yang et al., 2008; Schroeder et al., 2008; Caputo et al., 2008). More importantly, they have a homologue expressed in the pollen of *Arabidopsis*, making it an excellent candidate to be tested for the molecular identity of the anionic currents in pollen.

Anions in Plants

Plasma membrane anion transporters play fundamental roles in plant cell biology, especially when it comes to stomatal closure and plant nutrition and while in the pollen tube case the advances have been slow in understanding their role and even more their molecular identity, in these other cell systems the advances have been much more comprehensive.

Anions are always required in homeostatic concentrations in the cytosol as means to maintain the bulk electroneutrality of the cell. In addition, all free ion concentrations homeostasis is often tightly regulated as many physiological processes require the presence of specific concentrations of these ions to occur, and offsetting this internal balance often leads to problems for the cell. In most cells though, the intracellular concentrations of inorganic cations often exceeds that of inorganic anions, since the excess positive charges is also balanced by the presence of negatively charged intracellular macromolecules and other small organic anions and the electrochemical potential.

Thus, it is no surprise during evolution specific proteins that transport and interact with different ions have evolved resulting in a multitude of regulatory systems, feedback mechanisms and transduction pathways with ions involved. One of the most transversal phenomena regarding anion transport across species is the regulation of cellular

osmolarity. While most cells keep a mostly constant osmolarity, others, such as the guard cells in plants, do not. Guard cells mediate the opening and closure of the stomata and this is done by changing their osmolarity as a means to open or close the stomata in a tightly regulated process by many different effectors (Siegel et al., 2009). This process is deeply interconnected with the transport of ions and other solutes across the plasma membrane by specific membrane transporters. These transporters generate an osmotic gradient that leads to the passive flow of water, which in turn, generates turgor pressure needed to increase changes in cell volume and is generally associated with Cl^- fluxes. All this is made possible in plant cells due to the presence of the cell wall that can counteract the massive increase in turgor while keeping cell shape.

In the roots many different anions, such as sulphate (SO_4^{2-}), phosphate (PO_4^{3-}), nitrate (NO_3^-), malate and citrate, all have crucial roles in plant physiology and nutrition. Malate and citrate are intermediates of the Krebs cycles, for instance, while most of these anions are also involved in the regulation of the uptake of other ions in roots, most importantly phosphate and iron or in the resistance to aluminium in acidic soils (López-Bucio et al., 2000; Piñeros & Kochian, 2001; Durrett et al., 2007; Ryan et al., 2009).

Electrophysiology Techniques

The mechanism involved in generating the action potential were first described by Alan Hodgkin and Andrew Huxley, while working on the giant squid axon of *Loligo Sp.* (Hodgkin et al., 1952). These experiments were performed in a voltage clamp configuration, that were based on the technique developed by Cole and Marmont around the 1940's (Dean et al., 1940; Marmont, 1949).

The discovery of the mechanism involved in the excitation and inhibition of the nerve cells membranes was awarded with the Nobel Prize of Physiology/Medicine in 1963. With the development of the electrophysiology field, many other currents, channels and mechanism have been studied and described. This present work is based on the electrophysiological concepts first postulated by these investigators, using a more advanced methodology of voltage clamp known as the patch clamp, described by Sakmann and Neher (Hamill et al., 1981; Sakmann & Neher, 1984) also recognized by the Nobel committee.

Electric Properties of Living Cells

The membranes of all living cells evidence electrical properties, and as such, they can be described as a RC circuit. The RC circuit is a simple electrical circuit comprised of a resistance and a condenser in parallel. The condenser can be thought as the equivalent to the phospholipid layer on the membrane, thus acting as a barrier to the free flow of ions from one side to the other, while the resistance is the equivalent to the ionic channels through which the ions may flow from one side to the other. On top of that, any ionic gradient between the two sides of the membrane can be thought as a battery in series with the resistance, thus altering the flow of ions depending on the established gradients.

The presence of specific ion channels in the membranes and their asymmetric distribution gives rise to a voltage potential difference across the membrane, the membrane potential (V_m). This voltage potential is formed by the charge separation across the two sides of the membrane and it is due to the chemical gradient, i.e. from the concentration differences inside and outside the membrane.

The concentration difference across the membrane is kept due to active transport. A well-known example of an active transport is the ATPase Na^+-K^+ pump that, amongst other functions, is also responsible for maintaining the cell resting potential in neurons by transporting sodium and potassium ions against their gradients at the expense of ATP. This mechanism is fundamental to regulate and maintain the high concentration of K^+ and low concentrations of Na^+ inside the cells that would otherwise diffuse and dissipate both gradients.

In resting conditions, the inside of the membrane is negative relatively to the outside and, at that given moment, the drive for ions to move according to their concentration gradient is mostly counter-acted by the membrane potential, effectively preventing their net movement (Hille, 1992). This point, when equilibrium is attained, is called the reversal, Nernst or equilibrium potential for a given ion, being defined by:

$$E_{ion} = \frac{RT}{z_{ion}F} \ln\left(\frac{[ion]_o}{[ion]_i}\right)$$

Where R is the ideal gas constant, T is absolute temperature in Kelvin, z is the ion's valence, F is the Faraday constant and [ion] are the ionic concentrations inside (i) and outside (o) the membrane. From this relationship comes that the reversal potential for each ionic species depends only on its concentration inside and outside the membrane.

The overall membrane potential however depends on the membrane permeability and concentrations inside and outside for each specific permeable ionic species. This relationship is known as the Goldman-Hodgkin-Katz equation:

$$V_m = \frac{RT}{F} ln\left(\frac{\sum P_{Cation}[Cation]_o + P_{Anion}[Anion]_i}{\sum P_{Cation}[Cation]_i + P_{Anion}[Anion]_o}\right)$$

Where P is the membrane permeability for a given ion.

This equation assumes that the probability of any given ion to cross the membrane at a given moment is independent of the movement of the other ions present. The larger the gradient and permeability of a given ion, the larger its weight on membrane resting potential.

Ionic channels can either be sensitive to voltage or not. Channels that are not sensitive to voltage, i.e. whose opening and closure are independent of membrane voltage are called passive channels. Voltage sensitive channels, by opposition, have a part of its molecule – the gate – that changes its conformation depending on the membrane voltage. Thus, the channel conductance depends on the state of its activation and/or inactivation

gates. Activation gates open with membrane depolarization, while inactivation gates open with hyperpolarization voltages (Armstrong & Hille, 1998).

The Patch Clamp Technique

In this work we have used the patch clamp technique (Hamill et al., 1981; Sakmann & Neher, 1984), which is a specific application of voltage clamp. When applying voltage clamp to whole cells we can study the current properties in terms of its conductance, voltage dependency, selectivity and pharmacology. In voltage clamp, we are able to control the membrane potential (V_m) and to simultaneously measure the current that crosses the membrane.

This technique, initially developed by Cole, Marmont, Hodgkin, Huxley and Katz in the late 40's undergone several improvements over time (Dean et al., 1940; Marmont, 1949; Hodgkin et al., 1952), being distinguished with a Nobel Prize for Physiology/Medicine to Erwin Neher and Bert Sakmann in 1991. The patch clamp technique itself uses only a single electrode to simultaneously control the voltage and measure the electrical current.

In this work, the whole-cell configuration of patch clamp was used. With this configuration, the whole membrane as a whole can be studied by clamping its membrane potential and measuring the overall currents generated by all the active channels in all of the cell membrane. A typical patch clamp setup consists of an amplifier that measures the membrane potential of the cell, by determining the difference of potential between the inside and the outside of the cell ($V_m=V_i-V_o$), measured by the patch electrode and by the reference electrode, respectively. A second amplifier compares V_m with the V_c (the command potential imposed by the experimenter). Whenever V_m becomes different from V_c, the second amplifier will produce enough current to counteract the potential difference on the cell membrane. This dynamic adjustment (reducing the potential difference) happens immediately after the voltage pulse by a feedback look.

When, for instance, a cationic channel opens in response to a depolarizing event, the cations move across the membrane according to their chemical gradient. In voltage clamp, the second amplifier will generate a similar current of opposite signal, keeping V_m matched to V_c. This generated current is recorded, and because it is equal except in polarity to the ionic current, it mimics its properties over time. Therefore, any change in membrane permeability, will affect how much more or less current is needed to keep V_m constant.

Whole-cell patch clamp is thus a particular case of voltage clamp, in which the electrode used has a narrow opening of around 0.5 to 1 µm.

After attaining a seal between the membrane and the pipette, with a resistance in the order of 10^9 Ω (giga seal), a portion of the membrane is disrupted by applying suction to the pipette. This allows for a continuum between intracellular environment and the pipette solution, allowing for a direct control of the composition and concentration of all ionic species inside the cell. The high resistance of the seal prevents the leak currents between pipette and reference electrode and the passage of ions in bath solution to the cytoplasm.

With the disruption of the cell membrane in contact with the pipette, one can control the intracellular composition as well as the extracellular composition, and thus calculate expected equilibrium potentials for each permeable ion. Furthermore, by designing solutions where some permeable ions are substituted by non-permeable ions not relevant for the study in question, one can isolate specific ion currents. This along with the voltage clamping of the cell membrane potential allows for great control of the membrane and its channels, making it a very powerful technique to study ion channels and transporters.

Care has to be taken in to compensating electric artifacts, by adjusting a series of electric compensatory circuits to abolish transitory peaks that could impair the obtained results (Hamill et al., 1981), that normally involve adding proportional amounts of current through the pipette to counterbalance losses in current. Series resistance compensation is done through the amplifier with frequency-dependent gain and by reducing the electrode resistance, while transitory compensation is performed by reducing the transitory peak current and membrane capacitance.

Another source of noise to consider is the junction potential (E_j). The potential difference arises from the concentrations differences and ion motility present in the ionic solutions on the pipette and bath and must be corrected for each measurement. To further improve the quality of the measurements the patch pipette filament are bathed in silver chloride, that reduces the dielectric properties of the silver wire, further reducing the errors introduced by it.

The Vibrating Probe Technique

The vibrating probe technique is a non-invasive scanning ion-selective electrode technique, and is well suited for the study of extracellular ion dynamics in plants and other systems as well. One of its main advantages against other electrophysiological techniques is the fact of being non-invasive, allowing it to be used in live systems without interfering with the cells. That was the case of the pollen tube, that allowed a broad characterization of the extracellular fluxes that permeated it's membrane, while the pollen tube was growing (Kunkel et al., 2006).

The technique was developed initially by Jaffe and Nuccitelli as a vibrating probe with a spherical platinum-black electrode sensor at its tip, allowing the measurement of voltages with respect to a coaxial reference electrode. This probe vibrated at around 200 cycles per second in a horizontal plane between two extracellular points 30 µm apart. The resulting measured currents of any steady voltage difference would output a sinusoidal current with the aid of lock-in amplifier tuned to the vibration frequency. Since the electric field would be nearly constant over this small distance, it is approximately equal to the voltage difference divided by the distance. Thus, the current density in the direction of vibration is then given by this field multiplied by the medium's conductivity (Jaffe & Nuccitelli, 1974; Weisenseel et al., 1975).

The first use of the vibrating probe as a selective electrode was designed for Ca^{2+} and developed by Jaffe and Levy over a decade later (Jaffe & Levy, 1987), using a direct coupled device it used and Ag-AgCl wire for reference in a 3M KCl salt bridge, away from an artificial source of Ca^{2+}. It vibrated at a frequency of 0.5KHz using a bench-top square-wave oscillator damped with a RC network to smooth the vibratory motion. The system measured the voltage across an ion selective liquid ion exchanger (LIX) membrane in the tip of the microelectrode. Further developments changed the DC coupled device with a capacitor coupled (AC) device, which vibrated two extremes of a straight path, pausing at each end. It measured the voltage differences sensed by the LIX membrane and it was positioned by piezo pushers driven by an oscillator circuit (Kühtreiber & Jaffe, 1990).

Prior to using a vibrating probe technique to study any system it is imperative to use calibration solutions, usually three different molar concentration raging from 1 to 10 mM, for instances, of an appropriate saline solution of the ion we're about to measure. Adjustments should be made to adjust the range of the calibration to the dynamic range of the measurements being made. The system is then calibrated by establishing a Nernst

slope to infer the systems linearity and response to potential variations due to the difference ionic concentration is the control solutions. After establishing this and ensuring that the system is stable, measurements can be initiated.

This technique records potential differences alone. However, since it can detect them selectively by measuring only specific ion species, it makes it possible to determine the fluxes that created that potential by applying Fick's first law:

$$J = -D\frac{dC}{dr}$$

Where *D* is the diffusion rate for the ion species in study, *dr* is the excursion distance and *J* is the ionic flux. The *dC* is the differential concentration obtained by the calibration with the Nernst slope:

$$C = 10^{\frac{V-i}{s}}$$

With *i* being the interception point of the axis and the *s* the slope of the calibration curve.

Another important factor for good vibrating probe experiments is the probe itself, as each ion requires a specifically designed probe. Probes are made from capillary tubes and need to have a very thin opening that will be later on filled in with the appropriate ionophore. The size of the tip and the amount of the ionophore column, as well as the amount of saline solution (KCl) to back-fill them, all play an important role in increasing the efficiency of the probe and reducing the noise rate.

Objectives

Anionic transport plays a fundamental role in pollen tube growth and development, yet the molecular identification of the genes responsible for this transport has not been successful so far. Previous work in our group identified for the first time the presence of anionic currents in pollen grains protoplast by using the patch clamp technique, validating previous reports on the existence of large anionic effluxes on the pollen tube and demonstrating their dependency of $[Ca^{2+}]_{in}$.

The main goal of this work is to extend this previous study, including the role of pH in regulating the anionic currents and identifying their molecular identity.

Materials and Methods

Plant Growth Conditions

Arabidopsis thaliana wild type seeds (WT), ecotype Columbia, were obtained from the Nottingham Arabidopsis Stock Center (NASC). Pots with 300 mL capacity (Desch Plantpak) were used to grow *Arabidopsis thaliana* plants. These were filled with a 3:1 mixture of soil and vermiculite. The soil mixture was soaked with water and left to drain. The non-systemic insecticide DESTROYER 5G (5% (w/w) chlorpyrifos) from AGRIPHAR was then added in a concentration of 0.1 g per pot. All seeds were incubated at 4 ºC for 3 to 4 days – stratification process.

The WT seeds were then transferred to pre-prepared pots (5 seeds per pot) and left to germinate in a growth chamber. Germination Medium consisted of Murashige and Skoog Basal Medium supplemented with 1% (w/v) Sucrose, 0.05% (w/v) MES, 1x Gamborg's B5 vitamins, 8% (w/v) Agarose, pH 5.7. All *Arabidopsis thaliana* plants were germinated and grown in a growth chamber with a short day light regime (8h day/16h night) for 4 to 6 weeks and then transferred to a long day light regime (16h day/8h night) to promote flowering. The light was supplied by fluorescent lamps and its intensity varied between 60 and 80 µmol m^{-2} s^{-1} (µE m^{-2} s^{-1}). The temperature in the chamber ranged from 22 ºC during the day to 18 ºC during the night. The humidity levels ranged between 60 and 65%.

The *Arabidopsis* T-DNA insertion line was obtained from GABI-Kat and homozygous plants were selected by PCR.

Lilium longiflorum (Thunb.) plants were purchased from local flower suppliers.

Pollen Protoplast Production

Arabidopsis thaliana and *Lilium longiflorum* pollen grain protoplasts were isolated as described in Tavares et al., 2011, with just minor modifications and in line with what has been done by previous groups (Tanaka et al., 1987; Fan et al., 2001; Mouline et al., 2002; Tavares, 2011; Tavares et al., 2011).

For *Arabidopsis* experiments, roughly 30 to 50 freshly blossomed flowers were collected in the same day and shaken for 1 min, before adding 2 mL of standard solution (Table 1). These were then shaken for 2 min releasing the pollen grains from the anthers. The pollen in solution was then separated by using a 29 µm mesh filter.

For *Lilium* experiments, previously aliquoted pollen grains, that had been collected directly from the anthers and stored at -20ºC, were used. 2 mL of standard solution was added and, depending on how long the pollen had been stored, these were shaken from 1 to 3 min (longer for older pollen).

Table 1 - Protoplast Solutions. Osmolarity adjustment were made with sorbitol. pH was rectified with NMG-OH. Enzymatic solution concentrations are in % (w/v).

Standard Solution		Enzymatic Solution	
KNO_3	1.0 mM	Cellulase	1.0%
KH_2PO_4	0.2 mM	Macerozyme	0.5%
$MgSO_4$	1.0 mM	BSA	0.2%
KI	1.0 µM		
$CuSO_4$	0.1 µM	in Standard Solution	
$CaCl_2$	5.0 mM	kept at -80ºC	
MES	5.0 mM		
Glucose	0.5 M		
Sorbitol	1.0 M		
pH	5.8 (NMG-OH)		
Osmol	1.5 $Osmol.kg^{-1}$		

Either species pollen was left to hydrate for 10 min in standard solution at room temperature. Pollen was then centrifuged for 5 min at 1600 rpm or at 3500 rpm, for *Arabidopsis* or *Lilium* pollen respectively. The supernatant was then removed and 2 mL of enzymatic solution was added (Table 1). Pollen was incubated at 30ºC with mild agitation (less than 100 rpm) for a period of 90 to 150 min, depending on the pollen age and species. *Lilium* pollen normally requires less time, unless it has been stored for a longer period, while *Arabidopsis* takes longer for the enzymatic digestion to occur. Enzymes cellulose RS “Onozuka” and macerozyme R-10 were purchased from Duchefa (Haarlem, the Netherlands), as other companies enzymes testes failed to meet the requirements for this protocol.

After enzymatic digestion, the resulting pollen protoplasts and pollen grains are centrifuged for 5 min at 1300 rpm or at 1600 rpm, for *Arabidopsis* or *Lilium* respectively. The enzymatic solution (supernatant) is removed and another 2 mL of standard solution are added to wash the solution of the enzymes. The protoplasts suspension is centrifuged two more times, removing the supernatant, and re-suspending it with standard solution to

wash it off. After the last centrifugation, one bath solution is added instead of standard solution, depending on the experimental plan. The protoplasts were then kept in ice and used for patch clamp experiments in the same day. This protocol has been successful in creating protoplasts routinely, especially for *Lilium* pollen. The yield for *Arabidopsis* is much lower, but routinely generated enough protoplast per session for several seal tries and/or multiple experiments.

Electrophysiological Essays

After pollen grain protoplasts are ready, they are placed inside a 34 mm diameter Petri dish with a custom-made 1 mL central chamber with glass bottom. Adding 100 µL of protoplast solution (bath solution) along with 400 µL of the bath solution desired for that experiment. The Petri dish is then placed in the microscope stage and protoplasts are left for 20 min to set at the bottom.

The recording solutions used were designed in order to have the main permeable ion as Cl^- (B1-B10, P1-P2, Table 2), or NO_3^+ (B7 and B11, Table 2). Other permeable cations, namely K^+ and Na^+ were replaced by NMG^+ (N-Methyl-D-glucamin), a non-permeable cation. It was previously reported that the presence of TEA had no effect on the measured currents (Tavares et al., 2011), suggesting that the solution design and cation substitution was enough to quench any cation currents. Gadolinium (Gd^{3+}) was used as both a means to block divalent cation currents and as a mean to improve seal formation (Wang et al., 2004; Tavares et al., 2011).

Table 2 depicts the ionic composition of all the external (B1-11) and internal solutions (P1-2) used in this work for *Arabidopsis* experiments. In the case of *Lilium* experiments, all the solutions are the same, apart from the osmolarity, which is decreased to 700 mOsm. For each solution, pH was adjusted with NMG-OH, in combination with the use of appropriate buffers in each respective solution. The use of a Ca^{2+} chelator in the pipette solutions was intended to keep the free [Ca^{2+}] inside the pipette constant, around 6.04 nM. This value was estimated using webmaxclite v1.15, available online (http://www.stanford.edu/~cpatton/webmaxc/webmaxclite115.htm). ATP was also added to the pipettes solutions to power up any anionic transporter present in the membrane. HEPES was used as a buffer for solutions with pH above 6.7, while MES was used for solutions with pH below or equal to 6.7. All chemicals were purchased from Sigma, unless stated otherwise.

Table 2 - Recording solutions. B1 to B11 are bath solutions (extracellular) and P1 to P2 are pipette solutions (intracellular). Concentrations are in mM. pH is dimentionless and Osm is in mOsm. The pH was adjusted with NMG-OH, and osmolarity was adjusted with sorbitol. Free $[Ca^{2+}]_{in}$ in the pipette solutions was estimated to be 6.04 nM by using software Webmaxclite v1.15. NMG^{+} was used as a non-permeant cation as a substitute for other cations. Gd^{3+} was used to block Ca^{2+} and other cation currents.

	NMG-Cl	NMG-NO_3	$CaCl_2$	$MgCl_2$	$GdCl_3$	MgATP	MES	EGTA	Hepes	pH	Osm
B1 (Control)	**129**	**5**	**3**	**1**	**1**		**5**			**5.8**	**800**
B2 (pH 5.6)	129	5	3	1	1		5			**5.6**	800
B3 (pH 6.0)	129	5	3	1	1		5			**6.0**	800
B4 (pH 6.4)	129	5	3	1	1		5			**6.4**	800
B5 (pH 6.8)	129	5	3	1	1				**5**	**6.8**	800
B6 (pH 7.2)	129	5	3	1	1				**5**	**7.2**	800
B7 (Cl 14)	**3**	5	3	1	1		5			5.8	800
B8 (Cl 30)	**29**	5	3	1	1		5			5.8	800
B9 (Cl 70)	**59**	5	3	1	1		5			5.8	800
B10 (Cl 280)	**269**	5	3	1	1		5			5.8	800
B11 (NO_3)	**0**	**134**	3	1	1		5			5.8	800
P1 (Control)	**139.4**	**5**	**0.3**			**5**		**5**	**5**	**7.2**	**800**
P2 (pH 6.8)	139.4	5	0.3			5		5	5	**6.8**	800

The equilibrium potentials for all the solutions combinations used are shown in Table 3, for the permeable ions Cl^-, NO_3^- and H^+ (the only ions with different reversal potentials under these solution combinations). The reversal potential for Ca^{2+} and Mg^{2+}, which are also present in these solutions and are also permeable, is of 165.01 mV and 15.32 mV for all solutions used. These values are predicted by the Nernst equation.

Table 3 - Equilibrium Potentials for the permeable ions in solution for all the experimental conditions tested, as predicted by the Nernst equation. The equilibrium potential for Ca^{2+} is 165.01 mV and for Mg^{2+} is 15.32 mV for all the solutions combinations used. All values are in mV. Values in bold denote the changes in reversal potential compared to the control condition. In the control condition (P1/B1) the most relevant reversal potential is that of Cl^-, also marked in bold.

V_{rev} (mV)		B1	B2	B3	B4	B5	B6	B7	B8	B9	B10	B11
P1	Cl-	**0.00**	0.00	0.00	0.00	0.00	0.00	**57.94**	**38.76**	**17.44**	**-17.44**	**64.01**
	NO_3^-	0.00	0.00	0.00	0.00	0.00	0.00	0.00	0.00	0.00	0.00	**-82.74**
	H^+	81.11	**92.70**	**69.53**	**46.35**	**23.18**	**0.00**	81.11	81.11	81.11	81.11	81.11
P2	Cl^-	0.00										
	NO_3^-	0.00										
	H^+	**57.94**										

The reference electrode is then dipped in the bath and connected to the headstage. Reference electrodes were initially composed of homemade electrodes with Ag/AgCl wires embedded in a 0.5 M KCl-agar bridge, and later were substituted by a dry reference electrode that provided a much more stable readings (DRIREF-2; World Precision Instruments).

The Ag/AgCl electrode permits a smooth transition between the electric current carried by electrons and the current carried by the ions in solution. This was achieved by a silver/silver chloride (Ag/AgCl) interface - a silver wire coated with AgCl. When the electrons flow from the copper wire, through the silver wire, into the Ag/AgCl electrode, they convert the Ag^+ into Ag, the Cl^- ions then become hydrated and enter the solution. If the electrons flow in the reverse direction, the Ag atoms in the wire donate their electrons (one per Ag atom) and combine with the Cl^- in solution to make insoluble AgCl (Axon Instruments, 1993; Halliwell et al., 1987).

A protoplast is selected under an amplification of 200x to 300x (depending on setup), by choosing a smooth membrane protoplast, detached from its grain and isolated from others.

A microelectrode was then backfilled with the appropriate pipette solution (P1 or P2, Table 2) and an Ag/AgCl electrode was inserted inside, electrically connecting it to the

headstage via the pipette holder. The microelectrode was then dipped in to the bath solution, closing the electric circuit with the reference electrode. Micropipettes were previously pulled from borosilicate glass capillary with a 1.5 mm external diameter and 0.86 mm internal diameter (GB150F-8P; Science Products GmbH) with a vertical puller (PB-7, Narishige).

At this point, we can measure the microelectrode resistance. Ideal microelectrodes produced this way presented a resistance between 6 to 10 MΩ. A PVC tube connected to the pipette holder provided a means to apply pressure with the aid of a syringe, which helps in establishing a stable seal and the breaking of the membrane to enter whole-cell configuration.

Using macro and micromanipulators, the microelectrode is positioned above the chosen protoplast and we proceed to establish a tight seal between microelectrode and protoplast by monitoring the current to determine when contact is made. We then apply pressure in the microelectrode to facilitate seal formation. Ideally the seal resistance should be higher than 1 GΩ, as the higher resistance allows for reduced noise levels by leak currents from the seal between pipette and membrane (Axon Instruments, 1993). Once a Giga-seal is established capacitive transients are compensated via the fast and slow pipette capacitance compensation commands in the amplifier.

With further application of negative pressure, we disrupt the patch of membrane in contact with the microelectrode tip thus establishing an electrical continuity between the pipette solution and the interior of the cell, thus reaching to whole-cell configuration.

At this point, we can apply different voltage protocols to test the cell membrane response to different voltage potentials. We used two different protocols to test the membrane, the activation and tail protocol as shown in Figure 1. Both voltage protocols keep cells at a holding potential of -100 mV, since this potential mimics what is expect to be the resting membrane potential for these cells, and it has been shown that it maintains seal stability between voltage tests. For the activation protocol, the membrane is tested with increasing test potentials of 1.2 sec starting from -200 to +200 mV in 20 mV steps. The cell is kept for 3 sec between each test potential at holding potential, in order to make sure the currents have time to stabilize. For the tail protocol, the cells are clamped at +180 mV for 1 sec in order to get all the channels in a maximum conductivity state. This is then followed by increasing test potentials of 500 ms ranging from -180 to +180 mV with 20 mV steps. Between each test potential, the voltage is then clamped at the holding potential for 5 sec, giving even more time for the currents to stabilize.

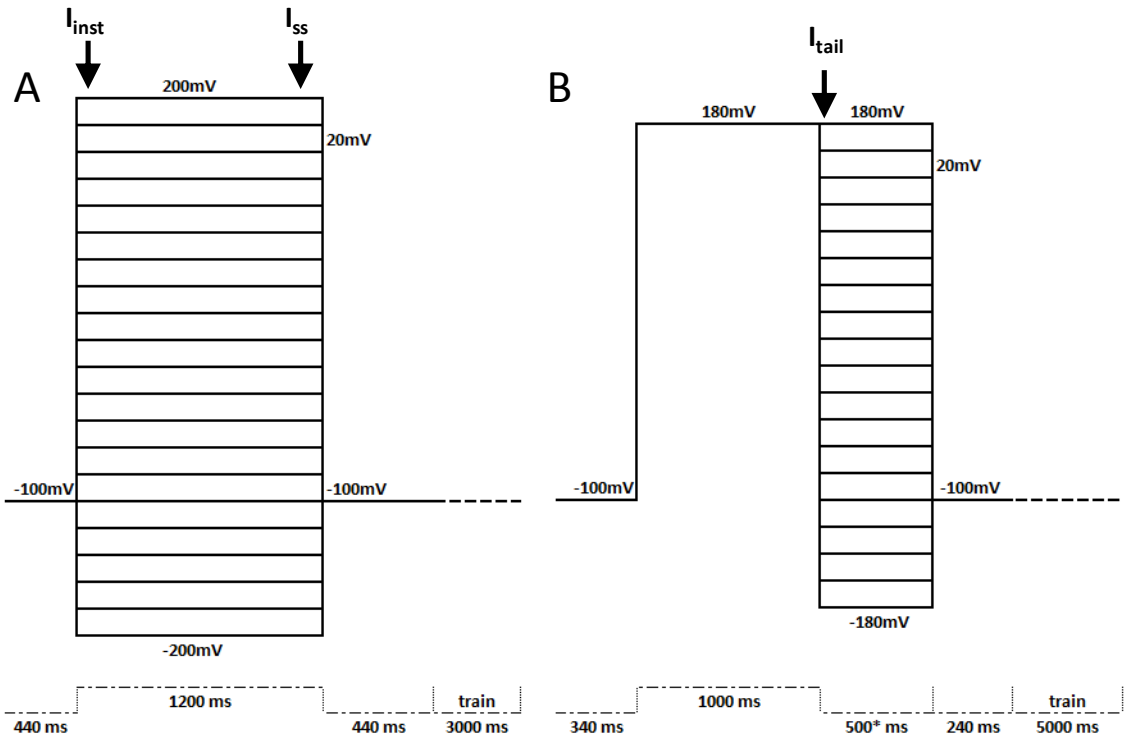

Figure 1 – Voltage Protocols. (A) Activation Protocol. (B) Tail Protocol. The black arrows mark the position where the currents are average to plot the corresponding I-V curves, for the Instantaneous (I_{inst}), steady state (I_{ss}) and tail (I_{tail}) current.

We have used an additional fast ramp protocol mostly as a quick way to measure the cell response to activation. We also used it to check for any quick transient currents that we might be missing with the other longer acquiring protocols, but failed to detect any such currents. In the end, it was mainly used as a quick way to check if the cell had entered whole-cell configuration or not, since in these cells the transition from cell attached to whole-cell is not always evident.

We always apply the activation protocol prior to the tail protocol, since the latter, especially when the seal is still stabilizing, may cause destabilization and even loss of the seal due to the high positive voltage used repeatedly. This has been minimized by the longer train used (10 sec between each run) and by spacing out measurements between each voltage protocol.

As soon as we enter whole-cell, the currents undergo a process of Rundown. For that reason, we try to run the first activation protocol as soon as possible, and we then follow the rundown process over time with the activation protocol alone. Tail protocol is only used after the first activation protocol is recorded, and before any other change, such as the end of rundown or after any bath exchange, in order to ensure that we have at least one measurement with each protocol at each specific checkpoint in the experiment.

On a typical experiment, we would have several checkpoints of interest. The first one being the first measurement as we enter whole-cell configuration. This we call the Initial Current (the current before rundown). Then, we monitor the currents as they undergo rundown and until the current amplitudes are stable for more than 15 min. This point we call Final Current (the current after rundown). We can only test new conditions on the Final Current, as we need to have a stable current in order to analyze the differences caused by any alteration to the system afterward. We either perform a bath solution exchange or apply an inhibitor to the bath solution. In either case, we allow the cell to stabilize after the change and monitor the currents with the activation protocol; after they stabilize, we can perform any additional bath solution exchanges if that is the experiment planned.

Alternatively, we can start with different initial solutions, to test different responses to the current lost by rundown or with different intracellular solutions. In these cases, we follow the same procedure as before as well.

Bath solutions were changed by injection at a continuous flow rate of approximately 20 $cm.s^{-1}$ through a 500 µm pvc tube, placed at one extreme of a 1 ml circular measuring chamber, and removal at the same rate from the opposite side. Protoplasts, especially from Lilium, are difficult to lift without losing the seal, and moving them to the perfusion tube often leads to loosing the seal. Alternatively, manual perfusion was also used with the same results, removing fix amounts of bath solution and adding set amounts of a new bath solution.

Anionic current inhibition was tested with NPPB, a known inhibitor of Cl^- currents, was also used sporadically in this work. NPPB was first dissolved in DMSO, in a stock solution of 25 mM concentration and kept at 4ºC, previous to use. Before applying to the experiment, it was first dissolved in bath solution. It has been shown that DMSO also has an effect on anionic currents, amounting to almost half the effect of NPPB (Tavares et al., 2011).

All current measurements of pollen protoplasts were done under voltage-clamp condition with standard whole-cell recording techniques (Hamill et al., 1981). Data was acquired at 50 kHz with a low-pass filter of 5 kHz. Clampex 8.0 software (Axon Instruments) was used to generate the command potentials and to collect the data in the computer for posterior analysis. The raw data obtained was then used to create Current-Voltage (I/V) curves and the analysis is further detailed on the Data Analysis section of the Materials and Methods.

All experiments were performed below room temperature, around 19ºC.

Patch Clamp Setup

The patch clamp setup consisted of the following equipment. A microscope mounted on top of an anti-vibrating table and inside a Faraday cage, a patch-clamp amplifier, a micro- and a macromanipulator, a digidata and a computer.

In detail, we used an IMT-2 inverted microscope (Olympus) with a WHK 10x/20 eyepiece and Plan 20x or 40x LWC-CD objective lens, mounted on top of a PBH51514 breadboard (Thor Labs) and a custom made frame with PWAO74 dumpers (Thor Labs). This was encased inside a custom-made copper Faraday cage. The pre-amplifier headstage CV203BU (Axon) was connected to a Axopatch 200B amplifier (Axon), outside the faraday cage. A Digidata 1200A (Axon) was used to interface the amplifier with the acquisition software Clampex 8.0 (Axon) on a computer. A micromanipulator MMO-203 (Narishige) and a macromanipulator MM-3 (Narishige) were used to move the headstage, pipette holder and pipette.

It is also fundamental to ground each piece of equipment inside the Faraday cage to reduce any source of electrical noise. This is achieved by grounding all equipment to a common ground and shielding any source of noise. In addition, the illumination of the microscope was substituted by a DC power source light.

Data Analysis

All raw data obtained was analyzed with Clampfit 8.0 (Molecular Devices). Liquid junction potentials were calculated in Clampex 8.0 (Molecular Devices) and were used to correct all whole-cell recordings in each proper solution combination (Table 4).

Table 4 – Liquid Junction Potentials. Calculated with Clampex 8.0 for all the experimental conditions tested. All values are in mV.

Vj (mV)	B1	B2	B3	B4	B5	B6	B7	B8	B9	B10	B11
P1	-0.4	-0.4	-0.4	-0.4	-0.4	-0.4	-26.1	-21.0.	-11.5	+13.1	-1.5
P2	-0.4	-	-	-	-	-	-	-	-	-	-

The liquid junction potentials (or diffusion potential) are a result from the difference in concentrations and ion mobility between two different salt solution at a given interface of

contact (Halliwell et al., 1994). This value affects the actual potential that is applied to the membrane during patch-clamp experiments and must be corrected for each solution combination (Axon Instruments, 1993).

All linear and nonlinear data fitting was performed with the ORIGIN 6.1 software (OriginLab Corporation, Northampton, MA, USA). Statistical significances were determined using the t-Test in Origin 8.1 and differences were considered significant if $p < 0.05$.

Current-Voltage relationship (I/V curves) were obtained by averaging raw data for 3 ms after 0.5 ms of any transient peak of either the activation or tail protocol test potentials for the instantaneous currents and tail currents respectively. For the steady state current, raw data was average for the last 50 ms of each test potential of the activation protocol. On occasion, individual changes to the measuring points had to be made in case of any unusual behavior, such as seal instability or transients not fully compensated.

Furthermore, all currents amplitudes were normalized with the respective membrane capacitance (C_m) producing current density values (pA/pF) that were then used for the proceeding analysis and I/V curves.

For each experimental condition and parameter, data from different cells in the same conditions was averaged. Data is shown as mean ± SE (n), where SE stands for standard error and n is the number of cells/experiments.

Asymptotic forward (gF) and backward (gB) conductance (outward and inward slope conductance) were obtained from the most positive and negative portions of the I/V curves, where the current values are directly proportional to the electromotive force, by means of a least-mean-square linear fit.

Equilibrium potentials for permeable ions in solution were calculated with the Nernst equations, reflecting each combination used (Table 3).

The relative permeability was determined by measuring the shift in reversal potential (V_{rev}) upon changing the bath solution with a Cl^- rich solution to a solution NO_3^- rich solution (B1 → B11) and vice-versa. The permeability ratio was estimated by rearranging the Goldman– Hodgkin–Katz equation:

$$P_{NO_3^-}/P_{Cl^-} = e^{\left(-\frac{\Delta V_{rev} F}{RT}\right)}$$

Where ΔV_{rev} is the difference between the reversal potential with the NO_3^- and that with Cl^-; F is Faraday's constant; R is the gas constant; and T is temperature in degrees Kelvin.

Conductance-Voltage relationship (G/V curves) were derived from I/V curves according to $G = I_{SS}/(V_m - V_{rev})$, where I_{ss} is the steady-state current at the end of the test potential V_m, and V_{rev} is the reversal potential of the current. Conductances values were then normalized for the maximum response and fitted with a Boltzmann type equation:

$$G/G_{max}(V_m) = A0 + \frac{A0 - A1}{\left[1 + e^{(V_m - V_h)/V_s}\right]}$$

With V_h being the potential for the half-maximal chord conductance which indicates at which potential the transition between two states of conductances occurs, V_s is the slope factor of the curve and measures the current sensitivity to potential variations, and A1 and A0 are the minimal and maximum values of conductance.

The activation currents could be fitted with the following empirical equation:

$$I(t) = \sum_{i=0}^{n} I_i e^{-t/\tau_i} + I_{inst}$$

Where I(t) is the total current, I_{inst} is the instantaneous current component, I_i is the time dependent current component, τ_i is the time factor, t is the time. The n value ranges from zero to 2, being 2 the most common case for currents elicited at high positive potentials, while the currents elicited with negative potentials typical only exhibit the instantaneous component or just one time-dependent component.

In order to calculate corresponding anion fluxes that the elicited currents could produce the following formula was used: $Flux = I/zFC_m$, where I is the current, z the ion charge, F the Faraday's constant (96485 s.A.mol^{-1}, C_m is the membrane capacitance (1 uF.cm^{-2}). Using this formula it was possible to convert current density (pA/pF) into ion fluxes (pmol.cm^{-2}.s^{-1}).

The Vibrating Probe

For use with the self-referencing ion-specific vibrating probe, pollen from *Nicotiana tabacum* SR1 was used. Plants were grown in soil in a culture chamber at 25ºC using long-day conditions. Pollen was harvested from mature flowers, dried for 48h at room temperature and stores at -20ºC for later use. The germination medium used contained 1.6 mM H_3BO_3, 5 µM $CaCl_2$, 5 µM MES and 6% sucrose with a pH 5.8, an optimized medium for use with the vibrating probe. Pollen grains were germinated in liquid medium,

under mild agitation. After germination, pollen tubes were allowed to grow for 2 to 4 hours allowing them to grow for a few hundred micrometers in Petri dishes before measurements were made.

The vibrating probe technique was used to measures extracellular ion fluxes for H^+, K^+, Ca^{2+} and anions in the growing pollen tube of *Nicotiana tabacum* as previously described (Kühtreiber & Jaffe, 1990; Kochian et al., 1992; Holdaway-Clarke et al., 1997; Shipley & Feijó, 1999; Feijó et al., 1999; Zonia et al., 2002; Kunkel et al., 2006).

Micropipettes were pulled from 1.5 mm borosilicate glass capillaries (TW150-4, World Precision Instruments) with a P-97 Flamming Brown Puller (Sutter Instruments) and baked at 220ºC overnight. Furthermore, the micropipettes were made hydrophobic by silanization (dimethyl-dichlorosilane, Sigma), after an 30min followed by 2h in oven.

Microelectrodes with tips opening of less than 3 µm (or less than 1 µm for K^+ measurements) were backfilled with 15 to 30 mm (or 20 to 40 mm for K^+) of the following electrolytes: H^+-specific electrode: 40 mM KH_2PO_4 and 15 mM KCl, pH 7.0; Ca^{2+} and anions electrode: 100 mM $CaCl_2$; K^+ electrode: 100 KCl. The microelectrode were then front-loaded with 20 to 30 µm (80-120 µm for K^+) of their respective selective exchange cocktail (H^+ Ionophore Cocktail B, Ca^{2+} Ionophore Cocktail A, K^+ Ionophore I Cocktail B, anions Chloride Ionophore I Cocktail A, Fluka).

Electrodes were calibrated in solutions containing three different concentrations in a background specific to the experiment/ion. Only electrodes that showed a Nernstian response were used.

A silver electrode wire pre-treated 10 min with bleach was inserted into the back of the electrode and established electrical continuity with the bathing solution. Signals were measured between the probe and a dry reference half-cell electrode (World Precision Instruments) inserted into the sample bath and amplified using a custom-built electrometer (Applicable Electronics).

Electrode vibration and positioning was achieved with a stepper-motor-driven three-dimensional positioner. Data acquisition, preliminary processing, control of the 3D electrode positioner and the stepper-motor controlled fine focusing of the microscope stage were performed with ASET software (Science Wares).

The self-referencing vibrating probe oscillated along an excursion of 10 µm (20 µm for K^+) measurements. Typical cycles acquisition were completed in 3 to 5 seconds depending on the tunable settling time after each movement, with two measurement periods (one at each extreme) and the respective excursion time.

The measurement close to the membrane was then subtracted by the one further away. Ion fluxes were obtained by perpendicularly vibrating the electrode tip within up to 1-3 µm of the pollen membrane on tubes longer than 200 µm. At this distance the fluxes are assumed to be uniform (Smith et al., 1994).

Background references were taken at more than 1 mm from any cell and the values were subtracted from the µV differential recordings during data processing using a custom-made script in SciLab 4.1.

The vibrating electrode system was attached to a Nikon Eclipse TE-300 inverted microscope that was housed inside a copper sheet Faraday cage supported on a vibrating-free platform.

The efficiency of the vibrating probe system was determined using a method adapted from previous works (Kühtreiber & Jaffe, 1990; Gilliham et al., 2006). An ionic gradient was measured both statically and with the electrode stepping between two points (50 µm apart in 4 s cycles) at various distances (10 to 500 µm) from an artificial source. The static measurements were used to calculate an empirical constant (U), which defines the diffusion characteristics of the gradient source and allows the generation of ΔV as a function of distance from the source to compare with that measured stepping between the two points every 4 sec. The ratio between the theoretically and experimentally derived values yielded a value for the efficiency of the flux measurement using this experimental configuration.

Frequency analysis of the ionic fluxes was performed using AutoSignal v1.7 (Systat Software) as done previously in our group (Michard et al., 2008; Ramos et al., 2009). For each set of flux oscillations to be analyzed a de-trend was applied, consisting of a linear least square fit subtraction to remove the very low frequency trend of the data. Fourier and wavelet analysis were used to dissect the frequency components of the oscillations. For Fourier analysis, a Fast Fourier Transform Radix 2 algorithm was used, ensuring that each data set was a continuous acquisition without breaks and with a constant sampling rate. Peaks were detected using a local maxima detection algorithm and considered relevant according to their significance levels (the higher the significance level the less likely for a detected spectral signal to arise from random noise). Significance levels are given in the results. For wavelet analysis, a continuous wavelet time-frequency spectrum was obtained with a non-complex Morlet wavelet (wave number, 16). A peak-type critical limit was used instead of the traditional confidence levels, as implemented in the software.

Results

The anionic currents of *Arabidopsis* pollen

From initial work done in our lab, anionic currents in pollen protoplasts have been described by applying whole-cell configuration of the patch clamp technique under symmetrical Cl- concentration (Tavares, 2011; Tavares et al., 2011).

The control experimental condition in which this was performed was by using the pipette solution P1 (intracellular side) with the bath solution B1 (extracellular side) which we refer to as control condition (See Table 2 on page 23). This solution combination P1/B1 (control) has proven to be very stable for patch clamping whole-cell grain protoplasts. It equilibrates an high [Cl^-] inside and outside the protoplast, with a steep pH gradient of 7.2 inside against 5.8 outside, with just enough Ca^{2+} present for seals to be established successfully and all other permeable ions removed from solution, or in very small concentrations. This eliminates any chemical gradients and isolates the voltage dependence of the currents on membrane potential, while ensuring that the dominant conductance measurable will be that of Cl^-. Furthermore, the presence of Gd^{3+} has proven to be essential for the establishment of stable seals between pipette and protoplast, allowing to further reduce the [Ca^{2+}] outside, as well as providing a safe guard for any contamination of the results by divalent cation currents.

Large outward rectifying voltage dependent anionic currents permeate Arabidopsis pollen plasma membrane

Under these control conditions voltage protocols as depicted in Figure 1 on page 26 were applied, eliciting large anionic outward rectifying currents as can be seen one example in Figure 2. The currents exhibit a strong outward rectification, but also conduct in the negative potentials, within the physiological range. The activation protocol clamped the membrane voltage at a holding potential of -100 mV, which were followed by test potentials (V_m) that ranged from -200 to +200 mV, in 20 mV steps. The tail protocol clamped the membrane voltage at an holding potential of also -100 mV, followed by a activation step at +180 mV to activate the outward current for 1 second, followed by test potentials in 20 mV steps from -180 to +180 mV.

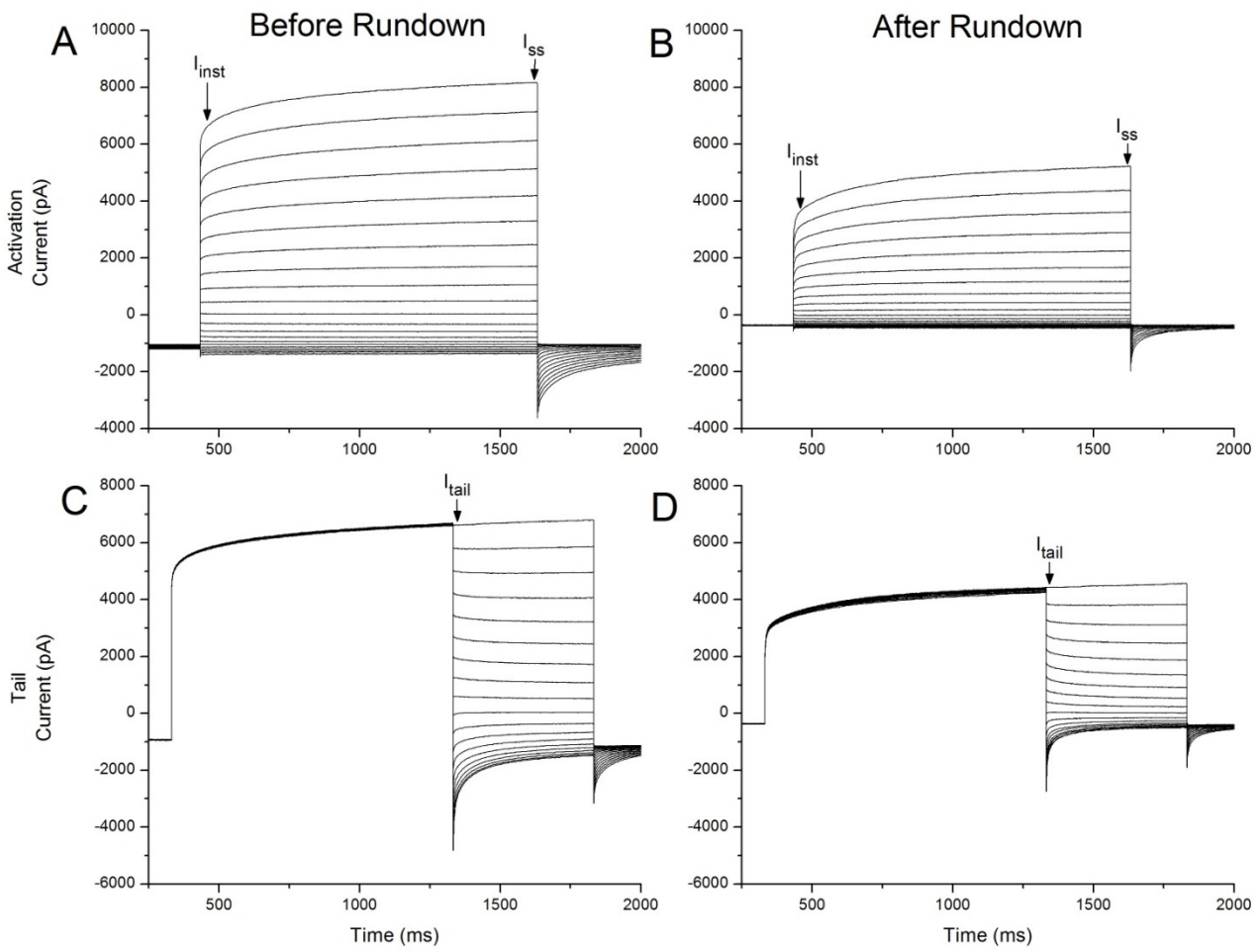

Figure 2 – Typical *Arabidopsis thaliana* wild type activation and tail currents, before and after rundown under control condition. Panel A and B show typical whole cell currents elicited with the activation protocol, denoting a strong outward rectification and a time dependent activation of the anionic currents. The activation current undergoes rundown, as seen from Panel A to B with overall current reduction. Panel C and D show typical whole cell currents elicited with the tail protocol, denoting a transient peak current after depolarization. The tail current also undergoes rundown, as seen from Panel C to D with the overall current reduction. Black arrows mark the position where the currents are averaged to plot the corresponding I-V curves, for the Instantaneous (I_{inst}), steady state (I_{ss}) and tail (I_{tail}) current.

Another interesting aspect is the fact that the activation currents are a composite current, with two distinct components – an instantaneous current and a time-dependent activation current. Previous work done in our group has also evidenced that this time-dependent activation is composed of a fast and a slow-time dependent activation, at the potentials tested. These time dependent activation curves have been shown to have time constants in the order of <50 ms for the fast one, and >300 ms for the slow ones (Tavares, 2011).

Anionic currents in Arabidopsis pollen protoplasts undergo a process of current rundown

As soon as whole-cell configuration was attained in stable seals, a time-dependent exponential decrease in current amplitude (rundown of the current) was always observed. This is a common feature of many channels' currents that are intracellularly regulated by unidentified effectors not present in the pipette solutions (Marty & Neher, 1995), which occurs most likely due to a dilution during the perfusion of the pipette solution in to the dense pollen protoplast cytoplasm. This response has been reported for anionic channels as well (Becq, 1996; Binder et al., 2003) and can be observed for the anionic currents in pollen protoplasts of *Arabidopsis* in Figure 2 from panel A to B (activation current rundown) and from panel C to D (tail current rundown).

The exact nature of this current lost during rundown is so far unknown, but is likely attributed to a population of channels present in the plasma membrane, or alternatively to the gradual dilution of some modulation effectors that regulate the anionic conductance's of all or some of the channels population in the membrane. This can occur by changing their open probability, for instance, or even their individual conductance over time.

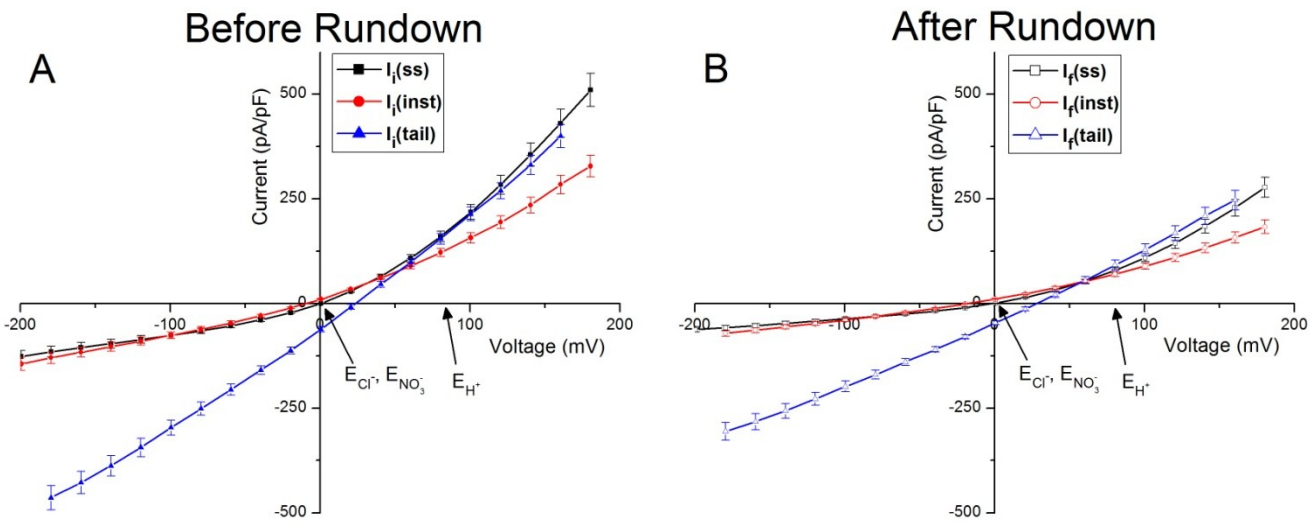

Figure 3 - Current-Potential (I-V) curves for all three current components measured, before and after rundown, under control condition. Steady state (I_{ss} ■), instantaneous (I_{init} ●) and tail (I_{tail} ▲) current components of the initial currents before rundown (A) and the final currents after rundown (B). The black arrow (➔) marks the position for the calculated equilibrium potential for Cl- (E_{Cl^-} = 0.0 mV), NO_3^- (E_{NO3^-} = 0.0 mV) and H^+ (E_{H^+} = 81.1 mV) for the control condition (P1/B1).

Until the rundown process is completed, the current amplitude is changing over time, which makes it undesirable to perform further tests before the current level stabilizes, as it would be difficult to ascertain which changes relate to the experimental test. This

process takes in average 80 ± 9 min in *Arabidopsis* wild type pollen grain protoplasts, ranging from 30 min to 180 min, and on rare occasions even more.

By plotting the normalized I-V curves as described in Material and Methods, for the instantaneous and steady state currents elicited by the activation protocol and the tail peak current for the corresponding protocol (Figure 3), we can better quantify the properties of the anionic currents before (Figure 3A) and after rundown (Figure 3B) for the three different currents measured (Table 5). Here we show the averaged I-V currents for all the experiments performed under control conditions (P1/B1) with the error bars representing the corresponding standard error. All currents - instantaneous, steady state and tail current - evidence strong rundown over time after whole-cell configuration is attained across all potentials. For maximum current values and rundown quantification, we considered the values obtained from potentials of ±160 mV, which were representative for values obtained from either positive or negative potentials. On average, the percentage of current lost by rundown was constant between all positive currents or all negative currents, but not between them. We did not use the currents obtained with maximum and minimum voltage, because in some experiments these extreme voltage values induced a seal destabilization that affected the results (and in some cases resulted in the seal being lost). Therefore, we often trimmed the protocols to avoid those potentials when the protoplast stability was affected by it on a case-by-case scenario. We never observed this effect at potential values of ±160 mV or lower.

Table 5 - *Arabidopsis thaliana* wild type average normalized initial currents and percentage of current lost by rundown. I_{init} is the initial current density (pA/pF) measured at ±160 mV before rundown for each of the current components (steady state I_{ss}, instantaneous I_i and tail current I_t). RD% refers to the percentage of current lost during rundown, measured at ±160 mV. Data is represented as mean ± SE. *, refers to statistical significant differences between comparable items within the same table column (p < 0.05).

		V_m (mV)	I_{init} (pA/pF)	n	RD %	n
wt	I_{ss}	+160	365 ± 51	(53)	55 ± 3	(53)
		-160	-78 ± 11		48 ± 3	
	I_i	+160	258 ± 38 *	(53)	53 ± 3	(53)
		-160	-89 ± 13		44 ± 3	
	I_t	+160	400 ± 55	(38)	46 ± 5	(31)
		-160	-406 ± 50 *		33 ± 4 *	

The steady state current and the instantaneous currents have very similar rundown properties. In fact, the major difference from these two currents falls in the range of the positive potentials, where the slow-time dependent activation current is more pronounced, and therefore the steady-state current magnitude is much larger than the instantaneous one. It is often usual for the instantaneous current to have slightly larger currents in the negative potential range, but the difference is often small. That said, both

currents share equal percentage of current loss during rundown, in the range of 54% for positive currents and 46% for negative currents (Table 5). The tail currents on the other hand are different from the activation currents, showing little rectification, and having lower percentage of current lost by rundown, 46% for positive currents and 33% for negative currents (Table 5). Even so, only the tail current obtained at negative voltages shows statistical difference from the other two current components, while the tail current obtained at positive voltages is statistically similar to the one obtained for the steady state current, but not with the instantaneous current.

Previous work done in our lab showed that a percentage of the current that remained after rundown was also inhibited by NPPB, and the percentage of inhibition was around 16% for the positive potential currents and 12% for negative potential currents. These experiments were repeated, and the results confirmed the previous observations.

By analyzing the current lost by rundown (I_{RD}), obtained by point-by-point subtracting of the raw data of the initial current (I_{init}) by the current after rundown (I_{final}), it has been possible to confirm that the current lost during this time is also due to anionic transport. Nevertheless, the current lost does have substantial different parameters that differentiate them from the currents that remain after rundown. This has been proposed as evidence for the existence of a different set of anionic channels that mediate this current lost by rundown (Tavares et al., 2011).

Furthermore, unlike in animal cells, where NPPB is a specific and strong inhibitor of Cl^- currents, in plants, this is not the case. In fact, it has been challenging to find a strong inhibitor that works well across different anionic channels or currents in plants, since the known classic anionic inhibitors have only small inhibiting strength, as is the case for NPPB, DPC, DIDS, Niflumic Acid and others. Still, many groups, reported that these inhibitors still have an effect in Cl^- conductance's, extracellular fluxes, intracellular gradients and pollen tube growth and germination (Zonia et al., 2001, 2002; Matveeva et al., 2003; Breygina, Smirnova, et al., 2009; Breygina et al., 2010). It has been proposed that the portion of the remaining current after rundown that is inhibited by NPPB, may be derived from a different channel population than the NPPB-insensitive population. Although, it is also plausible that NPPB may be only affecting the conductance's or properties of these current populations by partially blocking them (Tavares et al., 2011).

To assess if the currents elicited by negative potentials were not leak currents, a linear fit of the negative portion of the currents was applied and then used to correct the I-V curves by subtracting the resulting linear curve from that fit. The resulting I-V curve was not physiologically possible, with currents in the first quadrant that increase with

hyperpolarizing currents, which indicates that the measurements were not leak currents, but actual inward anionic currents as previous described by our group.

Furthermore, both rundown and inhibition current reductions were observed across all potentials tests and current components, which further points to the fact that the anionic channels present in the pollen membrane are able to transport anions across the membrane in both directions (both inward and outwardly).

Rundown of the anionic currents changes the conductance of the channels

By applying a least-mean square fit to the initial or to the last four points of each of the currents components, we can obtain the slope conductance for these curves (Table 6), as described in the Material and Methods. These values denote that the currents measured are strongly outwardly rectifying, as previously stated, specially the steady state current.

Both steady state and instantaneous currents have a statistically significantly reduced slope conductance ratio after rundown, along with their corresponding forward conductance (gF) values. These differences are not observed in the tail current slope conductance ratio, or its respective gF parameter, despite the tail current amplitude reduction shown before during rundown. In terms of forward conductance (gF) only the instantaneous current is statistically different from the other two current components, while the same is true for the backward conductance (gB) of the tail current. When looking at the conductance ratios, all three currents (I_{ss}, I_{inst}, I_{tail}) are statistically different between themselves, either before or after rundown, denoting the intrinsic differences from each of these current measurements.

Table 6 - Slope conductance values and ratio for *Arabidopsis thaliana* wild type currents before and after rundown. I_{init} is the initial current, and I_{final} is the final current before and after rundown for each of the current components (steady state I_{ss}, instantaneous I_i and tail current I_t). gF, gB and gF/gB refer to the forward conductance, backward conductance and their ratio (gF and gB are in nSiemmens). Data is represented as mean ± SE. *, refers to statistical significant differences between comparable items within the same table column, while § refers to statistical differences between comparable items in the initial and final currents ($p < 0.05$).

		I_{init}				I_{final}			
		gF (nS)	gB (nS)	gF/gB	n	gF (nS)	gB (nS)	gF/gB	n
wt	I_{ss}	41.4 ± 4.6 §	5.4 ± 1.2	**19.8 ± 2.2 *§**	(52)	30.0 ± 4.7 §	3.6 ± 0.8	**14.0 ± 1.8 *§**	(53)
	I_i	23.2 ± 2.8 *§	7.5 ± 1.4	**6.3 ± 0.7 *§**	(52)	15.0 ± 2.5 *§	5.5 ± 1.1	**3.8 ± 0.4 *§**	(53)
	I_t	32.5 ± 4.1	23.0 ± 3.2 *	**2.1 ± 0.3 ***	(38)	23.6 ± 4.2	17.0 ± 3.5 *	**2.3 ± 0.6 ***	(31)

If we take a closer look at the I-V curves shown in Figure 3, we can better appreciate the differences between the different currents in the physiological range and closer to the expected reversal potential for Cl^- in the control group (Figure 4). Of particular interest is

the differences between the steady state and instantaneous currents, that although similar do present several interesting differences.

Rundown of the anionic currents causes slight changes to the reversal potentials of the different current components

Perhaps the most important parameter to take notice between steady state currents instantaneous and tail currents is the reversal potential (V_{rev}) of these curves (Table 7). The steady state reversal potential ($V_{rev}[I_{ss}]$), for both the current before and after rundown, are within the expected values for Cl^- in our control conditions (E_{Cl^-} = 0 mV with B1/P1 – with Cl^- being the dominant permeable ion in solutions and in high and symmetrical concentrations). The average $V_{rev}[I_{ss}]$ of $I_{initial}$ is -2.1 ± 0.7 mV and I_{final} is -2.0 ± 1.2 mV. These values however shift substantially from the expected value for both the instantaneous and tail current reversal potential ($V_{rev}[I_{inst}]$ and $V_{rev}[I_{tail}]$), with values for $V_{rev}[I_{inst}]$ in $I_{initial}$ of -15.7 ± 1.6 mV and I_{final} of -23.3 ± 1.8 mV (which are statistically different) and for $V_{rev}[I_{tail}]$ in $I_{initial}$ of 22.7 ± 3.9 mV and I_{final} of 27.6 ± 5.2 mV, which can also be observed in Figure 4, marked by the black arrows for each of the currents mentioned. All V_{rev} values are statistically different between current components in each measurement, but only $V_{rev}[I_{inst}]$ changes significantly during rundown.

Table 7 - Reversal potentials for *Arabidopsis thaliana* wild type currents before and after rundown. I_{ss}, I_i and I_t stand for the steady state, the instantaneous and the tail current respectively. I_{init} is the initial current, and I_{final} is the final current before and after rundown for each of the current components. V_{rev} refers to the reversal potential (mV). Data is represented as mean ± SE. *, refers to statistical significant differences between comparable items within the same table column, while § refers to statistical differences between comparable items in the initial and final currents ($p < 0.05$).

		I_{init}		I_{final}	
		V_{rev} (mV)	n	V_{rev} (mV)	n
wt	I_{SS}	-2.1 ± 0.7 *	(52)	-2.0 ± 1.2 *	(53)
	I_i	-15.7 ± 1.6 *§	(52)	-23.3 ± 1.8 *§	(53)
	I_t	22.7 ± 3.9 *	(38)	27.6 ± 5.2 *	(31)

These values are in line with what has been described previously in our group, where the main focus was on characterizing the steady state currents, whose reversal potential matches perfectly with the expected values for anion currents alone. It is however important to understand the nature of the discrepancies for the instantaneous and tail currents reversal potential.

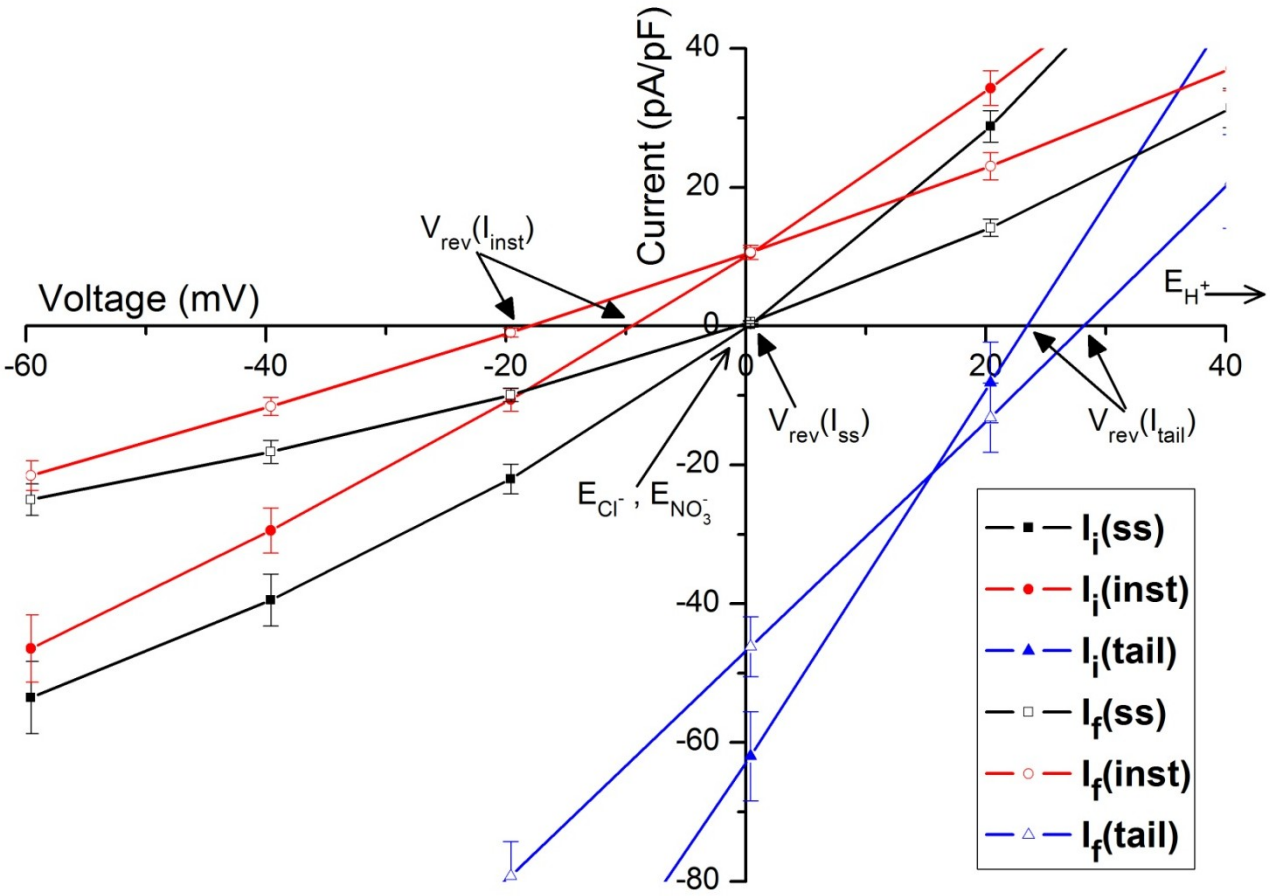

Figure 4 - Detail of I-V curves from Figure 3 in the vicinity of equilibrium potential of Cl^-. Steady state (I_{ss} ■ before rundown, □ after rundown), instantaneous (I_{init} ● before rundown, ○ after rundown) and tail (I_{tail} ▲ before rundown, △ after rundown). Black arrows (➔) point to the reversal potential (V_{rev}) of all currents before and after rundown. Open arrows (➔) mark the position of the calculated equilibrium potential for Cl- (E_{Cl^-} = 0.0 mV), NO_3^- (E_{NO3^-} = 0.0 mV) and H^+ (E_{H^+} = 81.1 mV) for the control condition (P1/B1).

The $V_{rev}(I_{tail})$ shift can be explained by the $[H^+]$, that under control conditions is calculated to be E_{H^+} = 81.11 mV (Table 3), enough to account for the observed shift. Another explanation would be endogenous cationic currents, such as K^+. However this is unlikely, since previous work in our lab has shown no effect on the anionic currents in the presence of TEA, a strong K^+ blocker (Tavares, 2011; Tavares et al., 2011). The only other permeable ions present in solutions, Ca^{2+}, Mg^{2+} and NO_3^- (Table 2), would not account for the observed V_{rev} shifts either since for NO_3^- the equilibrium potential is equal to that of Cl^- (E_{NO3^-} = 0 mV), while for the other two divalent cations, their fluxes should be completely abolished by the presence of Gd^{3+} in solution, a strong bivalent cation inhibitor. Furthermore, in some experimental conditions, shown in later sections of this thesis, the $V_{rev}(I_{inst})$ reaches values past the equilibrium potential for Mg^{2+} of -20.33 mV. However, this shift is consistent and reproducible across experiments, clearly revealing an additional effect on these anionic currents when we look at the transient reversal potential of the

anionic current elicited after a hyperpolarization holding potential. This leaves the $V_{rev}(I_{inst})$ shift unexplained, as none of the permeable ions in solution could account for such a shift.

Chord conductance of the rundown currents reveals different properties for the currents lost during rundown and the current that remains

By converting the anionic currents to their corresponding chord conductances, and plotting the normalized values against membrane potential (Figure 5), as described in the Material and Methods chapter, we can extract further information from the channels behaviors responsible for the anionic currents. The normalized chord conductance can be fitted with a Boltzmann-type equation, describing how the channels conductances respond to different membrane potentials. The slope factors (V_s) and the potential for the half-maximal chord conductance (V_h) that derive from these fits, are shown in Table 8, alongside with the minimal and maximum values of normalized conductance (A1 and A0).

Table 8 – Normalized chord conductance Boltzmann fits parameters for *Arabidopsis thaliana* wild type steady state rundown currents. A1 and A0 are the minimal and maximum values of normalized conductance, V_h is the potential for the half-maximal chord conductance and indicates at which membrane potential the transition between the maximum and minimum states of conductance occurs, V_s is the slope of the G/G_{max} curve and a measure of the sensitivity of the currents to variations in membrane potential. I_{init} is the initial current, and I_{final} is the final current after rundown. I_{RD} is the current obtained by subtraction of the I_{final} from I_{init}, the current lost by rundown. Data is represented as mean ± SE

	I_{SS}	A1 (kS)	A0 (kS)	V_h (mV)	V_s (mV^{-1})
wt	I_{init}	0.13 ± 0.01	1.15 ± 0.03	89 ± 4	62 ± 3
	I_{final}	0.16 ± 0.01	1.23 ± 0.09	114 ± 12	67 ± 7
	I_{RD}	0.15 ± 0.01	1.07 ± 0.01	62 ± 3	63 ± 2

The most striking result from this analysis is that the current lost by rundown (I_{RD}) has a distinct membrane potential sensitivity, which is also why the I_{init} is halfway between the I_{final} and the I_{RD}, since the I_{init} is in essence a composite of these two. This difference is only seen in the V_h parameter, while all the others show no striking difference. Previously it was also shown that the current sensitive to NPPB did not had any significant difference in these parameters compared to the non-NPPB-sensitive current, which amounts to ~90% of the current that remains after rundown (I_{final}) (Tavares et al., 2011).

Taken together, all these results evidence the existence of strong outward rectifying anionic currents in pollen grain protoplast, able to conduct anionic current both inward and outwardly, with three distinctively anion currents based on inhibition and rundown profiles (Tavares et al., 2011). The novelty is the fact that there are subtle discrepancies when it comes to the I_{inst} and I_{tail}, compared to the I_{ss}, that hint the presence of another

ion also contributing to the anionic currents studied. It should be noted that these discrepancies are essentially only observed in transient currents and its effect is camouflaged when the steady state current is measured, within just a few hundred milliseconds.

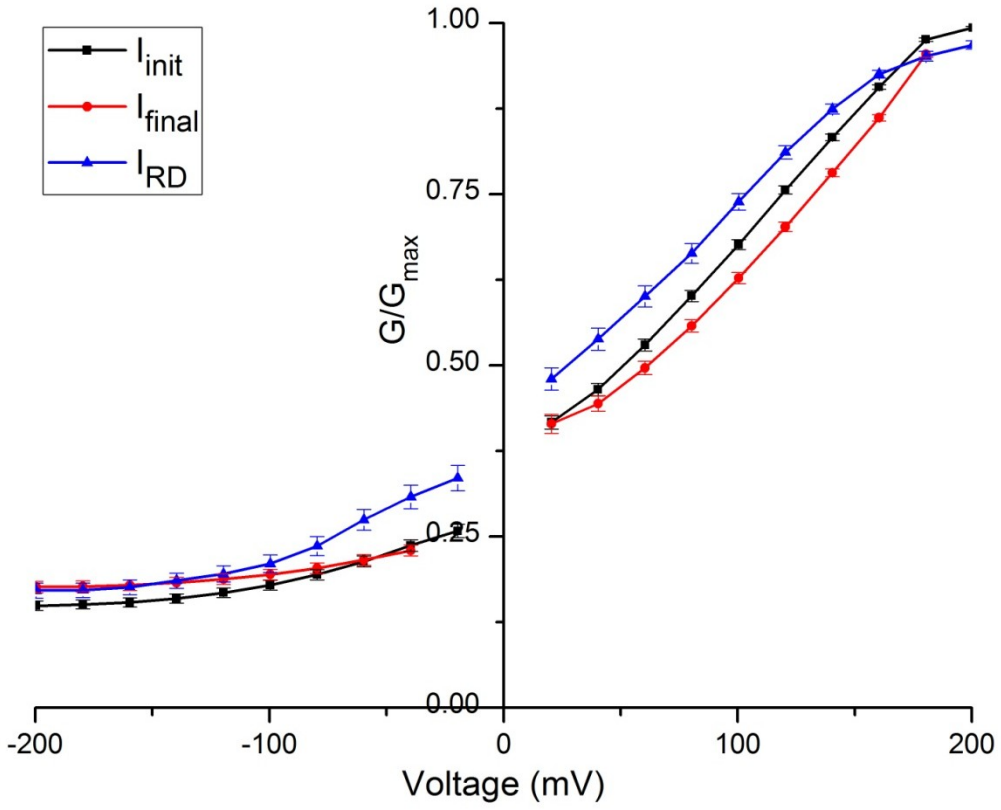

Figure 5 – Normalized average chord conductance curves of *Arabidopsis thaliana* wild type steady state rundown currents. I_{init} is the initial current, and I_{final} is the final current after rundown. I_{RD} is the current obtained by subtraction of the I_{final} from I_{init}, the current lost by rundown.

To address this, we hypothesize that H^+ currents may be the source of the discrepancies observed in the anionic currents. It has been known that H^+ and Cl^- fluxes in growing pollen tubes have an interesting correlation, being always in counter phase. In addition, both are fundamental for proper pollen growth and the importance of H^+ as a novel second messenger has also come to light. Some putative anion channels in plants have been shown to be in fact H^+/A^- exchangers. Along with all this, under the experimental conditions tested, the steep H^+ gradient also provides a reasonable explanation for some of the results observed. As such, H^+ could be a likely candidate to explain these observed differences.

Role of external pH on the anionic currents of *Arabidopsis* pollen

To test this hypothesis, we have manipulated the control solution's pH and buffer to test for different extracellular pHs. The control solution (P1/B1) has a internal alkaline pH (7.2) with a external acidic pH (5.8), and we've tested the effect of several different external pH (5.6, 6,0, 6.4, 6.8, 7.2, respectively solutions B2 to B6 on Table 2) on the anionic currents as described before. All bath solution exchanges were performed after rundown process had been completed and currents amplitude was stable. An example of the activation currents obtained under external alkalinization in wild type background can be seen in Figure 6, with the current after rundown at pH_o 5.8 (panel A), and going to pH_o 6.4, 6.8 and 7.2 (in panels B, C and D respectively). For tail currents, an example from the same cell at pH_o 5.8 and 6.8 is also shown (panels E and F).

Alkaline external pH strongly modulates anionic currents in Arabidopsis pollen

Figure 6 shows the dramatic effect of increasing external pH to the anionic currents in wild type pollen protoplasts, leading to a progressive loss of rectification and an overall increase in current amplitude, particularly at higher pH. In average the increase of the steady states currents at external pH 5.8 to 6.8 is a 4.46 fold change for negative currents (calculated at -160 mV) and a 2.80 fold change for positive currents (calculated at +160 mV); for the instantaneous currents is a 3.69 fold change for the negative currents and 3.20 for the positive currents; for the tail currents is a 1.84 fold change for the negative currents and 2.64 for the positive currents.

These effects of pH are observed in all current components as can be seen more readily in Figure 7 with the I-V curves for all three current components (I_{ss}, I_{inst} and I_{tail} in Panel A, C and E of Figure 7 respectively) across the different external pH tested. These effects of external pH on the currents were reversible. Furthermore, when the bath solution was acidified to 5.6 revealed a similar increase in overall currents as the experiments with alkalinization of the bath solution. This would suggest that the control solution in use is in a plateau of minimal current amplitudes, where deviations from those values lead to large increase in anionic currents activity.

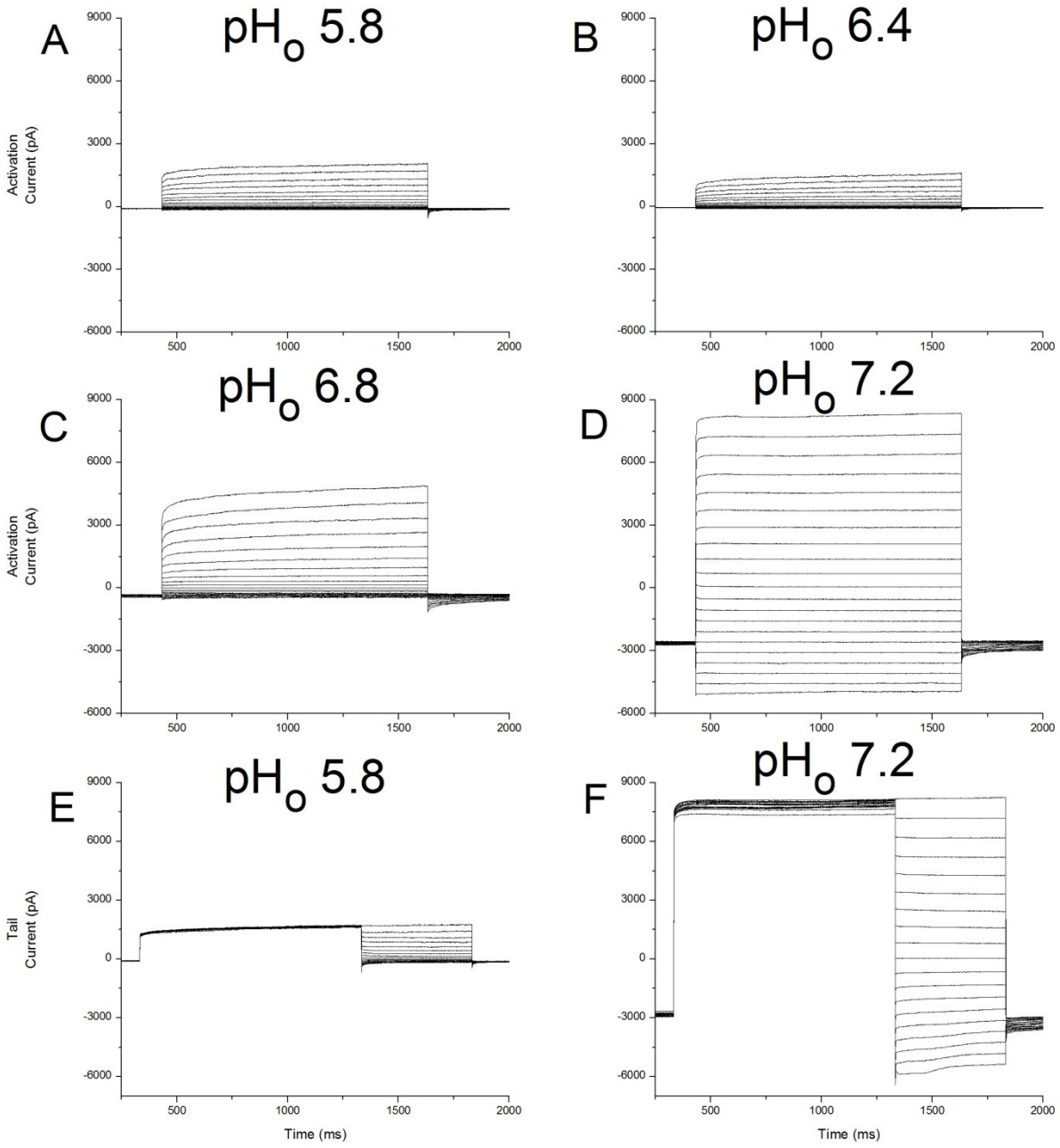

Figure 6 – Typical *Arabidopsis thaliana* wild type activation and tail currents under different external pH conditions. (A) Activation current at control condition after rundown, pH_o 5.8. (B-D) Activation currents after bath exchange to pH_o 6.4, 6.8 and 7.2. (E) Tail current at control condition after rundown, pH_o 5.8. (F) Tail current after bath exchange to pH_o 6.8.

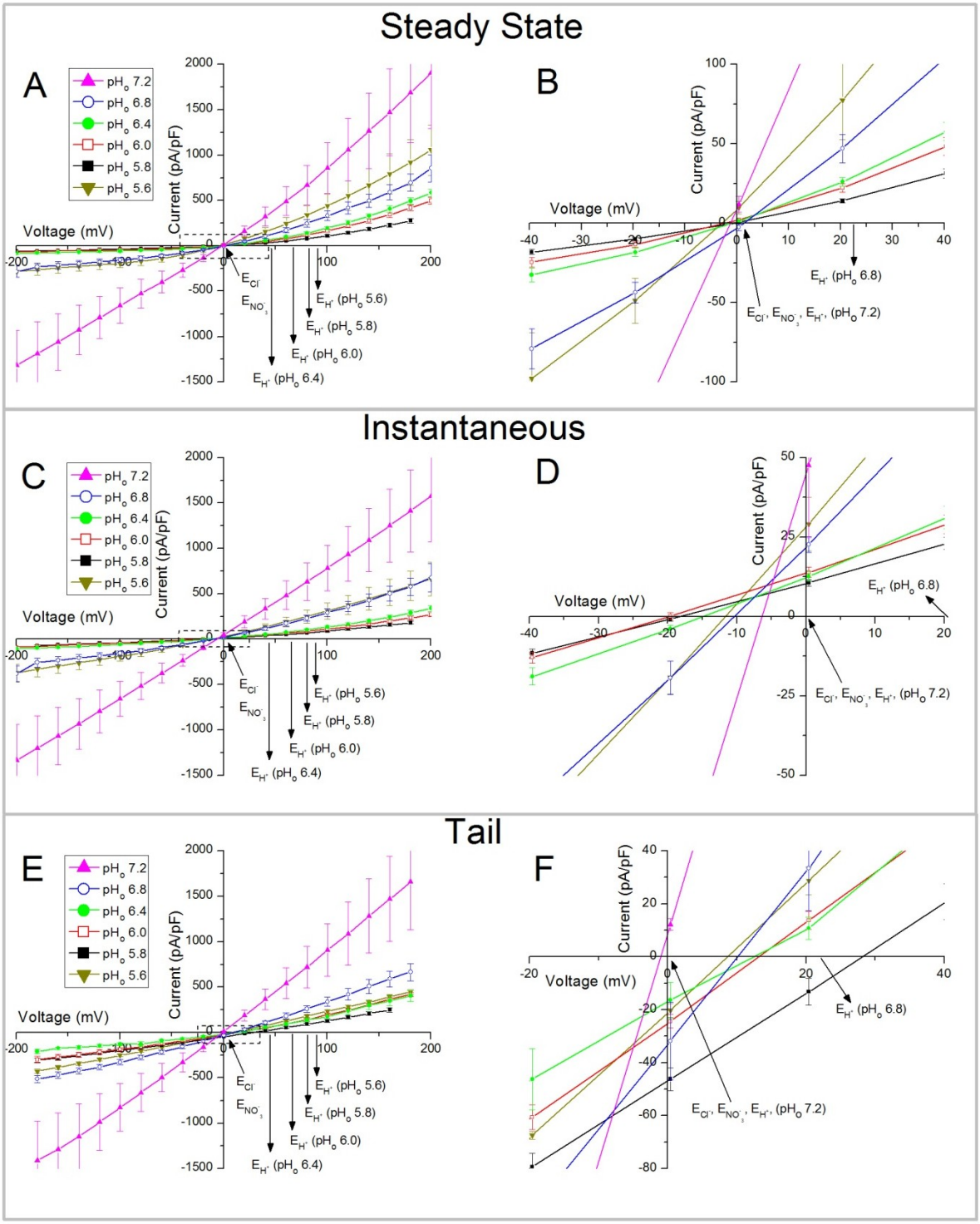

Figure 7 – Current-Potential (I-V) curves for all three current components measured under different extracellular pH conditions. (A) steady state currents, with detail near V_{rev} in panel B. (C) instantaneous currents, with detail near V_{rev} in panel D. (E) tail currents with detail near V_{rev} in panel F. The dotted box in plots A, C and E mark the region shown in detail in plots B, D and F respectively. The black arrows (➔) mark the position for the calculated equilibrium potential for Cl- (E_{Cl}-), NO_3^- (E_{NO3}-) and H^+ (E_H+) for the each different extracellular pH tested.

Interestingly, as the test experiment gets farther away from the control condition pH of 5.8, the more likely it is to experience seal instability, often leading to loosing the seal, particularly at the higher alkalinization points. Given the large amplitude of the currents observed at those conditions, one could assume that maintaining those ion fluxes for a extended period of time would lead to homeostatic imbalance in the protoplast or even membrane integrity, that could eventually lead to disruption of the seal. For that reason, it was also very difficult to test different initial pH conditions, other than the control, since the most interesting external pHs to test the rundown process, also lead to the aforementioned membrane seal instability.

External pH modulates anionic channels conductance in Arabidopsis pollen plasma membrane

Looking at the corresponding effects of external pH to the anionic currents slope conductance's (Table 9) we can appreciate the changes to rectification observed in the raw data and I-V curves before. Comparing the forward and backward conductance ratios at different external pH, the major differences are only observed at the most extreme pH tested, where the rectification is dramatically changed, though the tendency can be observed, even though there is no statistical significance, for pH_o 6.8. This is not visible for the tail currents conductance ratio, since these currents are already only very slightly rectified. But is obvious for both instantaneous and steady state currents, and it's expected to have similar effects under more acidic pH then the ones tested as well. Those conditions would fall farther from the expected physiological conditions and were therefore not tested.

The differences are however more meaningful when looking at the forward and backward conductance's on their own, where statistically different values can be seen as early as pH_o 6.0 for some of those parameters. This demonstrates the strong effect of pH in these channels conductance's, with an increase in currents amplitudes as shown before, for both steady state and instantaneous currents. However, these effects are not so readily seen in the tail currents, except on limited occasions, which again, might suggest that the tails currents are intrinsically different then the other two or that the effects are simply masked by their higher variability.

It is also interesting to notice that the forward conductance (calculated from the currents elicited by positive voltages) seem to be more easily affected by external pH then the backward conductances (calculated from the currents elicited by negative voltages, the physiological region of membrane potential). However, it seems that as the pH change increases, the reaction from the forward conductance falls short to the effect observed for the backward conductances, which increase quite dramatically, thus causing the large loss

of rectification. With the consequence of the conductance ratios at these external pH (6.0 and 6.4) actually increase, dropping only after the backward conductance increases substantially.

Table 9 – Slope conductance values and ratio for *Arabidopsis thaliana* wild type currents under different external pH conditions. Values in bold are the control condition (pH_o 5.8). Current components (steady state I_{ss}, instantaneous I_i and tail current I_t). gF, gB and gF/gB refer to the forward conductance, backward conductance and their ratio (gF and gB are in nSiemmens). Data is represented as mean ± SE. *, refers to statistical significant differences between comparable items within the same table column, while § refers to statistical differences from the control pH values to other tested pH conditions ($p < 0.05$).

			pHo 5.6			pHo 5.8			pHo 6.0		
			g (nS)	gF/gS	n	g (nS)	gF/gS	n	g (nS)	gF/gS	n
wt	I_{SS}	gF	52.1 ± 10.9	11.9 ± 4.5	(4)	**30.0 ± 4.7**	**14.8 ± 1.8 * (59)**		62.6 ± 12.4 *§	20.8 ± 4.4 *	(8)
		gB	8.2 ± 3.6 *			**3.6 ± 0.8**			8.1 ± 3.7		
	I_i	gF	25.9 ± 4.5	2.6 ± 0.7	(4)	**15.0 ± 2.5 ***	**3.8 ± 0.4 * (53)**		30.0 ± 6.2 *§	4.3 ± 0.9	(8)
		gB	12.2 ± 3.0			**5.5 ± 1.1**			11.8 ± 4.0		
	I_t	gF	44.1 ± 11.7	1.4 ± 0.1	(3)	**23.6 ± 4.2**	**2.3 ± 0.5 * (37)**		30.0 ± 14.8	2.6 ± 0.8	(4)
		gB	33.1 ± 9.9 *			**17.0 ± 3.5 ***			21.4 ± 13.2		
			pHo 6.4			**pHo 6.8**			**pHo 7.2**		
			g (nS)	**gF/gS**	**n**	**g (nS)**	**gF/gS**	**n**	**g (nS)**	**gF/gS**	**n**
	I_{SS}	gF	61.5 ± 14.8 §	21.4 ± 5.9 *	(6)	62.2 ± 6.4 *§	9.0 ± 2.4 *	(7)	42.5 ± 8.6	1.5 ± 0.1 §	(2)
		gB	6.1 ± 2.6			9.1 ± 1.8 §			27.6 ± 3.4 §		
	I_i	gF	29.9 ± 6.7	5.9 ± 2.0	(6)	40.9 ± 4.9 *§	4.6 ± 1.3	(7)	32.6 ± 7.0	1.1 ± 0.1 §	(2)
		gB	10.4 ± 3.6			11.7 ± 2.2 §			28.1 ± 3.6 §		
	I_t	gF	29.1 ± 18.9	2.5 ± 0.8	(3)	42.5 ± 6.7 §	1.7 ± 0.3 *	(5)	38.4 ± 8.3	1.3 ± 0.2	(2)
		gB	20.3 ± 16.5			28.5 ± 5.8 *			28.3 ± 2.4 §		

Anionic currents reversal potential is altered by changes in external pH, suggesting the presence of anionic/proton co-transport system

Looking at the reversal potentials of these curves (Figure 8, table 10), we can observe the gradual shift of reversal potentials towards zero with increasing external pH across all three different current components, which are statistically different from the control. While the steady state reversal potential shift is not statistically significant, the trend is consistently observed during experimental acquisition, despite its small magnitude. This is consistent with the hypothesis that the reversal potentials shifts are mediated by protons, as increasing external pH leads to a reduction of the H^+ gradient across the membrane and, therefore, to a equilibrium potential for H^+ closer to zero.

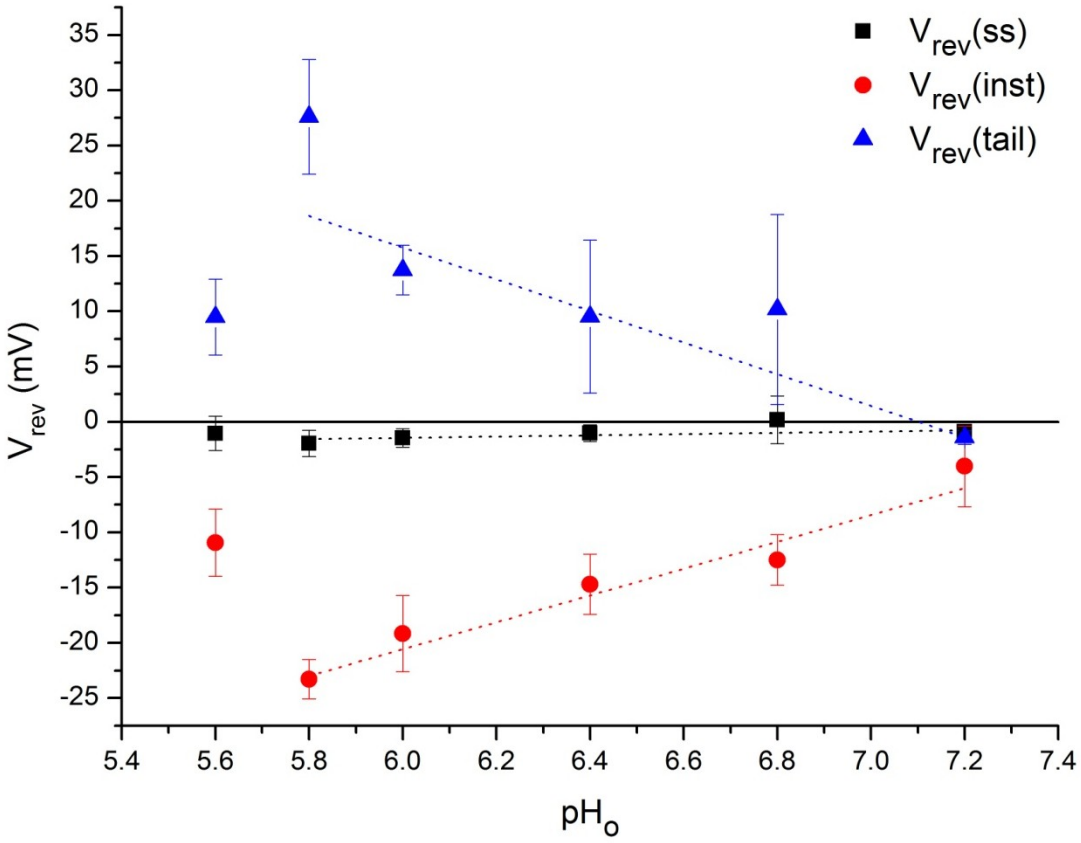

Figure 8 – *Arabidopsis thaliana* reversal potential under different external pH for steady state, instantaneous and tail currents. Current after rundown, control condition is at pH_o 5.8. Dotted lines represent the linear fit to the reversal potential to each according current component. Data points from pH_o 5.6 were not used for the fitting.

This evidence confirms the hypothesis that the shifts originally detected in the anionic currents that deviated from the expected values are in fact due to H^+ transport across the membrane. While this effect is minor when only the steady state currents are taken into account, its effect on the transient anionic currents is quite striking. Surprisingly, the same effect is also observed on the measurements under more acidic external pH, where significant shifts are also observed towards zero, which evokes the idea that our control condition of pH_o 5.8 is incidentally at a pivotal point of pH sensing. It's not unlikely, that at low pH the active channel(s) present in the plasma membrane may change, being activated or de-activated, or even just changing their conformation or behavior as it has been described for other anionic channels before (Matsuda et al., 2010) where the CLC-3 Cl^-/H^+ antiporter is as a bona fide co-transporter at higher extracellular pH, but at lower extracellular pH however, the Cl^- and H^+ transport become uncoupled, such that the CLC-3 then behaves as a Cl^- channel under those conditions, and can effectively behave as either a channel or co-transporter, dependent on external pH alone. This could be a possible explanation for this biphasic behavior observed in the anionic currents.

Table 10 – Reversal potentials for *Arabidopsis thaliana* wild type currents under different external pH. Values in bold are the control condition (pH_o 5.8). I_{ss}, I_i and I_t stand for the steady state, the instantaneous and the tail current respectively. V_{rev} refers to the reversal potential (mV). Data is represented as mean ± SE. *, refers to statistical significant differences between comparable items within the same table column, while § refers to statistical differences between comparable items in the initial and final currents ($p < 0.05$).

		pH_o 5.6		pH_o 5.8		pH_o 6.0		pH_o 6.4		pH_o 6.8		pH_o 7.2	
		V_{rev} (mV)	n	V_{rev} (mV)	n	V_{rev} (mV)	n	V_{rev} (mV)	n	V_{rev} (mV)	n	V_{rev} (mV)	n
wt	I_{SS}	-1.0 ± 1.5	(4)	**-2.0 ± 1.2 * **	**(53)**	-1.5 ± 0.9 *	(8)	-1.0 ± 0.8	(6)	2.4 ± 2.9	(7)	-0.9 ± 0.6	(2)
	I_i	-10.9 ± 3.0 *§	(4)	**-23.3 ± 1.8 * **	**(53)**	-19.2 ± 3.4 *	(8)	-14.7 ± 2.7 *§	(6)	-12.5 ± 2.3 *§	(7)	-4.0 ± 3.6 §	(2)
	I_t	9.5 ± 3.4 §	(3)	**27.6 ± 5.2 * **	**(31)**	13.7 ± 2.2 *§	(4)	9.5 ± 6.9 §	(3)	10.2 ± 8.6 §	(5)	-1.4 ± 0.6 §	(2)

By plotting the reversal potentials versus pH we can better analyze the dependence of these two parameters. A linear curve can be fitted to these data points, if the data point for external pH 5.6 is excluded, which shows a distinct behavior then the rest (Figure 8, dotted lines). For the steady state current there is no meaningful dependency, as this current is mostly dominated by Cl^- (and NO_3^-) and the effect of pH in the steady state reversal potential is negligible. As for the instantaneous and the tail currents reversal potentials, the external pH dependency is quite strong and visible as can be seen in Figure 8 and Table 10. When the H^+ gradient across the membrane is reduced (pH_o increases), the reversal potential moves closer to the expected equilibrium potential for Cl^- (as well as to the new H^+ equilibrium potential) both very close to 0 mV.

This is evidence that these current components are H^+ dependent, identifying H^+ as the other ionic species being transported along with anions in the pollen grain plasma membrane under our experimental conditions. Still, the relevance of this fit is that the slope obtained for these linear relationships falls short of the Nernst slope assuming only one ion was being transported. This can also be observed in Table 10 for the reversal potential values of any current. For example, between 5.8 and 6.8 the measured shift across a decade is less than the Nernst values of 58 mV/dec. This suggests that we may be in the presence of a H^+/A^- co-transport mechanism, which could explain the observed changes in reversal potentials of the anionic currents under different external pHs, as the reversal potential would be determined by both anions and H^+, particularly for the transient currents I_{inst} and I_{tail}.

Anionic channels membrane potential sensitivity is altered by external pH

By analyzing the normalized chord conductance of the steady state anionic currents under different external pH, we also observe the dramatic effect of increasing the pH on the bath medium (Figure 9). Particularly striking is the fact that as the external bath pH moves away from the control values (pH_o 5.8) the sensitivity to membrane voltage changes substantially, rendering the chord conductance curve for pH_o 7.2 almost linear,

indicating very little voltage sensitivity by the currents under these conditions and with the values in between showing this tendency already. Interestingly, as observed before, for more acidic external pH then the control, we mimic the same results as alkalinizing the extracellular medium, as seen for the chord conductance curve for pH_o 5.6 that yields similar results to that of pH_o 6.8.

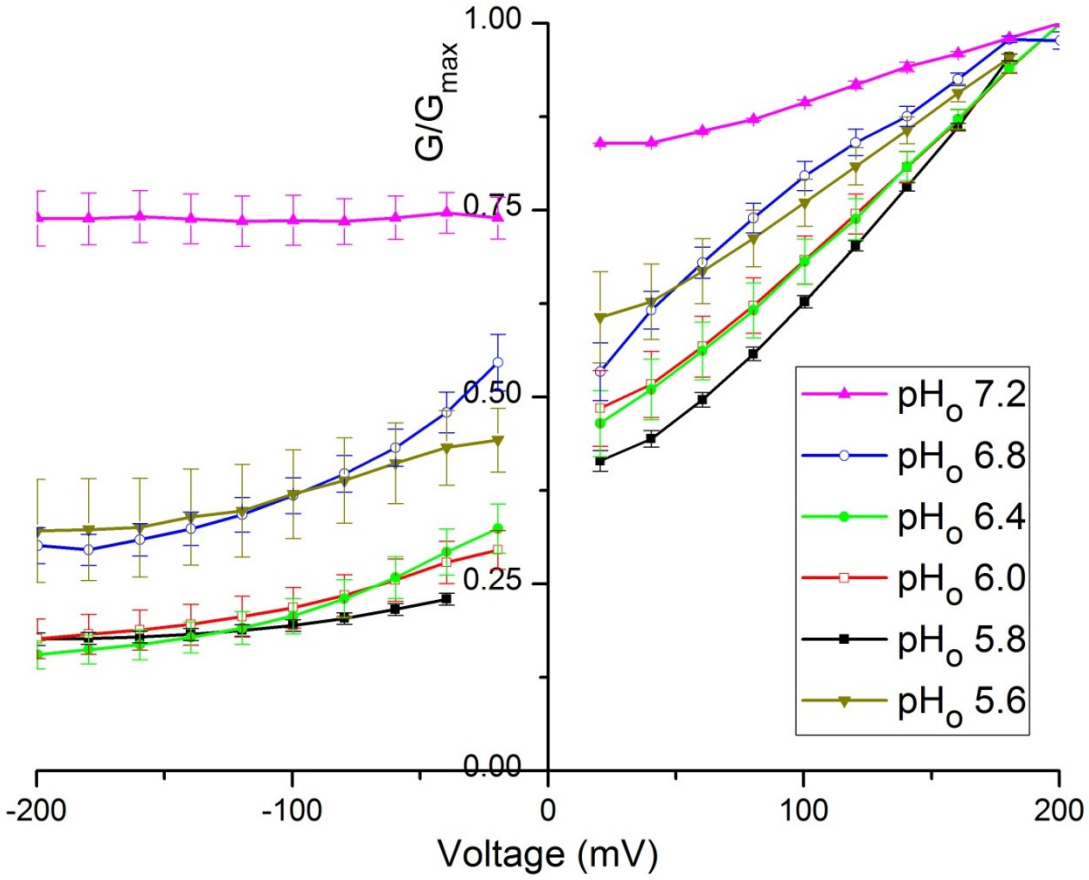

Figure 9 – *Arabidopsis thaliana* normalized average chord conductance for steady state currents under different external pH.

By fitting these curves with a Boltzmann-like equation, we can obtain fit parameters as described before that describes how the channels conductances respond to different membrane potentials under different external pH values (Table 11). We observe strong regulation of the channel's steady state conductance properties dependent on external pH, as we have observed for all current's amplitude, slope conductances, and for the instantaneous and tail currents reversal potential. As external pH increases the V_h parameter decreases, while the opposite is observed for the V_s parameter. These fit with the observed overall currents amplitude increase, particularly due to the increase in negative currents, which correlate well with the V_h shift, and gradual loss of rectification that can be also seen with the increase in the slope of the fit V_s.

Table 11 – Normalized chord conductance Boltzmann fits parameters for *Arabidopsis thaliana* wild type steady state currents under different external pH. A1 and A0 are the minimal and maximum values of normalized conductance, V_h is the potential for the half-maximal chord conductance and indicates at which membrane potential the transition between the maximum and minimum states of conductance occurs, V_s is the slope of the G/G_{max} curve and a measure of the sensitivity of the currents to variations in membrane potential. Values in bold are the control condition (pH_o 5.8). Data is represented as mean ± SE.

		A1 (kS)	A0 (kS)	V_h (mV)	V_s (mV^{-1})
wt I_{ss}	**pH_o 5.6**	0.27 ± 0.02	1.21 ± 0.06	94 ± 9	89 ± 9
	pH_o 5.8	**0.16 ± 0.01**	**1.23 ± 0.09**	**114 ± 12**	**67 ± 7**
	pH_o 6.0	0.15 ± 0.01	1.19 ± 0.06	105 ± 7	77 ± 6
	pH_o 6.4	0.12 ± 0.01	1.30 ± 0.05	108 ± 8	86 ± 5
	pH_o 6.8	0.25 ± 0.03	1.19 ± 0.06	74 ± 11	90 ± 12
	pH_o 7.2	0.73 ± 0.01	1.09 ± 0.03	68 ± 12	108 ± 10

Taken together, all this data reveals that the pollen grain protoplast anionic currents are indeed strongly regulated by external pH, displaying a wide and complex array of responses and pH modulation, along with the possibility of having at least one co-transporter activity linked to H^+ and anions. By bringing H^+ in to the mix, we have gained further knowledge in to the behavior and nature of the anionic transporters present in the plasma membrane of pollen, better understanding the previously observed discrepancies that could have not been explained by anions alone.

Anionic currents of *cacc* mutant line in pollen

The homozygotic knock-out mutant line GK-238B02 plants, with a T-DNA insertion on the At1g73030 gene encoding for a TMEM16A homologue, a Ca^{2+}-activated Chloride Channel (CaCC) in mammalian cells, was characterized by means of patch clamp experiments under the same conditions as described for wild type plants of *Arabidopsis thaliana* (ecotype Columbia). These KO plants did not show any observable macroscopic phenotype and pollen grains and tubes behavior *in vitro* had no apparent observable phenotype either. Nonetheless, the TMEM16A (Anoctamin1) electrophysiological profile in mammals has very intriguing similarities with the currents we have detected under our experimental conditions. Since some of the expected candidates for plasma membrane anion channels in pollen failed to localize to the plasma membrane or do not show any significant electrophysiological phenotype, like for instance the highly expressed in pollen CLC-c gene, this CaCC gene was selected to be investigated in further detail as a candidate for identifying a gene responsible for the anionic currents in pollen.

Under control conditions (P1/B1, Table 2), as described for the wild type experiments, stable seals where regularly obtained in whole cell configuration. By applying the activation and tail voltage protocols (Figure 1), we elicited comparable currents to those obtained with the wild type for the *cacc* mutant line (Figure 10).

Arabidopsis cacc mutant line also evidences strong outward rectifying anionic currents, but with longer rundown time

The *cacc* KO anionic whole cell currents also shows a strong outward rectification, conducting current in both directions, including in the physiological range for plasma membrane potential. As in wild type activation currents, the *cacc* line also evidences a composite activation current – with an instantaneous and a time-dependent activation component. Furthermore, this time-dependent activation is also composed of a fast and a slow time dependent activation, as in wild type, and with similar time constants in the order of <60 ms for the fast one and >350 ms for the slow one.

The mutant line, much like the wild type, also exhibits rundown of the currents in all its current components, however several differences distinguish the behavior between them. The first difference is easily noticeable during the course of the experiment, and pertains to the time it takes for currents to stabilize in the mutant line, compared to the wild type. In the *cacc* mutant background the rundown process takes in average 134 ± 12 min (n = 17), which makes it 66% longer then the wild type rundown. While in wild type, some

protoplasts exhibited a rather fast rundown process (~30 min), the shortest ever measured in the mutant line was just over 60 min, being normally longer than 110 min and sometimes reaching lengths of nearly 300 min. It is therefore assumed that CaCC is involved in the rundown process, as its absence leads to longer periods before current is stable, and therefore, it's safe to assume, that whatever molecule/signal is being depleted and causing rundown of the currents it also modulates CaCC activity and that CaCC accelerates the rate of decay of this effector.

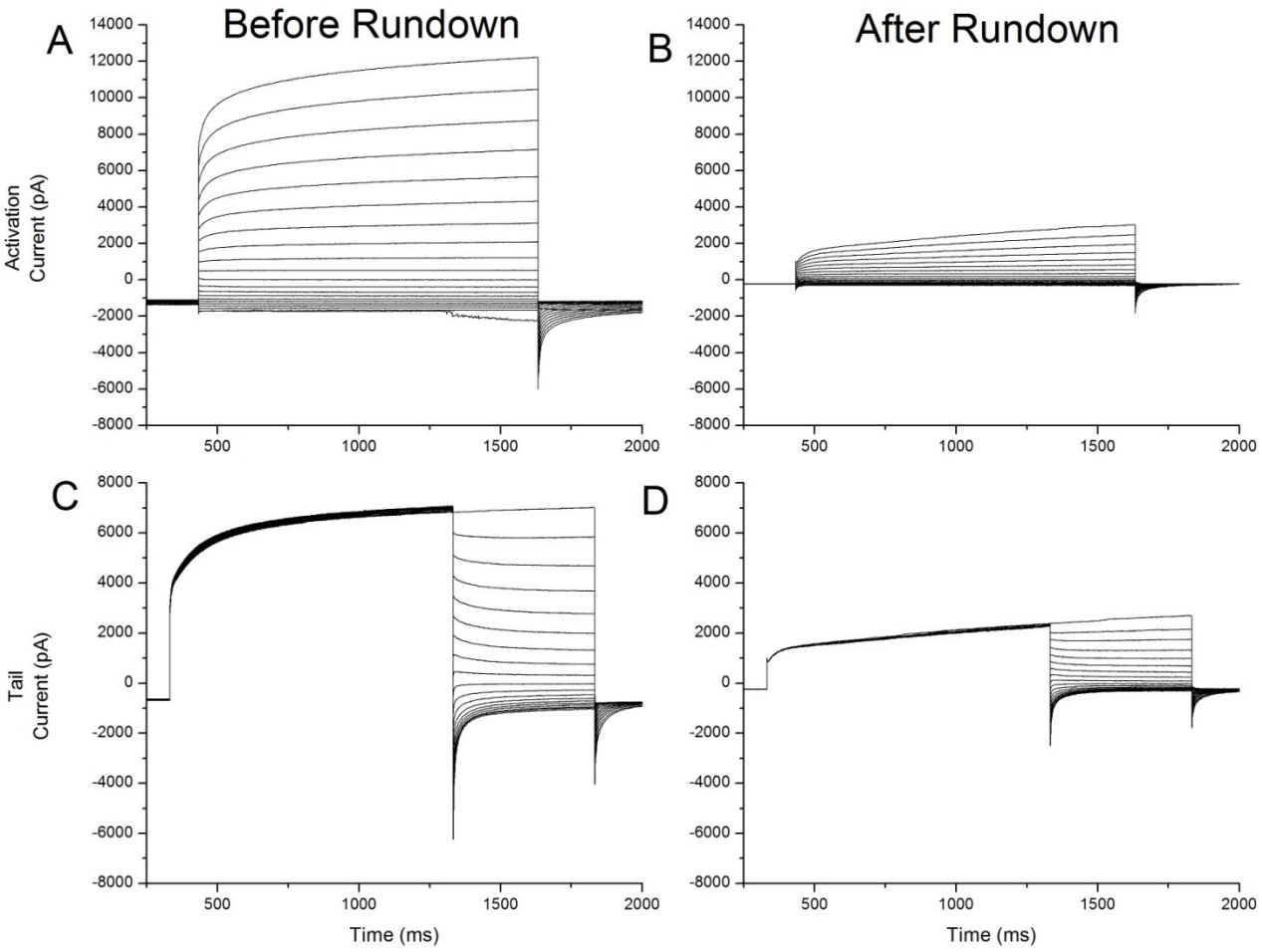

Figure 10 – Typical *Arabidopsis thaliana cacc* KO mutant activation and tail currents, before and after rundown under control condition. (A-B) Activation currents, denoting a strong outward rectification and a time dependent activation. Activation current undergoes rundown, as seen from panel A to B, with an overall current reduction. (C-D) Tail currents, denoting a peak current after depolarization. Tail current also undergoes rundown, as seen from panel C to D, with an overall current reduction.

Following the same procedure for plotting the I-V curves, for the instantaneous, steady state and tail currents before and after rundown, as previously described, we can better quantify the differences between the mutant and wild type (Figure 11, Table 12).

cacc mutant has increased anionic current amplitudes, but similar percentual loss of current with wild type

Of notice is the fact that all currents in the mutant are larger than in the wild type (Figure 12), with the current amplitudes for steady state and instantaneous currents being statistically different, while the tail currents have no significance difference. Still, they are still slightly larger in average then the ones in wild type. Looking at the percentages of rundown, they are also larger in the mutant for all currents components elicited at either positive or negative potentials. However, there is no statistically significance between mutant and wild type rundown percentages. So, while the currents are significatively larger, the percentual loss of current is maintained in the mutant, suggesting that a similar population of channels is still undergoing the same process of rundown, only with increased currents.

The percentage of current lost by rundown is mostly constant across current all membrane potentials and the small differences observed between the rundown from positive potentials and negative potentials are decreased compared to wild type. The tail currents have significantly different rundown percentages when compared with the other current components, as was observed for the wild type currents.

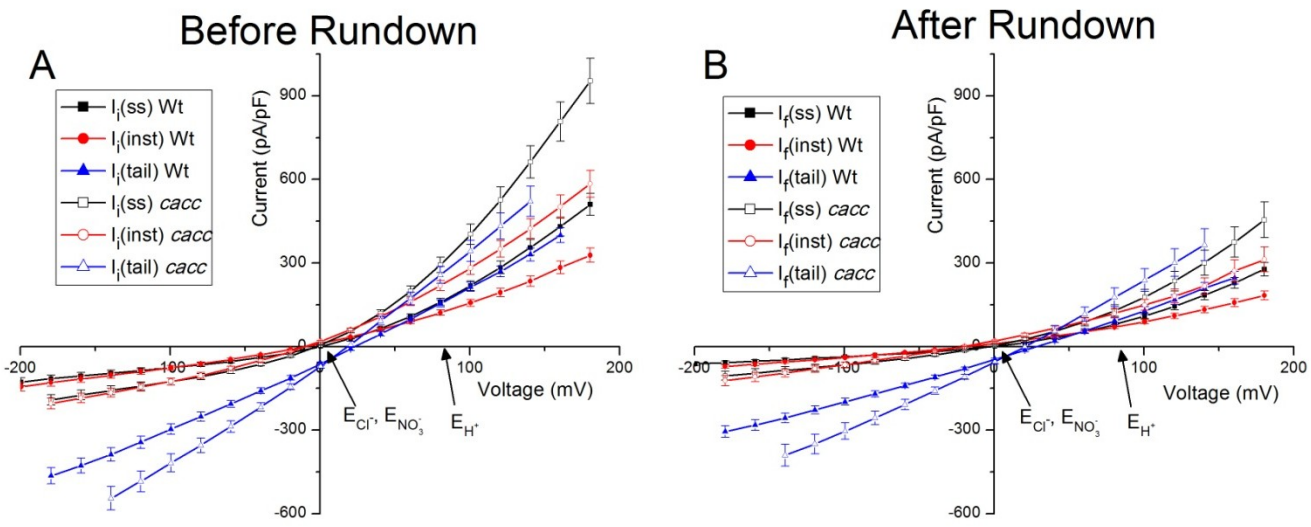

Figure 11 - Current-Potential (I-V) curves for all three current components measured (Steady state I_{ss}, Instantaneous I_{init}, Tail I_{tail}) for the initial currents before rundown (A) and the final currents after rundown (B) in *Arabidopsis thaliana* wild type (filled shapes, ■, ●, ▲) and *cacc* (open shapes, □, ○, △) mutant protoplasts. The black arrow (➔) marks the position for the calculated equilibrium potential for Cl- (E_{Cl^-} = 0.0 mV), NO_3^- (E_{NO3^-} = 0.0 mV) and H^+ (E_{H^+} = 81.1 mV) for the control condition (P1/B1).

These results, along with the fact that rundown times are substantially increased in the mutant came together pointing out to the fact that the CaCC gene may be competing for the same effector that is responsible for the rundown of the currents, without undergoing

rundown itself (or it's effect to the overall rundown current are small at the very least). Even so, the average currents after rundown in the mutant are still significantly larger than in the wild type, which in turns suggests that the absence of the CaCC provides overall larger currents, which can fit the hypothesis that the CaCC could be an transporter carrying anions against their gradient. In other words, its absence would lead to an increase in currents.

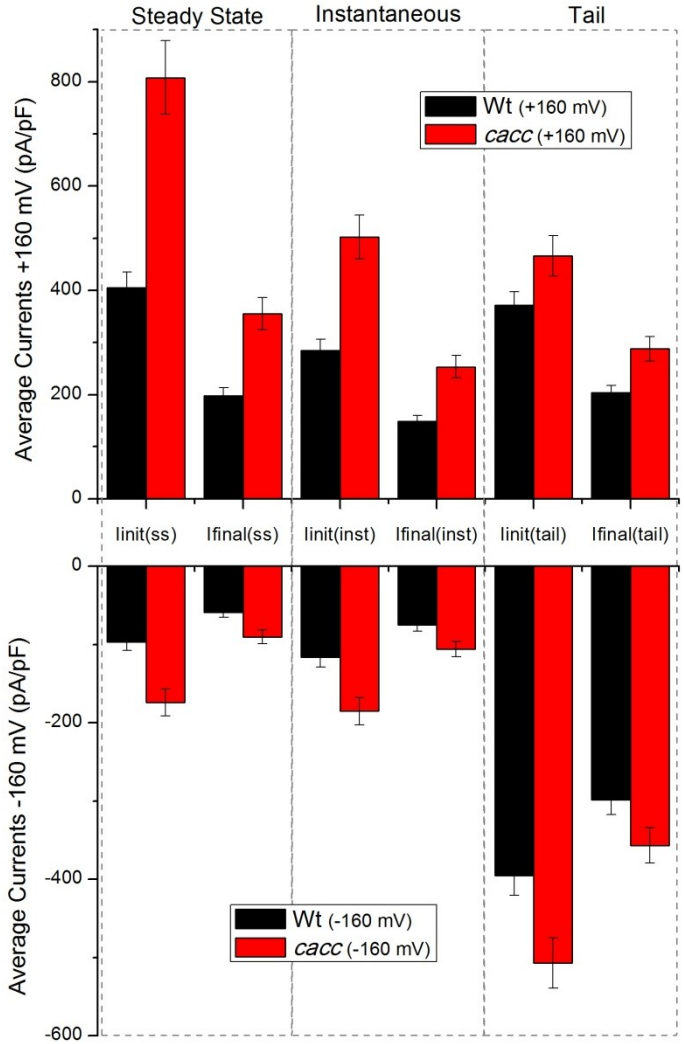

Figure 12 – *Arabidopsis thaliana* wild type and *cacc* mutant average current amplitude for the currents before and after rundown (I_{init} and I_{final}) at ±160 mV for all three current components.

Table 12 - *Arabidopsis thaliana* wild type and *cacc* mutant average normalized Initial currents and percentage of current lost by rundown. I_{init} is the initial current density (pA/pF) measured at ±160 mV before rundown for each of the current components (steady state I_{ss}, instantaneous I_i and tail current I_t). RD% refers to the percentage of current lost during rundown, measured at ±160 mV. Data is represented as mean ± SE. *, refers to statistical significant differences between comparable items within the same table column, while ¥ refers to statistical significant differences between wild type and *cacc* mutant ($p < 0.05$)

		V_m (mV)	I_{init} (pA/pF)	n	RD %	n
wt	I_{ss}	+160	365 ± 51	(53)	55 ± 3	(53)
		-160	-78 ± 11		48 ± 3	
	I_i	+160	258 ± 38 *	(53)	53 ± 3	(53)
		-160	-89 ± 13		44 ± 3	
	I_t	+160	400 ± 55	(38)	46 ± 5	(31)
		-160	-406 ± 50 *		33 ± 4 *	
cacc	I_{ss}	+160	542 ± 69 ¥	(24)	58 ± 5	(24)
		-160	-145 ± 30 ¥		56 ± 5	
	I_i	+160	502 ± 84 ¥	(24)	57 ± 3	(24)
		-160	-130 ± 19 ¥		54 ± 5	
	I_t	+160	417 ± 64	(21)	48 ± 6	(20)
		-160	-462 ± 48 *		37 ± 4 *	

Slope conductances are not significatively altered in the mutant, neither are the reversal potentials during rundown

When looking at the slope conductances in the mutant line, obtained as described previously for wild type, it is also observed that these currents are strongly outwardly rectified, specially the steady-state current, which actually gets even more outwardly rectified after rundown, which does not occur in wild type (Table 13). Again, the tail current slope conductance ratio remains essentially the same, although less rectified then the wild type.

Within the slope conductances for the different current components of the *cacc* mutant line there are some minor differences in significance, compared with the wild type pattern. This is the case for the forward conductance in the initial current, where in the wild type the instantaneous gF is statistically different from the other two, but in the mutant, only the steady state gF is statistically different. Still, the major result is that in terms of slope conductances, there is no statistically difference between the wild type and the mutant slope conductance of the anionic currents. Both exhibit the usual changes in slope conductance and current rectification during rundown, with just minor non-significant differences between them.

Table 13 - Slope conductance values and ratio for *Arabidopsis thaliana* wild type and *cacc* mutant currents before and after rundown. I_{init} is the initial current, and I_{final} is the final current before and after rundown for each of the current components (steady state I_{ss}, instantaneous I_i and tail current I_t). gF, gB and gF/gB refer to the forward conductance, backward conductance and their ratio (gF and gB are in nSiemmens). Data is represented as mean ± SE. *, refers to statistical significant differences between comparable items within the same table column, while § refers to statistical differences between comparable items in the initial and final currents ($p < 0.05$). There is no statistical difference in comparable elements between wild type and *cacc* mutant.

		I_{init}				I_{final}			
		gF (nS)	gB (nS)	gF/gB	n	gF (nS)	gB (nS)	gF/gB	n
wt	I_{SS}	41.4 ± 4.6 §	5.4 ± 1.2	**19.8 ± 2.0** *§	(53)	30.0 ± 4.7 §	3.6 ± 0.8	**14.8 ± 1.8** *§	(53)
	I_i	23.2 ± 2.8 *§	7.5 ± 1.4	**6.3 ± 0.7** *§	(53)	15.0 ± 2.5 *§	5.5 ± 1.1	**3.8 ± 0.4** *§	(53)
	I_t	32.5 ± 4.1	23.0 ± 3.2 *	**2.1 ± 0.3** *	(38)	23.6 ± 4.2	17.0 ± 3.5 *	**2.3 ± 0.5** *	(31)
cacc	I_{SS}	54.9 ± 7.6 *§	8.7 ± 2.5	**16.2 ± 2.7** *	(24)	28.4 ± 5.5 §	4.4 ± 1.4	**25.7 ± 7.6** *	(24)
	I_i	31.9 ± 5.0 §	9.8 ± 2.6	**6.0 ± 1.1** *§	(24)	16.9 ± 4.2 §	6.2 ± 1.6	**4.7 ± 1.5** *§	(24)
	I_t	34.7 ± 5.3	22.6 ± 3.5 *	**1.7 ± 0.1** *	(21)	25.9 ± 5.0	17.1 ± 3.1 *	**1.7 ± 0.3** *	(20)

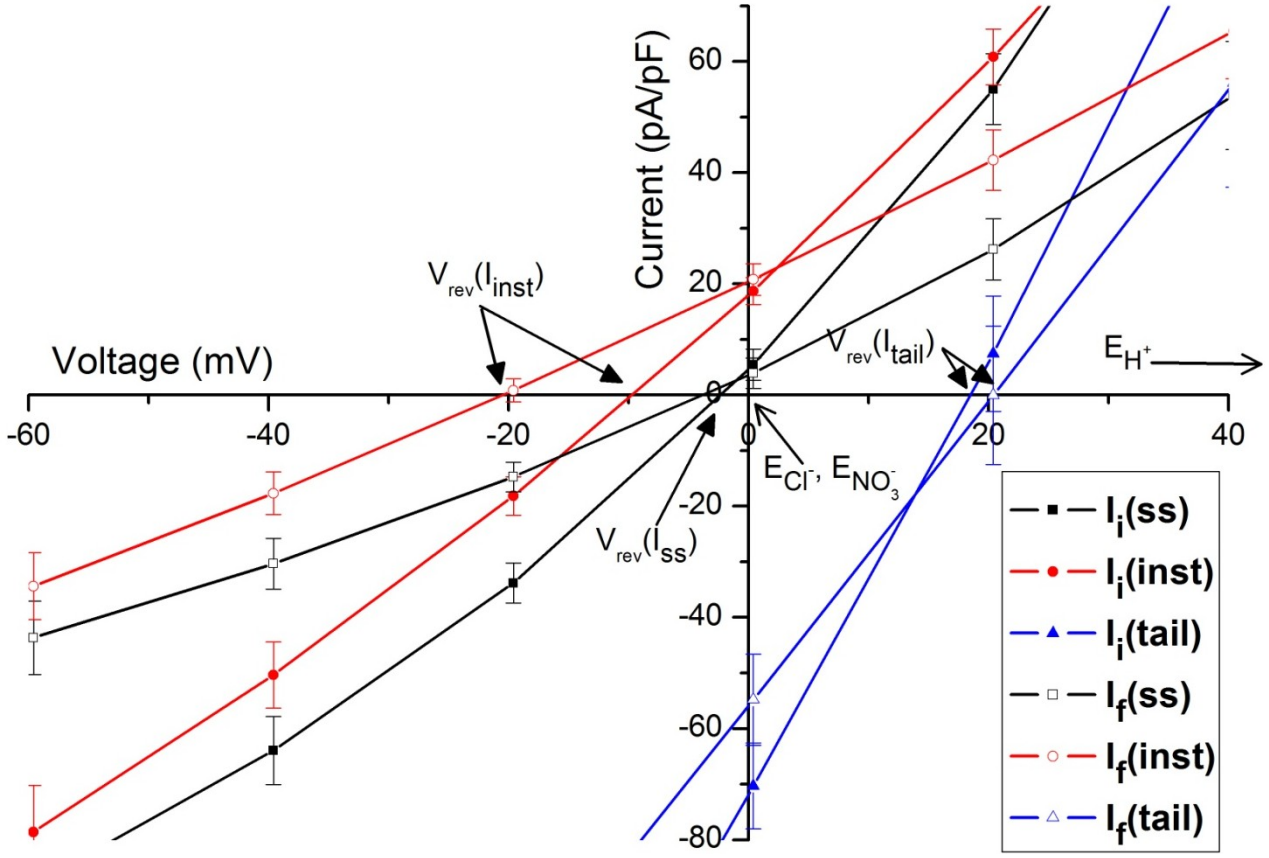

Figure 13 - Detail of I-V curves from the *cacc* KO mutant from Figure 11 in the vicinity of equilibrium potential of Cl^-. Steady state (I_{ss} ■ before rundown, □ after rundown), instantaneous (I_{init} ● before rundown, ○ after rundown) and tail (I_{tail} ▲ before rundown, △ after rundown). Black arrows (➔) point to the reversal potential (V_{rev}) of all currents before and after rundown. Open arrows (➔) mark the position of the calculated equilibrium potential for Cl- (E_{Cl^-} = 0.0 mV), NO_3^- (E_{NO3^-} = 0.0 mV) and H^+ (E_{H^+} = 81.1 mV) for the control condition (P1/B1).

Looking closer to the I-V curves from Figure 11, the differences between currents can be better observed in the region closer to the expected reversal potential (Figure 13). Again, the difference between steady state, instantaneous and tail current reversal potential is seen, with apparent shifts to those obtained from wild type during rundown. Looking closely at the reversal potentials for all these curves (Table 14), we again find that the steady-state reversal potentials falls within the expected values for the equilibrium potential of Cl^-, while the values for the reversal potential of the instantaneous current again shift towards the negative, and the reversal potential of the tail current towards the positive. None of the values is statistically significant between wild type and mutant, but both are statistically different between themselves, and of interest is the statistical difference between the reversal potential of the instantaneous current during rundown that also persists in the mutant. These results do not reveal any particular effect of the mutation in the anionic currents reversal potentials during rundown.

Table 14 - Reversal potentials for *Arabidopsis thaliana* wild type and *cacc* mutant currents before and after rundown. I_{ss}, I_i and I_t stand for the steady state, the instantaneous and the tail current respectively. I_{init} is the initial current, and I_{final} is the final current before and after rundown for each of the current components. V_{rev} refers to the reversal potential (mV). Data is represented as mean ± SE. *, refers to statistical significant differences between comparable items within the same table column, while § refers to statistical differences between comparable items in the initial and final currents ($p < 0.05$).

		I_{init}		I_{final}	
		V_{rev} (mV)	n	V_{rev} (mV)	n
wt	I_{SS}	-2.1 ± 0.7 *	(52)	-2.0 ± 1.2 *	(53)
	I_i	-15.7 ± 1.6 *§	(52)	-23.3 ± 1.8 *§	(53)
	I_t	22.7 ± 3.9 *	(38)	27.6 ± 5.2 *	(31)
cacc	I_{SS}	-0.6 ± 1.3 *	(24)	0.2 ± 2.8 *	(24)
	I_i	-12.6 ± 2.0 *§	(24)	-25.8 ± 3.5 *§	(24)
	I_t	25.6 ± 6.0 *	(21)	35.4 ± 9.2 *	(20)

Current after rundown in the mutant has a slightly different sensitivity to membrane potential then in wild type

Finally, by plotting the normalized chord conductance for the *cacc* KO mutant currents (Figure 14), as done before for the wild type currents, we can observe a similar behavior as in the wild type, where the current lost by rundown differentiates from the current after rundown. By fitting these curves with a Boltzmann like equation, we can extract further information (Table 15). The most striking result is that V_h for the current after rundown in the mutant is substantially increased compared to wild type, while on the other hand the current lost by rundown in the mutant seems to have a slightly less

stepper value for V_s. Even so, both wild type and mutant show the same effects on these currents in terms of their overall chord conductance, with an increase in V_h for I_{final}.

Table 15 – Normalized chord conductance Boltzmann fits parameters for *Arabidopsis thaliana* wild type and *cacc* mutant steady state rundown currents. A1 and A0 are the minimal and maximum values of normalized conductance, V_h is the potential for the half-maximal chord conductance and indicates at which membrane potential the transition between the maximum and minimum states of conductance occurs, V_s is the slope of the G/G_{max} curve and a measure of the sensitivity of the currents to variations in membrane potential. I_{init} is the initial current, and I_{final} is the final current after rundown. I_{RD} is the current obtained by subtraction of the I_{final} from I_{init}, the current lost by rundown. Data is represented as mean ± SE.

	I_{SS}	A1 (kS)	A0 (kS)	V_h (mV)	V_s (mV^{-1})
wt	I_{init}	0.13 ± 0.01	1.15 ± 0.03	89 ± 4	62 ± 3
	I_{final}	0.16 ± 0.01	1.23 ± 0.09	114 ± 12	67 ± 7
	I_{RD}	0.15 ± 0.01	1.07 ± 0.01	62 ± 3	63 ± 2
cacc	I_{init}	0.22 ± 0.01	1.10 ± 0.04	88 ± 6	61 ± 4
	I_{final}	0.29 ± 0.01	1.37 ± 0.08	158 ± 10	71 ± 5
	I_{RD}	0.24 ± 0.01	0.97 ± 0.02	57 ± 4	50 ± 4

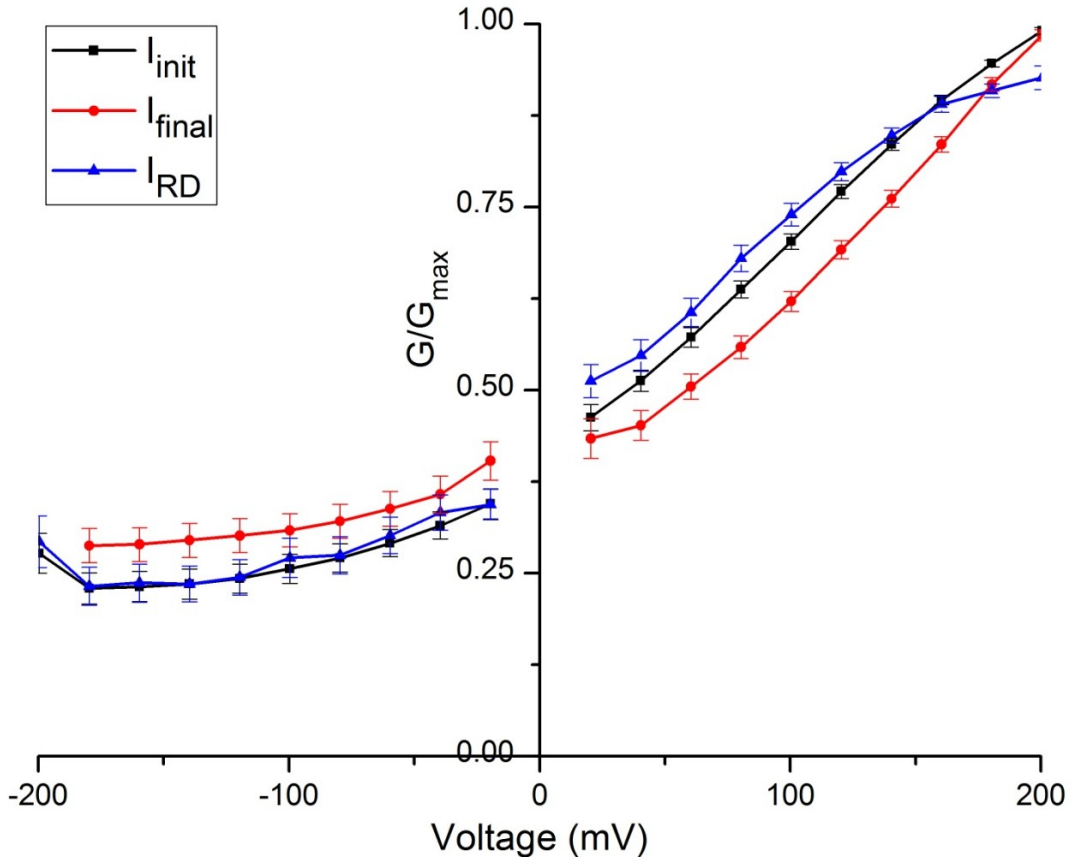

Figure 14 - Normalized average chord conductance curves of *Arabidopsis thaliana cacc* KO mutant steady state rundown currents. I_{init} is the initial current and I_{final} is the final current after rundown. I_{RD} is the current obtained by subtraction of the I_{final} from I_{init}, the current lost by rundown.

All in all, these results for the *cacc* mutant show an overall significant effect on the anionic currents on pollen protoplasts. These differences are mostly restricted to the amplitude of the anionic currents and the length of rundown, with most all other electrophysiological parameters measured showing no significant difference between their wild type counterparts. This may account for the lack of observable macroscopic phenotypes in this mutant, since the overall increase in current may not be sufficient to warrant any fitness disadvantage to the pollen tube growth alone. Next, we address the response of this mutant under different external pH conditions.

Role of external pH in *cacc* mutant anionic currents

Using the same experimental protocol as was used for the study of the wild type anionic currents under different external pHs, the anionic currents of the *cacc* mutant background were analyzed under the same conditions. Starting from the control condition and after rundown was completed (P1/B1, Table 2) with an bath pH of 5.8, we tested different solutions with different external pHs (B2 to B6, Table 2).

An example of the anionic currents in the mutant under different external pH can be seen in Figure 15, with the activation currents after rundown at pH_o 5.8 (panel A), and going through pH_o 6.4, 6.8 and 7.2 (panels B, C and D respectively). For the tails currents an example is shown at control pH_o 5.8 and another at pH_o 6.8 (panel E and F).

Anionic currents in the cacc mutant are insensitive to external pH changes

While there are some changes to the overall currents, the major difference compared to wild type is the absence of the overall increase in anionic currents under more alkaline bath pH and subsequent progressive loss of rectification at higher pH.

For a better look at the differences of the different currents components under these conditions the I-V curves for all three currents components are plotted in Figure 16 (with the steady state currents in panel A, the instantaneous in panel C and the tail currents in panel E). Again, no loss of overall rectification is seen and all currents seem to cluster around the current after rundown (pH_o 5.8). In fact the currents measured at external pH of 6.0 and 6.4 tend to be smaller than the control currents, while all other currents are slightly larger, but never with such a dramatic increase as in wild type.

In average the changes in current amplitude for the steady state currents is a 1.53 fold change for positive currents and 0.99 for negative currents (calculated at ± 160 mV), between currents from pH_o 5.8 to 6.8; for the instantaneous currents is a 1.10 fold change

for positive currents and 1.16 for negative currents; for the tail currents is a 1.30 fold change for positive currents and 1.52 for the negative currents. Again, denoting a clear drop in current amplitude when compared to the fold-change values obtained in similar conditions in wild type protoplasts.

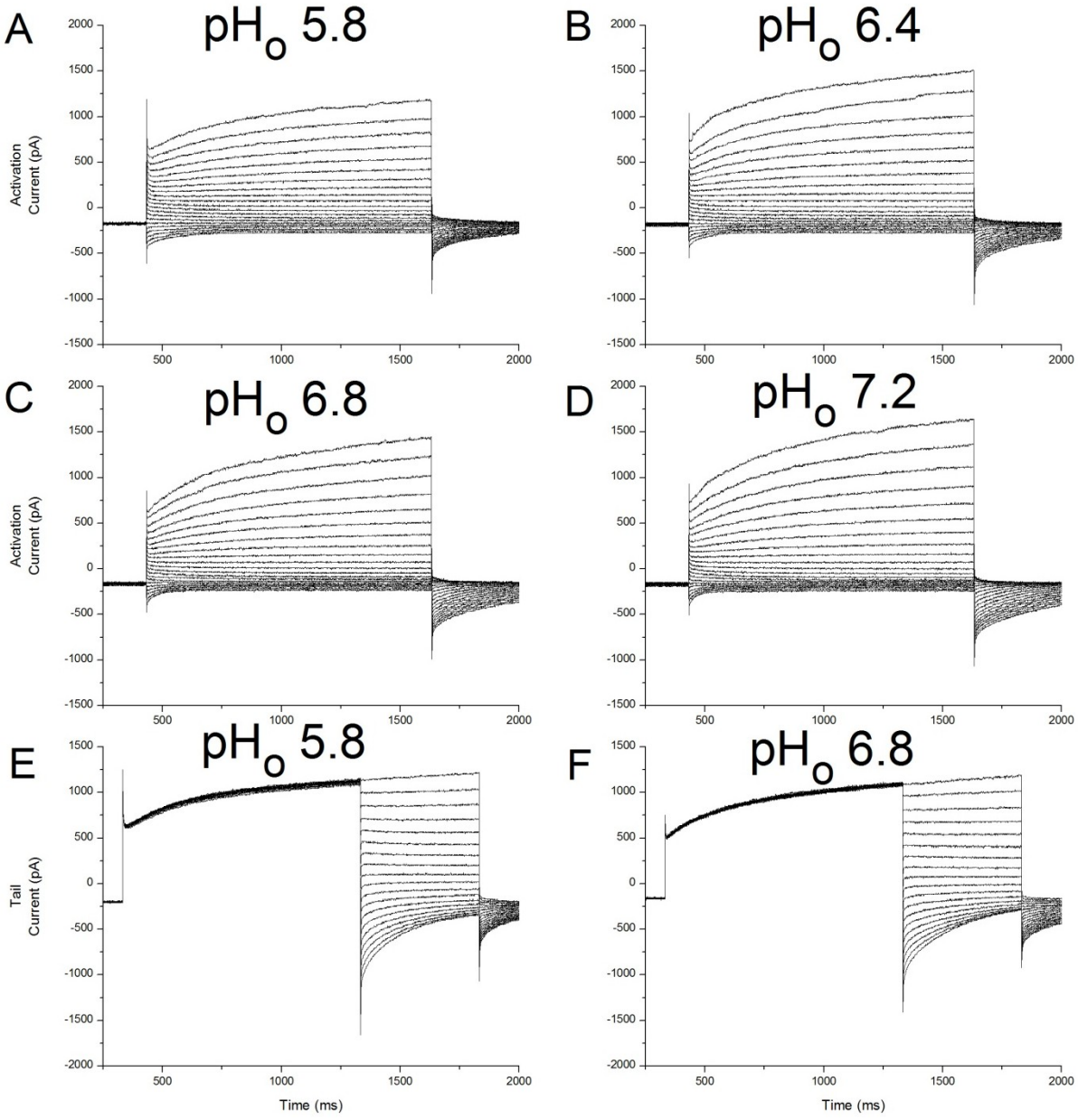

Figure 15 – Typical *Arabidopsis thaliana cacc* KO mutant activation and tail currents under different external pH conditions. (A) activation current at control condition after rundown, pH_o 5.8. (B-D) Activation currents after bath exchange to pH_o 6.4, 6.8 and 7.2. (E) Tail current at control condition after rundown, pH_o 5.8. (F) Tail current after bath exchange to pH_o 6.8.

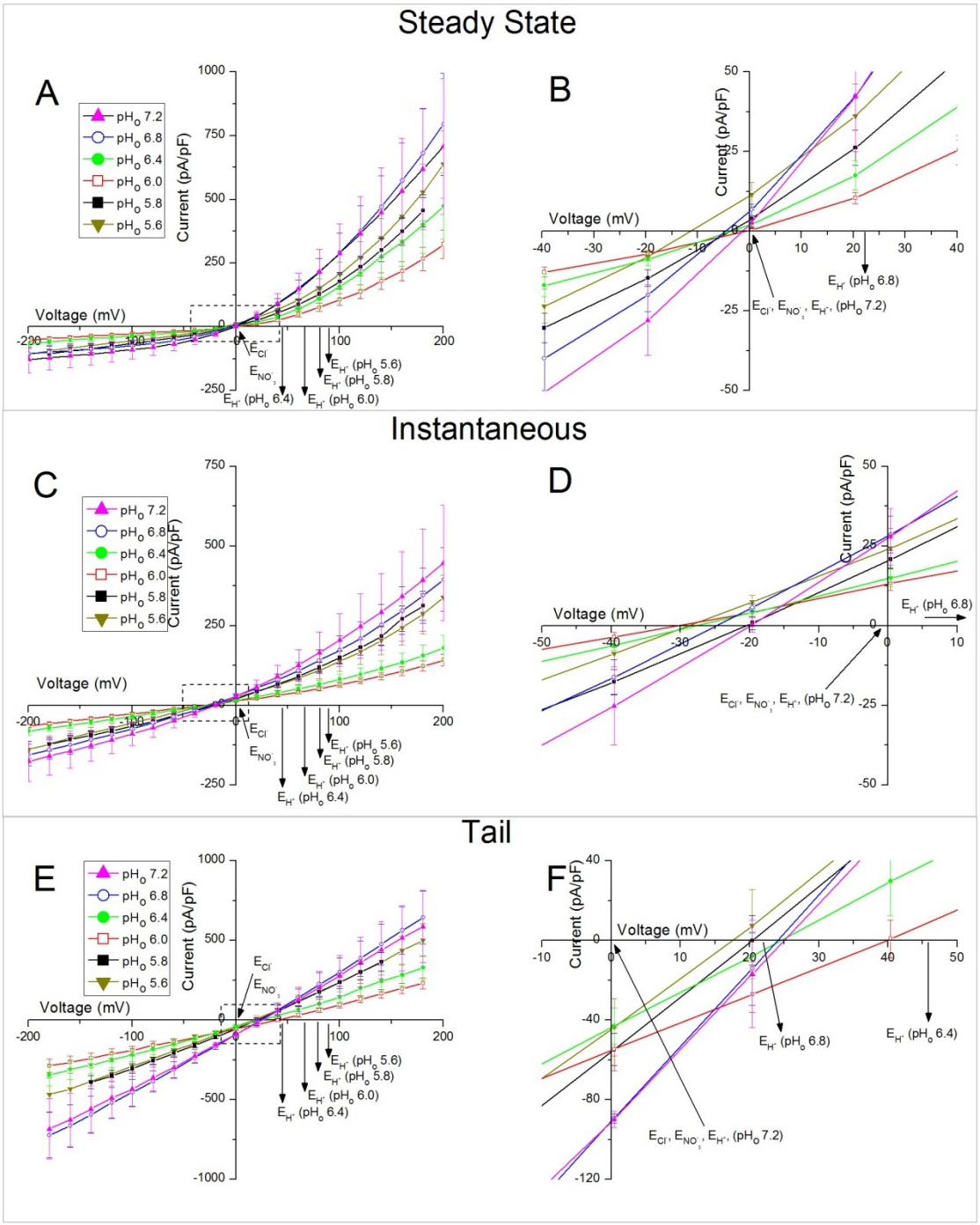

Figure 16 – Current-Potential (I-V) curves for all three current components measured under different extracellular pH conditions in the *cacc* KO mutant of *Arabidopsis thaliana*. (A) steady state currents, with detail near V_{rev} in panel B. (C) instantaneous currents, with detail near V_{rev} in panel D. (E) tail currents with detail near V_{rev} in panel F. The dotted box in plots A, C and E mark the region shown in detail in plots B, D and F respectively. The black arrows (➔) mark the position for the calculated equilibrium potential for Cl- (E_{Cl}-), NO_3^- (E_{NO3}-) and H^+ (E_H+) for the each different extracellular pH tested.

So, despite larger currents in control condition (pH$_o$ 5.8, for I_{final}) in the *cacc* mutant, the anionic currents in pollen protoplasts do not respond as readily to external pH changes as

in the wild type, having a much more equal response across different pH_o than the clearly pH_o dependent response observed in wild type.

It is interesting to observe that the response is rather similar between all three current components, and the response to acidification yields no dramatic effect either, contrary to what was seen before for the wild type. Furthermore, at the extreme pH measurements, seal destabilization was not nearly as pronounced as it was in the case of wild type at high alkaline pHs.

Channels conductance in the plasma membrane of Arabidopsis cacc mutant do not change dramatically as in wild type nor rectification is lost at higher alkaline pH

Looking at the slope conductances of these curves (Table 16), we can see how pH is affecting the currents in the *cacc* mutant. While there are still some changes to the slope conductance of the anionic currents, particularly at pH_o 7.2, where most slope conductances are statistically different from the control condition, for the most part the differences are slim and not regular.

However, the most relevant result is the fact that the anionic currents slope conductances from the cacc mutant are statistically different from those in the wild type protoplasts, particularly at higher extracellular pH. While these differences are not statistically significant when it comes to the slope conductance ratio, they are for the forward and backward slope conductance, clearly showing that the conductance state of the channels in the membrane is changed substantially in the mutant, under more alkaline pH. Furthermore, contrarily to the wild type, we do not seen a increase in forward or particularly on the backward individual conductances as pH increases, where in fact what's measured in a tendency to decrease these parameters instead.

cacc mutant anionic currents reversal potential is not dependent of pH, suggesting CaCC is the co-transporter

Another striking difference between the mutant and wild type is the effect on the reversal potentials of the anionic currents, particularly on the transient current I_{inst} and I_{tail}, where the larger shifts have been observed (Figure 17, Table 17). With increasing external pH, which in turn reduces the H^+ gradient across the plasma membrane, no change is observed regarding all current components reversal potentials, contrary to what has been previously observed in the wild type.

Table 16 – Slope conductances for *Arabidopsis thaliana* wild type and *cacc* mutant currents under different external pH conditions. Values in bold are the control condition (pH_o 5.8). Current components (steady state I_{ss}, instantaneous I_i and tail current I_t). gF, gB and gF/gB refer to the forward conductance, backward conductance and their ratio (gF and gB are in nSiemmens). Data is represented as mean ± SE. *, refers to statistical significant differences between comparable items within the same table column, while § refers to statistical differences from the control pH values to other tested pH conditions, and ¥ refers to statistically different values between wild type and *cacc* mutant ($p < 0.05$).

			pHo 5.6			pHo 5.8			pHo 6.0		
			g (nS)	gF/gS	n	g (nS)	gF/gS	n	g (nS)	gF/gS	n
wt	I_{ss}	gF	52.1 ± 10.9	11.9 ± 4.5	(4)	**30.0 ± 4.7**	**14.8 ± 1.8 * (53)**		62.6 ± 12.4 *§	20.8 ± 4.4 *	(8)
		gB	8.2 ± 3.6 *			**3.6 ± 0.8**			8.1 ± 3.7		
	I_i	gF	25.9 ± 4.5	2.6 ± 0.7	(4)	**15.0 ± 2.5 ***	**3.8 ± 0.4 * (53)**		30.0 ± 6.2 *§	4.3 ± 0.9	(8)
		gB	12.2 ± 3.0			**5.5 ± 1.1**			11.8 ± 4.0		
	I_t	gF	44.1 ± 11.7	1.4 ± 0.1	(3)	**23.6 ± 4.2**	**2.3 ± 0.5 * (31)**		30.0 ± 14.8	2.6 ± 0.8	(4)
		gB	33.1 ± 9.9 *			**17.0 ± 3.5 ***			21.4 ± 13.2		
			pHo 6.4			**pHo 6.8**			**pHo 7.2**		
			g (nS)	**gF/gS**	**n**	**g (nS)**	**gF/gS**	**n**	**g (nS)**	**gF/gS**	**n**
	I_{ss}	gF	61.5 ± 14.8 §	21.4 ± 5.9 *	(6)	62.2 ± 6.4 *§	9.0 ± 2.4 *	(7)	42.5 ± 8.6	1.5 ± 0.1 §	(2)
		gB	6.1 ± 2.6			9.1 ± 1.8 §			27.6 ± 3.4 §		
	I_i	gF	29.9 ± 6.7	5.9 ± 2.0	(6)	40.9 ± 4.9 *§	4.6 ± 1.3	(7)	32.6 ± 7.0	1.1 ± 0.1 §	(2)
		gB	10.4 ± 3.6			11.7 ± 2.2 §			28.1 ± 3.6 §		
	I_t	gF	29.1 ± 18.9	2.5 ± 0.8	(3)	42.5 ± 6.7 §	1.7 ± 0.3 *	(5)	38.4 ± 8.3	1.3 ± 0.2	(2)
		gB	20.3 ± 16.5			28.5 ± 5.8 *			28.3 ± 2.4 §		
			pHo 5.6			**pHo 5.8**			**pHo 6.0**		
			g (nS)	**gF/gS**	**n**	**g (nS)**	**gF/gS**	**n**	**g (nS)**	**gF/gS**	**n**
cacc	I_{ss}	gF	28.7 ± 8.2	10.9 ± 3.3 *	(3)	**28.4 ± 5.5**	**25.7 ± 7.6 * (24)**		19.2 ± 9.3 ¥	9.1 ± 2.7 *¥	(6)
		gB	4.1 ± 2.5			**4.4 ± 1.4**			2.1 ± 0.7		
	I_i	gF	13.4 ± 4.5	2.3 ± 0.3	(3)	**16.9 ± 4.2**	**4.7 ± 1.5 * (24)**		6.5 ± 2.6 §¥	1.8 ± 0.3 ¥	(6)
		gB	5.6 ± 1.5			**6.2 ± 1.6**			3.2 ± 1.1		
	I_t	gF	23.0 ± 5.7	2.0 ± 0.8	(3)	**25.9 ± 5.0**	**1.7 ± 0.3 * (20)**		14.5 ± 6.2	1.8 ± 0.4	(6)
		gB	12.6 ± 2.5			**17.1 ± 3.1 ***			9.1 ± 4.0		
			pHo 6.4			**pHo 6.8**			**pHo 7.2**		
			g (nS)	**gF/gS**	**n**	**g (nS)**	**gF/gS**	**n**	**g (nS)**	**gF/gS**	**n**
	I_{ss}	gF	18.6 ± 6.4 ¥	8.8 ± 3.0 *	(6)	18.3 ± 5.4 ¥	14.7 ± 1.5 *	(4)	13.5 ± 2.6 §¥	13.3 ± 1.0 *¥	(3)
		gB	3.1 ± 1.5			1.2 ± 0.3 *§¥			1.0 ± 0.3 *§¥		
	I_i	gF	5.9 ± 1.8 §¥	1.9 ± 0.4	(6)	7.7 ± 2.5 ¥	2.4 ± 0.5	(4)	6.6 ± 2.6 §¥	2.2 ± 0.7	(3)
		gB	3.7 ± 1.5			3.2 ± 0.7 *¥			2.9 ± 0.2 *§¥		
	I_t	gF	14.6 ± 4.9	1.5 ± 0.3	(6)	15.8 ± 3.6 ¥	1.3 ± 0.2	(4)	12.7 ± 1.3 §¥	1.3 ± 0.1	(3)
		gB	10.1 ± 3.4			11.9 ± 1.0 *¥			10.2 ± 1.5 *¥		

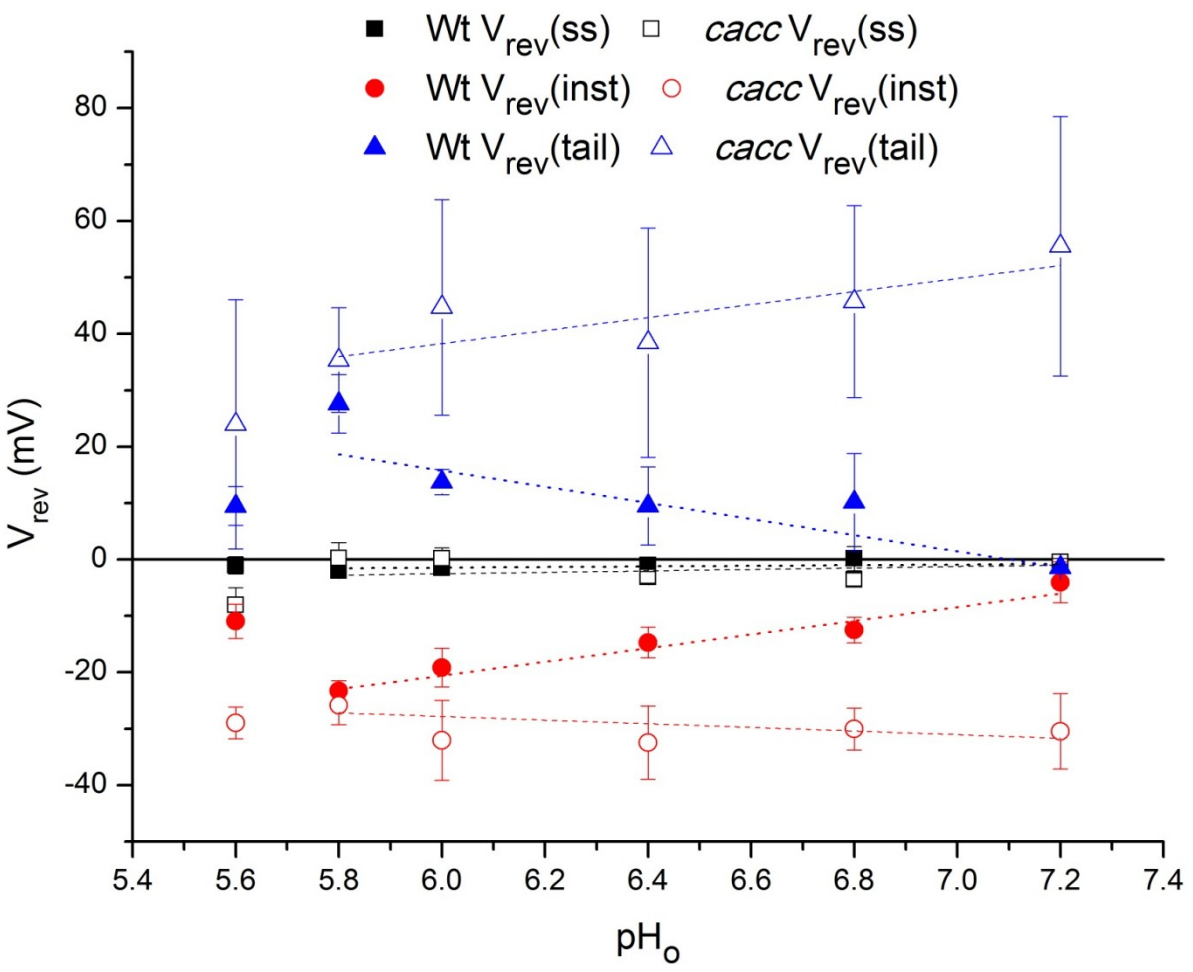

Figure 17 – *Arabidopsis thaliana* wild type and *cacc* mutant reversal potentials under different external pH for steady state, instantaneous and tail currents. Current after rundown, control condition is at pH_o 5.8. Dotted lines represent the linear fit to the reversal potential to each according current component. Data points from pH_o 5.6 were not used for the fitting.

This suggests that the CaCC gene is in fact mediating the H^+/A^- co-transport responsible for these observed shifts, and the pollen anionic currents become insensitive to $[H^+]$ when this gene is knocked out. By fitting a linear curve to the reversal potentials shifts versus pH as done for the wild type, the results are essential a straight line with no significant slope (Figure 17, dashed lines for open marks). This further supports the idea that CaCC may in fact be a co-transporter of H^+ and Cl^-, whose effect is mostly seen in transient currents and masked in the steady state currents.

This does not however explain the nature of the initial reversal shift from the expected anionic equilibrium potential observed in the instantaneous and tail reversal potentials in both wild type and *cacc* backgrounds. The results obtained for wild type suggested that this shift was H^+ based, given that by abolishing the pH gradient, this shift also disappeared. Yet, it would be expected that in the mutant this shift would naturally

disappear, instead of persisting at roughly -30 mV for instantaneous currents and +40 mV for the tail currents. It is then safe to assume that another mechanism must be involved in generating these shifts for the instantaneous and tail currents reversal potentials.

Table 17 – Reversal potentials for *Arabidopsis thaliana* wild type and *cacc* mutant currents under different external pH. Values in bold are the control condition (pH_o 5.8). I_{ss}, I_i and I_t stand for the steady state, the instantaneous and the tail current respectively. V_{rev} refers to the reversal potential (mV). Data is represented as mean ± SE. *, refers to statistical significant differences between comparable items within the same table column, while § refers to statistical differences between comparable items in the initial and final currents, and ¥ refers to statistically different values between wild type and *cacc* mutant ($p < 0.05$).

		pH_o 5.6		pH_o 5.8		pH_o 6.0		pH_o 6.4		pH_o 6.8		pH_o 7.2	
		V_{rev} (mV)	n	V_{rev} (mV)	n	V_{rev} (mV)	n	V_{rev} (mV)	n	V_{rev} (mV)	n	V_{rev} (mV)	n
wt	I_{SS}	-1.0 ± 1.5	(4)	**-2.0 ± 1.2 * (53)**		-1.5 ± 0.9 *	(8)	-1.0 ± 0.8	(6)	2.4 ± 2.9	(7)	-0.9 ± 0.6	(2)
	I_i	-10.9 ± 3.0 *§	(4)	**-23.3 ± 1.8 * (53)**		-19.2 ± 3.4 *	(8)	-14.7 ± 2.7 *§	(6)	-12.5 ± 2.3 *§	(7)	-4.0 ± 3.6 §	(2)
	I_t	9.5 ± 3.4 §	(3)	**27.6 ± 5.2 * (31)**		13.7 ± 2.2 *§	(4)	9.5 ± 6.9 §	(3)	10.2 ± 8.6 §	(5)	-1.4 ± 0.6 §	(2)
cacc	I_{SS}	-8.1 ± 3.1	(3)	**0.2 ± 2.8 * (24)**		0.2 ± 1.9 *	(6)	-3.1 ± 1.0	(6)	-3.5 ± 1.1 *	(4)	-0.4 ± 0.6	(3)
	I_i	-29.0 ± 2.8 *¥	(3)	**-25.8 ± 3.5 * (24)**		-32.1 ± 7.1 *	(6)	-32.4 ± 6.5 *¥	(6)	-30.0 ± 3.7 *¥	(4)	-30.4 ± 6.7 *¥	(3)
	I_t	24.0 ± 22.1	(3)	**35.4 ± 9.2 * (20)**		44.7 ± 19.1 *	(6)	38.5 ± 20.3	(6)	45.7 ± 17.0 *	(4)	55.5 ± 23.0	(3)

Given that the instantaneous currents are elicited after an hyperpolarization potential, and the tail currents after depolarization potentials, it's interesting to observe that both currents reversal potentials seem to give symmetrical values, only in opposite directions from the E_{Cl}-. These transient currents could still be driven by H^+, and in the absence of the CaCC gene, failed to be rectified by external pH. Perhaps a H^+ leak current could be behind these further deviations from the expected behavior for the tail anionic currents. This would fit well with what was already known from pollen tube H^+ fluxes and the expected membrane potentials at the pollen tube tip, which should be towards depolarization, since most known fluxes in the tip appear to be passive.

As for the instantaneous current, it has been well established that the presence of the H^+-ATPase in the plasma membrane is restricted from the tip and the membrane potential at the sub-apical and shank regions of the pollen tube should be hyperpolarized, potentially activating the H^+ pump. Thus, the instantaneous current and its observed reversal shift, even in the *cacc* mutant, could be induced by the hyperpolarization of the plasma membrane and activation of the H^+-ATPase, shifting the instantaneous currents reversal potential due to the active transport of H^+ out of the protoplast. This effect would then be masked by the anionic currents slow activation.

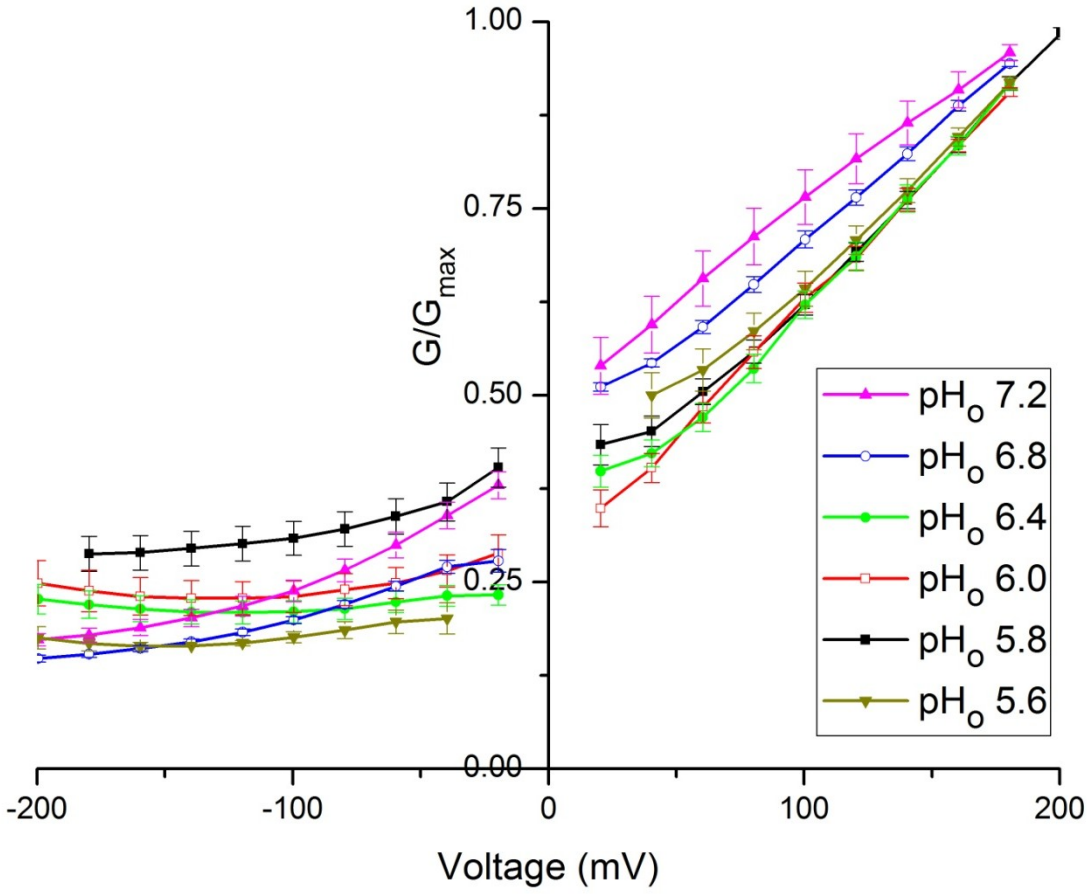

Figure 18 – *Arabidopsis thaliana cacc* KO mutant normalized average chord conductance for the steady state currents under different external pH.

cacc mutant voltage sensitivity is not affected by external pH

Finally, by analyzing the chord conductance of the anionic currents under different external pH in the mutant line (Figure 18), further evidence confirms the previous observations that the *cacc* mutant background lacks the same pH sensitivity observed in wild type. Performing the Boltzmann-like equation fits as done before we can better understand what is changing between wild type and this mutant (Table 18). While the changes to the V_h parameter are comparable with the ones obtained with wild type, with some changes in magnitude, the major difference is in fact the fact the in the *cacc* mutant the slope factor (V_s) does not increase with external pH as it did in the wild type. Thus, the normalized chord conductance curve shape does not change with external pH, only the half-maximal chord conductance changes, shifting the curve towards the left.

Table 18 – Normalized chord conductance Boltzmann fits parameters for *Arabidopsis thaliana* wild type and *cacc* mutant steady state currents under different external pH. A1 and A0 are the minimal and maximum values of normalized conductance, V_h is the potential for the half-maximal chord conductance and indicates at which membrane potential the transition between the maximum and minimum states of conductance occurs, V_s is the slope of the G/G_{max} curve and a measure of the sensitivity of the currents to variations in membrane potential. Values in bold are the control condition (pH_o 5.8). Data is represented as mean ± SE.

		A1 (kS)	A0 (kS)	V_h (mV)	V_s (mV^{-1})
wt I_{ss}	**pH_o 5.6**	0.27 ± 0.02	1.21 ± 0.06	94 ± 9	89 ± 9
	pH_o 5.8	**0.16 ± 0.01**	**1.23 ± 0.09**	**114 ± 12**	**67 ± 7**
	pH_o 6.0	0.15 ± 0.01	1.19 ± 0.06	105 ± 7	77 ± 6
	pH_o 6.4	0.12 ± 0.01	1.30 ± 0.05	108 ± 8	86 ± 5
	pH_o 6.8	0.25 ± 0.03	1.19 ± 0.06	74 ± 11	90 ± 12
	pH_o 7.2	0.73 ± 0.01	1.09 ± 0.03	68 ± 12	108 ± 10
***cacc* I_{ss}**	**pH_o 5.6**	0.15 ± 0.07	1.05 ± 0.06	89 ± 11	56 ± 7
	pH_o 5.8	**0.29 ± 0.01**	**1.37 ± 0.08**	**158 ± 10**	**71 ± 5**
	pH_o 6.0	0.22 ± 0.01	1.12 ± 0.04	114 ± 5	57 ± 4
	pH_o 6.4	0.20 ± 0.01	1.08 ± 0.07	106 ± 10	53 ± 6
	pH_o 6.8	0.12 ± 0.01	1.06 ± 0.05	57 ± 8	66 ± 7
	pH_o 7.2	0.15 ± 0.00	1.07 ± 0.02	51 ± 3	67 ± 2

These results point to the fact that the CaCC gene is responsible for H^+/A^- co-transport in the pollen plasma membrane, which effect is mostly visible in the transient currents and not in the steady state current, along with some regulatory function that modulates the currents according to the external pH.

Based on the reversal potential shifts under different external pH in the wild type instantaneous current, we can estimate a possible stoichiometry for the CaCC putative co-transporter H^+/A^- of 2:1, two protons per chloride/anion. It would be expected for protons to be transported along their gradient, energizing the co-transporter, and thus transporting anions against their gradient.

Anionic currents dependency on external [Cl^-] in *Arabidopsis* pollen

In the experiments shown before, for both wild type and *cacc* mutant lines of *Arabidopsis thaliana*, symmetrical [Cl^-] was used as the main permeable ion in solution. To verify the nature of the Cl^- currents, lower external [Cl^-] was tested by exchanging the bath solution from control solution B1 to one of B7 to B10 solutions (Table 2) (with measurement points at $[Cl^-]_{out}$ = 70 and 30 mM, for wild type *Arabidopsis*, and 15, 30, 70 and 280 for the *cacc* mutant). The bath exchange was only performed after the rundown process had been completed, and for comparison purposes only the current after rundown (I_{final}) is considered, with a $[Cl^-]_o$ of 140 mM.

Anionic currents in Arabidopsis pollen are modulated by external [Cl^-]

Upon decrease of external [Cl^-] changes to the anionic currents in wild type pollen protoplast were observed (Figure 19) to all current components. As expected the current was substantially decreased for positive potentials for the steady state, instantaneous and tail current respectively in the order of 72, 80 and 81% at $[Cl^-]_o$ = 70 mM and at 84, 91 and 85% for $[Cl^-]_o$ = 30 mM. These changes in current amplitude are also accompanied by reversal potential shifts towards more positive potentials for all current components, as it would be expected for anionic currents under this change in anionic gradient, as can be seen in Table 19, which validates the currents measured as being mediated by Cl^-.

However, the negative currents were also equally decreased in all current components, which were not entirely expected. In average the current reduction was in average 79, 76 and 55% at $[Cl^-]_o$ = 70 mM and of 87, 87 and 81% at $[Cl^-]_o$ = 30 mM, respectively for the steady state, instantaneous and tail current. In essence, similar current amplitude reduction as to what happen to the currents elicited at positive potentials. This would suggest that $[Cl^-]_o$ should be modulating the channel's activity or gating, as it's reduction in the external medium leads to a decrease in Cl^- efflux (at negative potentials), while the decrease in influx (at positive potentials) is to be expected and can be simply explained by the change in electrochemical gradient under these conditions.

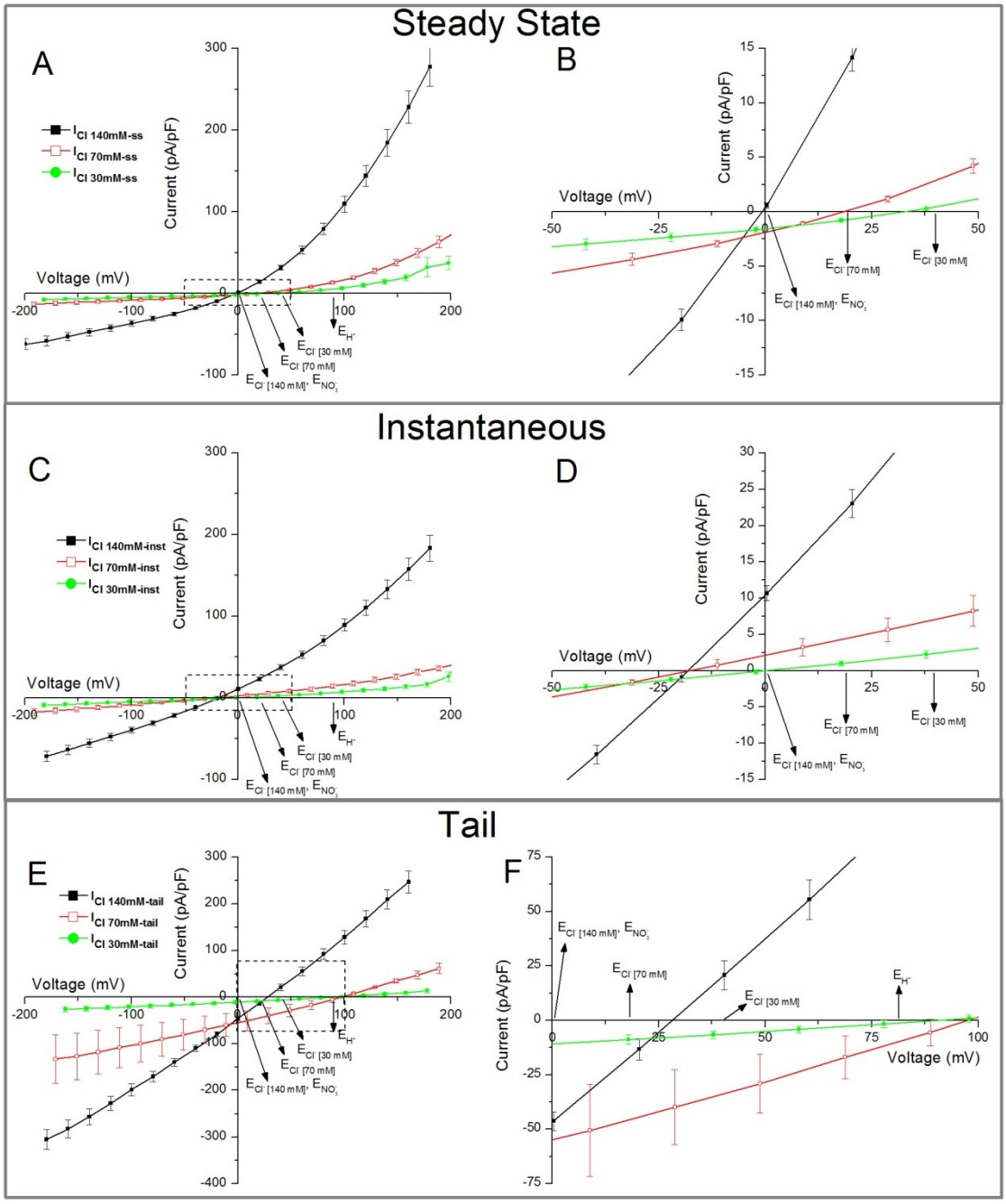

Figure 19 – Current-Potential (I-V) curves for all three current components measured under different extracellular [Cl^-] conditions in *Arabidopsis thaliana* wild type. (A) steady state currents, with detail near V_{rev} in panel B. (C) instantaneous currents, with detail near V_{rev} in panel D. (E) tail currents with detail near V_{rev} in panel F. The dotted box in plots A, C and E mark the region shown in detail in plots B, D and F respectively. The black arrows (➔) mark the position for the calculated equilibrium potential for Cl- (E_{Cl}-), NO_3^- (E_{NO3}-) and H^+ (E_H+) for the each different extracellular [Cl^-] tested.

This has been observed in other anionic channels as well. Such as the case of an outward-rectifying anion channel in wheat roots and leaves (Garrill et al., 1994; Skerrett & Tyerman, 1994), where the anion channel is notably gated by external anion

concentration, along with the R-type anion channel in both *Arabidopsis* and *Vicia faba*, that, among many other regulators, is also affected by external anion concentrations (Schmidt & Schroeder, 1994; Thomine et al., 1997). Interestingly, this effect was not observed under similar experimental conditions in the anionic currents of *Lilium longiflorum* pollen protoplasts (Tavares et al., 2011), which leads to the assumption that the anionic channels populations present in both species pollen have distinctive regulatory mechanism or even distinct anionic channels between them.

Table 19 - Reversal potentials for *Arabidopsis thaliana* wild type and *cacc* mutant currents under different external [Cl^-] conditions. Values in bold are the control condition ($[Cl^-]_o$ 140 mM). I_{ss}, I_i and I_t stand for the steady state, the instantaneous and the tail current respectively. V_{rev} refers to the reversal potential (mV). Data is represented as mean ± SE. *, refers to statistical significant differences between comparable items within the same table column, while § refers to statistical differences between comparable items in the initial and final currents ($p < 0.05$).

		$[Cl]_o$ 14 mM		$[Cl]_o$ 30 mM		$[Cl]_o$ 70 mM		$[Cl]_o$ 140 mM		$[Cl]_o$ 280 mM	
		V_{rev} (mV)	n	V_{rev} (mV)	n	V_{rev} (mV)	n	V_{rev} (mV)	n	V_{rev} (mV)	n
wt	I_{SS}			36.9 ± 3.1 *§	(7)	20.5 ± 3.1 *§	(3)	**-2.0 ± 1.2 ***	**(53)**		
	I_i			-3.2 ± 7.5 *§	(7)	-11.2 ± 9.0 *	(3)	**-23.3 ± 1.8 ***	**(53)**		
	I_t			89.5 ± 15.8 *§	(7)	82.9 ± 24.2 *	(2)	**27.6 ± 5.2 ***	**(31)**		
cacc	I_{SS}	41.3 ± 5.0 §	(2)	36.0 ± 6.7 §	(3)	16.6 ± 3.8	(2)	**0.2 ± 2.8 ***	**(24)**	-14.9 ± 4.4	(2)
	I_i	10.9 ± 13.6 §	(2)	-4.5 ± 11.5 *	(3)	-19.2 ± 16.3	(2)	**-25.8 ± 3.5 ***	**(24)**	-30.8 ± 7.5	(2)
	I_t	116.0 ± 33.0 §	(2)	101.3 ± 28.3 §	(3)	95.3 ± 50.3	(2)	**35.4 ± 9.2 ***	**(20)**	-6.4 ± --	(1)

cacc mutant anionic currents are also modulated by external [Cl^-], and evidence saturation at higher external concentration, suggesting the presence of other anionic co-transporters in the plasma membrane

In the case of the *cacc* mutant line the response to $[Cl^-]_o$ changes was similar to the observed effects in the wild type (Figure 20). Again, the I-V curves were obtained after stable rundown and tested with different bath solutions, just as in the case of wild type, but with measuring points at $[Cl^-]_o$ = 70, 30, 14 and 280 mM respectively. The overall results consists of a decrease in current amplitudes across all potentials and in all three current components with decreasing extracellular [Cl^-] with average current amplitude change of 72, 75 and 79% for the steady state, instantaneous and tail positive currents and of 71, 67 and 44% for the corresponding negative currents at $[Cl^-]_o$ = 30 mM. Again, the decrease in the currents elicited by negative potentials wasn't expected, unless it's assumed that the external [Cl^-] regulates the anionic channels conductivity states, since under this Cl^- gradient it would be expected to have an increase in the inward currents and a decrease in the outward currents.

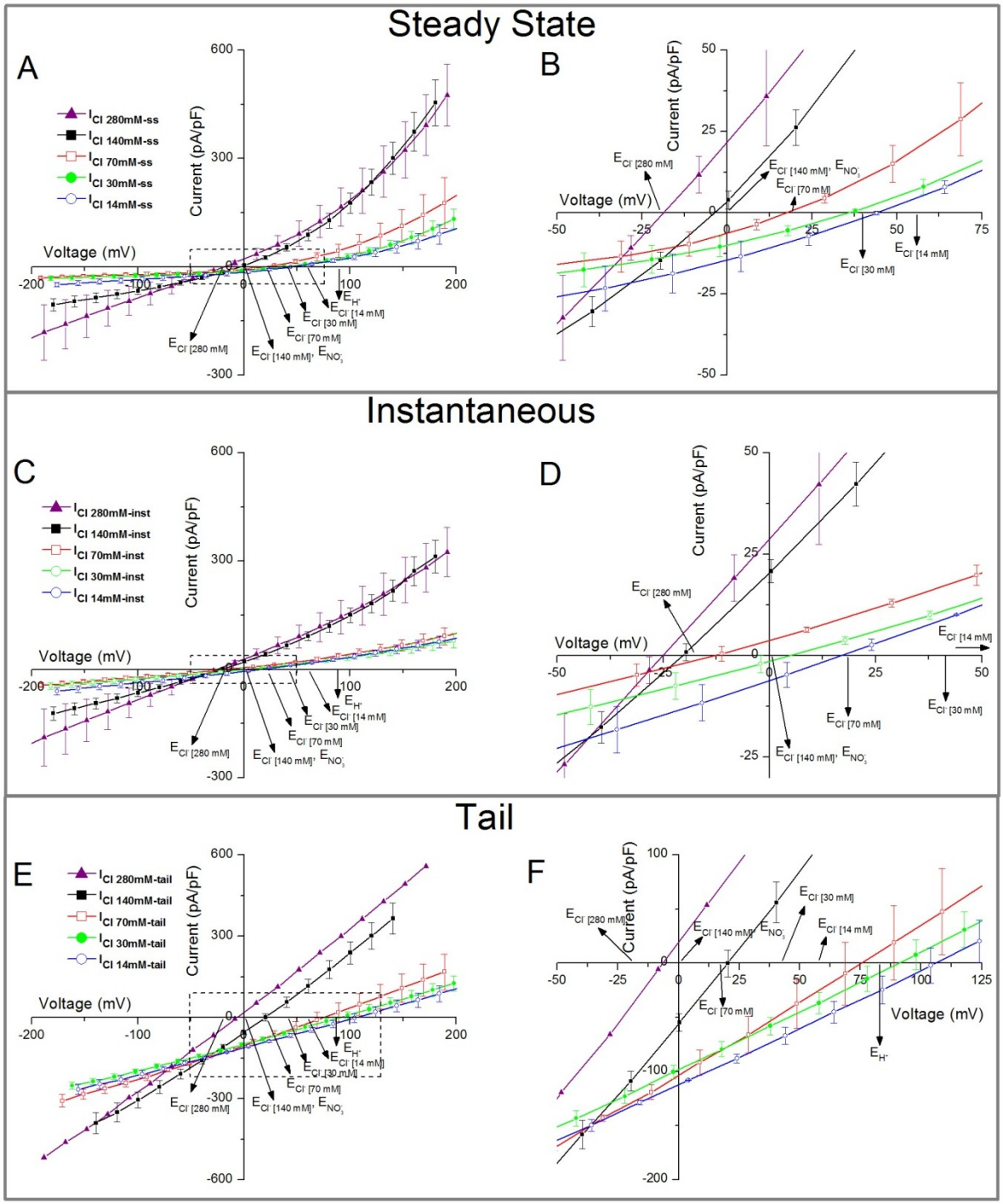

Figure 20 – Current-Potential (I-V) curves for all three current components measured under different extracellular [Cl^-] conditions in the *cacc* KO mutant of *Arabidopsis thaliana*. (A) steady state currents, with detail near V_{rev} in panel B. (C) instantaneous currents, with detail near V_{rev} in panel D. (E) tail currents with detail near V_{rev} in panel F. The dotted box in plots A, C and E mark the region shown in detail in plots B, D and F respectively. The black arrows (➔) mark the position for the calculated equilibrium potential for Cl- (E_{Cl}-), NO_3^- (E_{NO3}-) and H^+ (E_H+) for the each different extracellular [Cl^-] tested.

By increasing $[Cl^-]_o$ the anionic current an overall decrease in current amplitude for the positive currents of 10%, and an increase in the negative currents of up to 1.5 fold change with the exception of the negative tail currents which just have a mild increase of 1.06 fold change. Given the results obtained for the reduction of $[Cl^-]_o$ it would be expected to see the reverse effect under increase of $[Cl^-]_o$, however others groups have pointed out that increasing the external $[Cl^-]$ would impair pollen germination and growth (Breygina, Matveeva, et al., 2009), which might suggest that under these conditions the channel might be close to saturation. This would likely be firstly seen at the positive potentials that typical have larger current amplitudes, while for the negative potentials the expected current amplitude increase would still be seen, although more experiments would be needed to confirm this.

External $[Cl^-]$ modulates channel's conductivity in both wild type and mutant, while keeping the channel's rectification

Looking at the respective slope conductance for the anionic currents under these conditions, for both wild type and *cacc* mutant (Table 20) the first thing that emerges is the fact that the slope conductance ratio (gF/gB) essentially remains stable across different $[Cl^-]_o$ conditions. Despite some variations on this parameter, there is no statistic significance. However, looking at the forward and backward conductance, we observe the opposite, with nearly all measurements being statistically different from the control condition, revealing the change in conductance from the channels to a different anionic gradient. However, since the change is similar across membrane potential, the rectification is kept, in both wild type and *cacc* mutant.

Of interest is the fact that the results obtained at $[Cl^-]_o$ = 280 mM do not show that difference, supporting the interpretation that the channel might be already saturated at these concentrations and the changes in conductance are not significant. Asides that, the only differences detected between the wild type and the *cacc* mutant are two values for I_i(gB) and I_t(gF) at $[Cl^-]_o$ = 30 mM, which could indicate that in the mutant some aspects of the anionic currents might have different responses to these anionic concentration changes, but overall there seems to be very little changes between *cacc* mutant and wild type anionic currents response to external anion concentration.

Table 20 - Slope conductances for *Arabidopsis thaliana* wild type and *cacc* mutant currents under different external [Cl^-] conditions. Values in bold are the control condition ([Cl^-]$_o$ 140 mM). Current components (steady state I_{ss}, instantaneous I_i and tail current I_t). gF, gB and gF/gB refer to the forward conductance, backward conductance and their ratio (gF and gB are in nSiemmens). Data is represented as mean ± SE. *, refers to statistical significant differences between comparable items within the same table column, while § refers to statistical differences from the control condition and other tested conditions, and ¥ refers to statistically different values between wild type and *cacc* mutant ($p < 0.05$).

			[Cl]$_o$ 14 mM			[Cl]$_o$ 30 mM			[Cl]$_o$ 70 mM			[Cl]$_o$ 140 mM			[Cl]$_o$ 280 mM		
			g (nS)	gF/gS	n	g (nS)	gF/gS	n	g (nS)	gF/gS	n	g (nS)	gF/gS	n	g (nS)	gF/gS	n
wt	I_{SS}	gF				5.1 ± 2.2 §	10.7 ± 3.8	(7)	8.9 ± 0.4 §	21.9 ± 8.2	(3)	**30.0 ± 4.7**	**14.8 ± 1.8 * (53)**				
		gB				0.4 ± 0.1 §			0.6 ± 0.3 §			**3.6 ± 0.8**					
	I_i	gF				3.4 ± 1.8 §	4.2 ± 1.2	(7)	3.9 ± 0.9 *§	5.5 ± 2.2	(3)	**15.0 ± 2.5 ***	**3.8 ± 0.4 * (53)**				
		gB				0.6 ± 0.2 §¥			1.1 ± 0.5 §			**5.5 ± 1.1**					
	I_t	gF				4.3 ± 1.7 §¥	1.7 ± 0.4	(7)	8.5 ± 1.4 §	2.2 ± 0.7	(2)	**23.6 ± 4.2**	**2.3 ± 0.5 * (31)**				
		gB				4.0 ± 2.5 §			4.4 ± 1.9 §			**17.0 ± 3.5 ***					
cacc	I_{SS}	gF	7.7 ± 3.3 §	6.3 ± 4.5	(2)	12.6 ± 4.7	35.9 ± 22.4	(3)	12.1 ± 7.8	29.8 ± 27.3	(2)	**28.4 ± 5.5**	**25.7 ± 7.6 * (24)**		17.4 ± 9.7	7.1 ± 5.2	(2)
		gB	1.8 ± 0.8			1.0 ± 0.6 §			1.0 ± 0.7 §			**4.4 ± 1.4**			7.6 ± 6.9		
	I_i	gF	4.4 ± 1.2 §	1.8 ± 0.7	(2)	4.5 ± 1.6 *§	2.1 ± 0.6	(3)	5.1 ± 2.1 §	2.4 ± 1.1	(2)	**16.9 ± 4.2**	**4.7 ± 1.5 * (24)**		9.9 ± 5.7	3.7 ± 2.7	(2)
		gB	2.7 ± 0.4 §			2.2 ± 0.5 §¥			2.3 ± 0.2 §			**6.2 ± 1.6**			8.0 ± 7.3		
	I_t	gF	9.8 ± 0.3 §	1.3 ± 0.1	(2)	11.6 ± 1.3 §¥	1.4 ± 0.2	(3)	12.5 ± 2.5 §	1.3 ± 0.2	(2)	**25.9 ± 5.0**	**1.7 ± 0.3 * (20)**		22.6 ± --	1.2 ± --	(1)
		gB	7.9 ± 0.4 *§			8.4 ± 0.6 *§			9.7 ± 0.1 *§			**17.1 ± 3.1 ***			18.3 ± --		

Anionic currents reversal potentials follow changes in external [Cl^-] for both mutant and wild type, but fail to reach predicted values, confirming the presence of co-transporter of another ion species

By looking at the reversal potentials of these curves (Table 19) the gradual shift of reversal potentials for all current components can be observed as the external [Cl^-] changes, as it would be expected for anionic currents. Still, for both the wild type and the *cacc* mutant the underling result is that the observed shift fails to reach the expected value for E_{Cl^-}, which indicates that another ion or ions are contributing to the measured reversal potentials. The sole exception is the tail current reversal potential, which seems to be within range of the expected shifts for a Cl^- based current under our experimental conditions. Still, it's also interesting to observe that for [Cl^-]$_o$ = 280 mM, even the reversal potential for the tail current also fails to reach the expected values for E_{Cl^-}, which might be further indication of the channels change in behavior under these high external anionic concentrations.

By plotting the reversal potentials for each of the current components versus the respective external [Cl^-] we can observe their dependency (Figure 21). It is easy to observe the linear dependency of the reversal potential for all three current components to different external [Cl^-], going to more positive values with decreasing concentration and to more negative values with increasing concentrations. Again, it should be noted that the values measured that [Cl^-]$_o$ = 280 mM seem to break away from the linearity that can be

observed from the other measured points, which further indicates that at these concentrations the currents have reached a plateau of saturation.

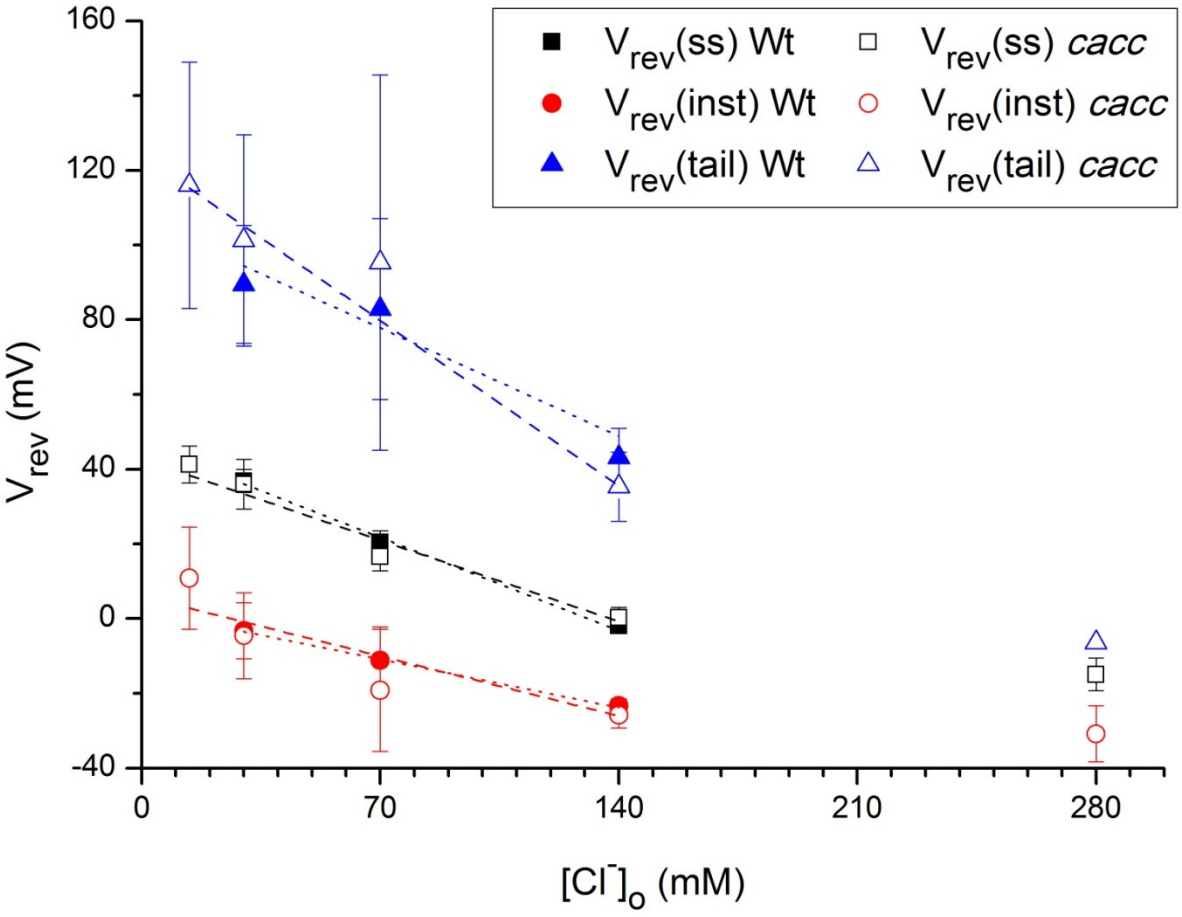

Figure 21 - *Arabidopsis thaliana* wild type and *cacc* mutant reversal potentials under different $[Cl^-]_o$ for steady state, instantaneous and tail currents. Current after rundown, control condition is at $[Cl^-]_o$ = 140 mM. Dotted lines represent the linear fit to the reversal potential to each according current component. Data points from $[Cl^-]_o$ = 280 mM were not used for the fitting.

By fitting a linear curve to these data points (Figure 21, dotted and dashed lines) we can observe that both the wild type and *cacc* mutant V_{rev} are dependent on $[Cl^-]_o$. However the slope obtained is lower then what is expected from a Cl^- channel alone (~58mV/decade) as was mentioned before, which is a clear indication of the presence of another ion/solute that is being transported along side with Cl^-. Interestingly the instantaneous current reversal potentials slope seems slightly lower than that of steady state or tail currents, which implies that the instantaneous currents is more strongly affected by other ions.

The absence of an effect in the *cacc* mutant under these conditions, compared to the wild type, implies that the CaCC gene contribution to the anion transport is small, and in fact, only observed under specific pH conditions. The lack of this transporter, while

affecting the overall anionic currents amplitudes and other properties as described before, does not substantially alter the plasma membrane sensibility to $[Cl^-]$, suggesting that other channels should be more dominant in terms of anionic currents.

The solutions used also include NO_3^- at 5 mM. The presence of another anion in solution was intentional, and it's presence would be sufficient to drive the reversal shifts away from the predicted E_{Cl}-, particularly as the $[Cl^-]_o$ is reduced to values close to the $[NO_3^-]_o$, though it's importance would be negligent as the $[Cl^-]_o$ is increased. It is thus important to determine the relative permeability between Cl^- and NO_3^- to better access each anion's contribution to the final anionic current, which will be address in the next chapter.

Changes in external [Cl-] uncouple positive and negative potentials response in both mutant and wild type

Regarding the chord conductance curves under different external $[Cl^-]$ the results can be seen in Figure 22 for the wild type and in Figure 23 for the *cacc* mutant. The first observation to be made is that under different external $[Cl^-]$ the normalized chord conductance curves no longer fit a Boltzmann curve, hinting for two distinctive processes eliciting the currents at negative and positive potentials that uncouple at asymmetrical anionic concentrations across the plasma membrane.

As external $[Cl^-]$ decreases, the normalized slope conductance increases in the negative potential range and decreases in the positive potential range, with the opposite effect for increasing external $[Cl^-]$ (for the mutant at least) comparatively with the control condition ($[Cl^-]_o$ = 140 mM). While it was impossible to fit the Boltzmann curves as before, it seems apparent that as external $[Cl^-]$ decreases that V_h shifts to more positive values, while the V_s does not appear to be dramatically changed. If taking in to account the non-normalized chord conductance, the A1 and A0 parameters for these curves fit perfectly what has been shown before for their currents, with a decrease in overall current with decreasing $[Cl^-]_o$. For increasing external $[Cl^-]$, it seems that again a saturation region is reached for the anionic currents, at least for the outward currents.

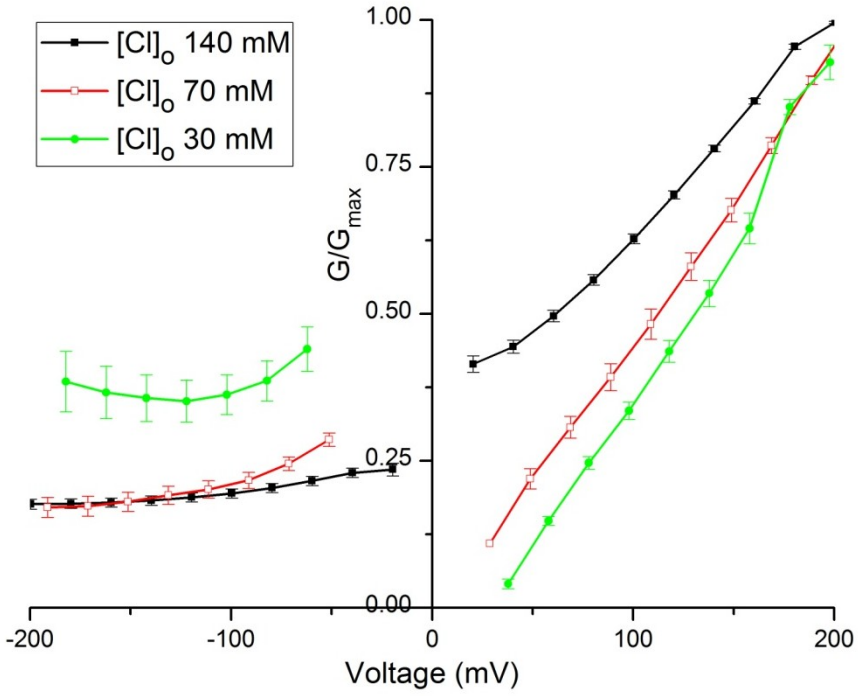

Figure 22 – Normalized average chord conductance curves of *Arabidopsis thaliana* wild type steady state currents under different external [Cl^-] conditions.

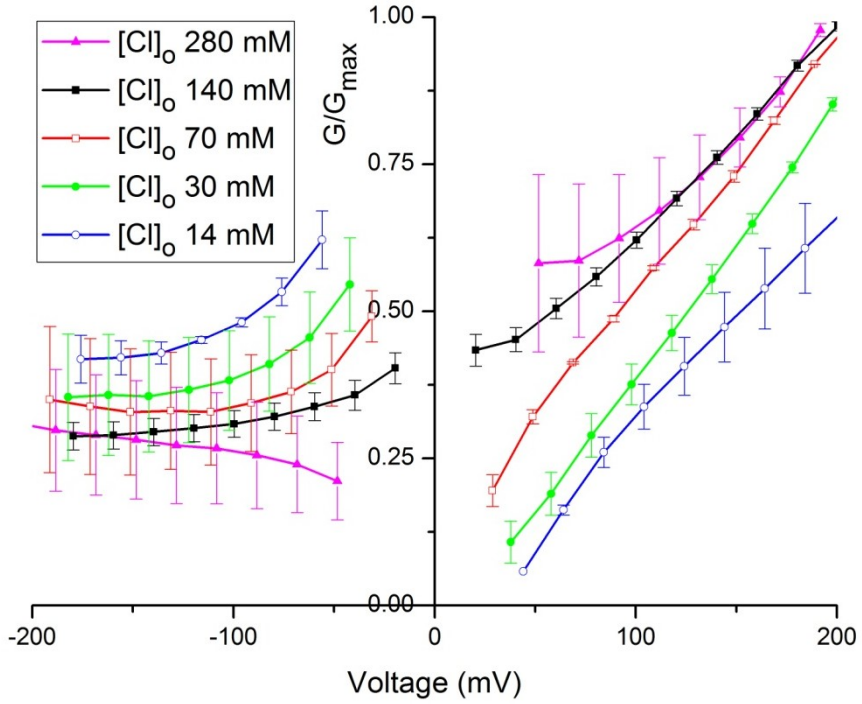

Figure 23 – Normalized average chord conductance curves of *Arabidopsis thaliana cacc* mutant steady state currents under different external [Cl^-] conditions.

Overall, these results evidence the anionic nature of the currents measured and the importance of NO_3^- to these currents. They do not reveal any significant effect to the currents in the *cacc* mutant under these conditions. Furthermore, they point to the fact that the anionic currents are regulated by their extracellular concentration within physiological range. Finally, under extracellular concentrations above 200 mM there is a potentially saturating effect that indicates the presence of other anion transporters in the plasma membrane, besides the CaCC gene, contributing significantly to the overall anionic currents, rather than just simple anionic channels.

Anion currents selectivity in *Arabidopsis* pollen

To determine the different contribution from Cl^- and NO_3^- to the measured anionic currents and calculate their relative permeability, the bath solution was substituted from a $[Cl^-]$ rich solution to a $[NO_3^-]$ rich solution (P1/B1 -> P1/B11, Table 2). All bath exchanges were performed after full rundown was attained, as usual.

Wild type anionic currents are equally permeable to Cl^- and NO_3^-, but not in cacc mutant, suggesting that CaCC is only responsible for Cl^- transport

By comparing the average wild type current amplitudes between the high extracellular $[Cl^-]$ with the high extracellular $[NO_3^-]$ we confirmed previous reports that there was little difference between them (Figure 24, Panel A, C and E), with the sole exception being that the tail currents at negative potentials diverged slightly, with decreased anionic currents under high $[NO_3^-]_o$. However, by comparing the *cacc* mutant anionic currents under similar conditions (Figure 24, Panel B, D and F), it's easily observed that in the mutant there is reduced overall anionic currents for all current components across all potentials for the high extracellular $[NO_3^-]$, compared to the high extracellular $[Cl^-]$ condition.

This can be better analyzed in Figure 25, where it is easier to see that the currents under high external $[NO_3^-]$ between wild type and *cacc* mutant are essentially similar, while under high external $[Cl^-]$ they show the already described amplitude differences. These results suggest that the CaCC gene would be responsible for a significant part of the Cl^- transport in the overall anionic currents previously observed. It would also suggest that it is acting as a H^+/Cl^- co-transporter, instead of an unspecific H^+/anion co-transporter, transporting Cl^- against its gradient. Nonetheless, the overall outlook for the population of anionic channels/transporters present in the plasma membrane in wild type seem to indicate that there isn't a clear preference for NO_3^- over Cl^-, probably resulting from a mix of different channels with different permeabilities preferences between those two anions.

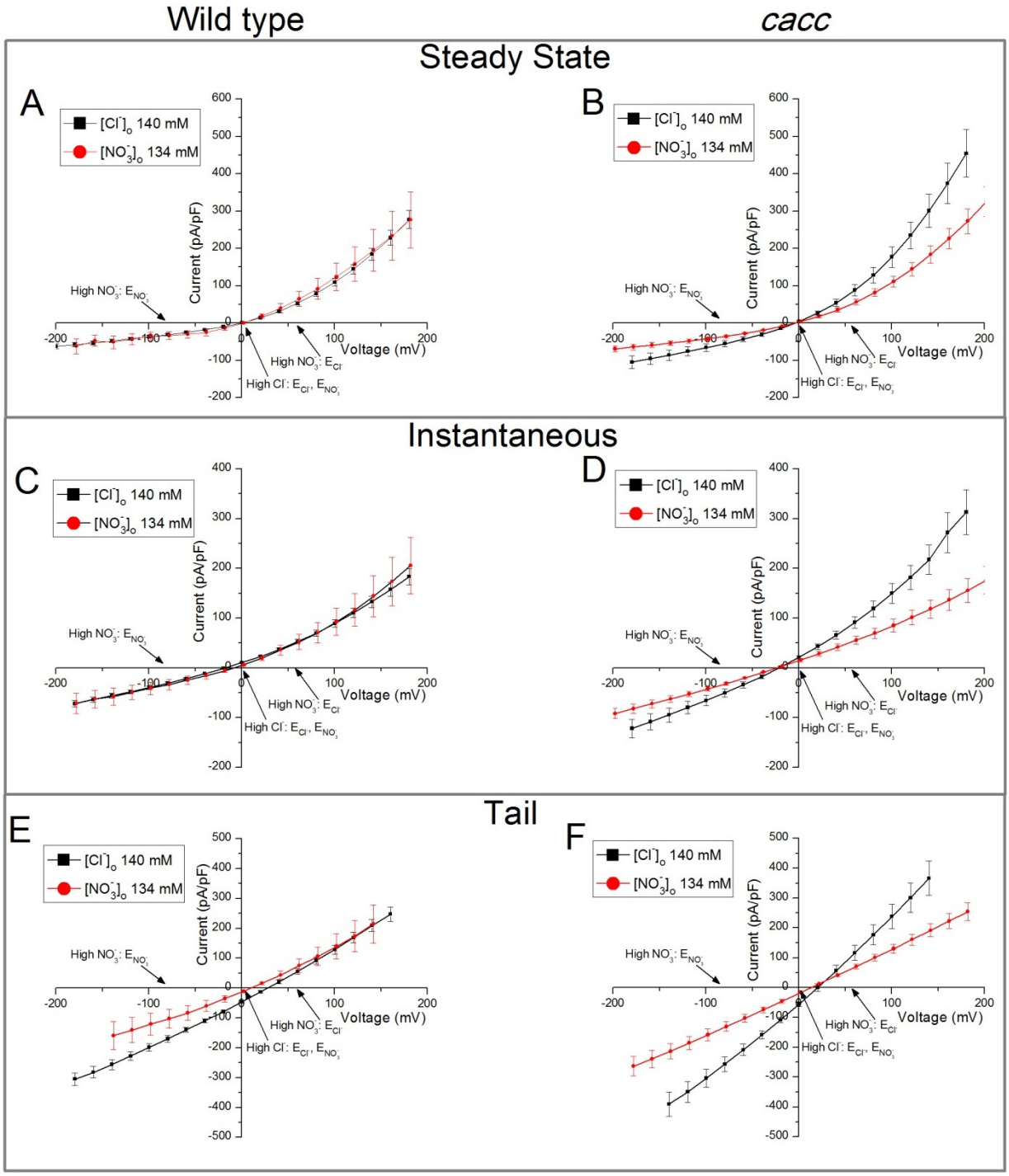

Figure 24 - Current-Potential (I-V) curves for all three current components measured under high extracellular [Cl^-] or high extracellular [NO_3^-] condition in *Arabidopsis thaliana* wild type (A, C and E) and *cacc* KO mutant (B, D and F). (A,B) steady state currents. (C,D) instantaneous currents. (E,F) tail currents. The black arrows (➔) mark the position for the calculated equilibrium potential for Cl- (E_{Cl}-) and NO_3^- (E_{NO3}-) for both conditions tested.

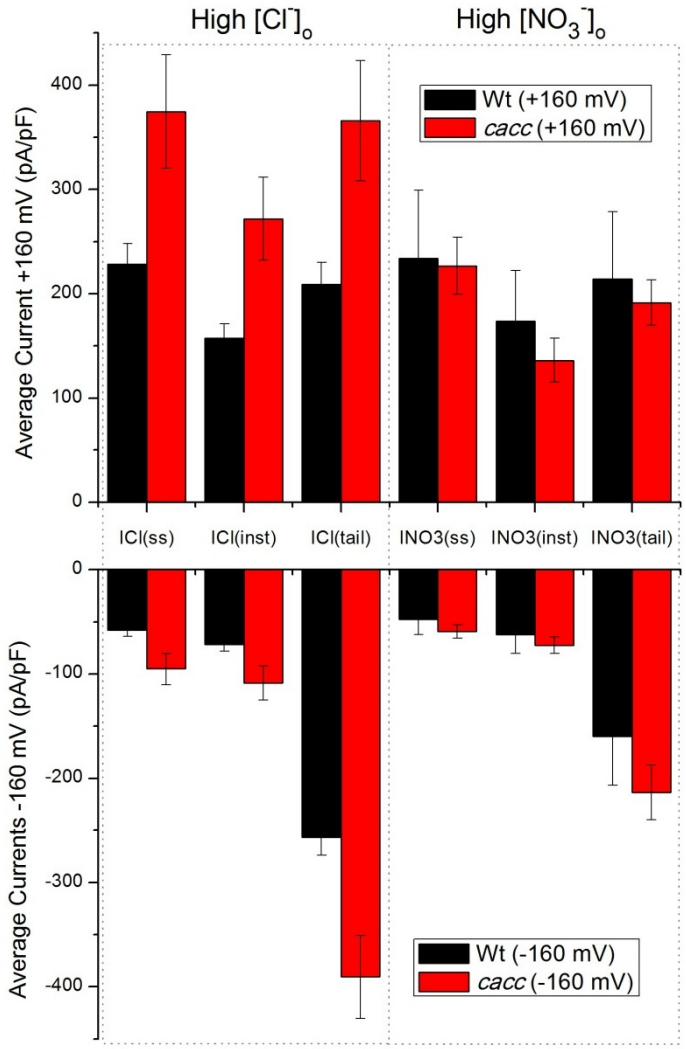

Figure 25 - *Arabidopsis thaliana* wild type and *cacc* mutant average current amplitude for the currents after rundown under external high [Cl^-] and high external [NO_3^-] conditions, measured at ±160 mV for all three current components.

Overall permeability of the plasma membrane is similar for Cl^- and NO_3^-

Looking at the reversal potentials of these curves (Table 21) the only significant changes between high $[Cl^-]_o$ and high $[NO_3^-]_o$ conditions are observed for the tail current reversal potentials, with lower values for high $[NO_3^-]_o$ then in the control condition. There is no difference between wild type and *cacc* mutant reversal potentials under these conditions. This suggests that the overall permeability of the plasma membrane anionic channels for Cl^- and NO_3^- should be very similar, and the absence of the CaCC gene does not affect that balance either, keeping the overall plasma membrane selectivity to those two anions unchanged. It should also be noted that the bath substitution was not entirely

symmetrical, which gave rise to different equilibrium potentials for both anions (E_{Cl^-} = +64.01 mV and E_{NO3^-} = -82.74 mV), however the total anion concentration was unchanged, which seems to be the crucial factor in regulating the reversal potential of these channels.

A partial substitution of $[Cl^-]$ by $[NO_3^-]$ in the bath solution was also tried in two different cells, and rendered no visible effects to the currents. Which further reinforce the idea that the important factor for the measured anionic currents reversal potential is the total anionic concentration present inside and outside, and not a particular anion concentration over another, at least for Cl^- and NO_3^- ions.

Table 21 – Reversal potentials for *Arabidopsis thaliana* wild type and *cacc* mutant currents under high external [Cl^-] or high external [NO_3^-] conditions. I_{ss}, I_i and I_t stand for the steady state, the instantaneous and the tail current respectively. V_{rev} refers to the reversal potential (mV). Data is represented as mean ± SE. *, refers to statistical significant differences between comparable items within the same table column, while § refers to statistical differences between comparable items in the initial and final currents ($p < 0.05$).

		High $[Cl^-]_o$		High $[NO_3^-]_o$	
		V_{rev} (mV)	n	V_{rev} (mV)	n
wt	I_{ss}	-2.0 ± 1.2 *	(53)	-4.1 ± 8.0 *	(8)
	I_i	-23.3 ± 1.8 *	(53)	-18.4 ± 11.4 *	(8)
	I_t	27.6 ± 5.2 *§	(31)	10.9 ± 3.0 *§	(6)
cacc	I_{ss}	0.2 ± 2.8 *	(24)	1.2 ± 3.4 *	(3)
	I_i	-25.8 ± 3.5 *	(24)	-21.4 ± 3.3 *	(3)
	I_t	35.4 ± 9.2 *§	(20)	12.8 ± 3.4 *§	(3)

The value found for P_{NO3}/P_{Cl} determined from the deviation of the averaged V_{rev} (as described in the Data analysis section of the Materials and Methods) was 1.16 for wild type and 0.93 for the *cacc* mutant. These experiments provide evidence that the pollen membrane channels act essentially as non-specific anion channels (at least for the most common inorganic anions, Cl^- and NO_3^-), with a very slight preference for NO_3^- in the wild type that's changed over to Cl^- in the *cacc* mutant.

Anionic channels membrane potential sensitivity is altered in the presence of high external [NO_3^-]

Looking back at the slope conductance ratios for these experiments (Table 22) the only observed difference is the decrease in outward rectification in the steady state for the *cacc* mutant in high $[NO_3^-]_o$ conditions, which differs significantly from the control condition and the similar condition in the wild type. However, most differences are seen

in the forward and the backward slope conductance of the currents under high $[NO_3^-]_o$ conditions. While these differences balance out when the slope conductance ratio is calculated, they are observed both between wild type and mutant and comparatively to the control condition of high $[Cl^-]_o$. This is an intriguing result, which might suggest that the presence of NO_3^- in the extracellular medium changes the conductance states of the anionic channels present in the plasma membrane. We have mentioned before that extracellular $[Cl^-]$ could be modulating these channels, and so, it is likely, that the presence of NO_3^- instead of Cl^- might have an effect on the channels conductivity or gating properties. It's interesting to note that the effect in the *cacc* mutant under high $[NO_3^-]_o$ conditions, seems to go in the opposite direction that in the wild type under similar conditions, even though their currents amplitudes are similar.

Table 22 – Slope conductances for *Arabidopsis thaliana* wild type and *cacc* mutant currents under high external $[Cl^-]$ or high external $[NO_3^-]$ conditions. Current components (steady state I_{ss}, instantaneous I_i and tail current I_t). gF, gB and gF/gB refer to the forward conductance, backward conductance and their ratio (gF and gB are in nSiemmens). Data is represented as mean ± SE. *, refers to statistical significant differences between comparable items within the same table column, while § refers to statistical differences between the two tested conditions, and ¥ refers to statistically different values between wild type and *cacc* mutant ($p < 0.05$).

		High $[Cl^-]_o$				High $[NO_3^-]_o$			
		gF (nS)	gB (nS)	gF/gB	n	gF (nS)	gB (nS)	gF/gB	n
wt	I_{SS}	30.0 ± 4.7 §	3.6 ± 0.8	**14.8 ± 1.8** *	(53)	10.3 ± 4.0 §	1.1 ± 0.5	**14.9 ± 3.8** *	(8)
	I_i	15.0 ± 2.5 *§	5.5 ± 1.1 §	**3.8 ± 0.4** *	(53)	5.8 ± 2.2 §	1.5 ± 0.5 §	**4.0 ± 0.6**	(8)
	I_t	23.6 ± 4.2 §	17.0 ± 3.5 *§	**2.3 ± 0.5** *	(31)	8.8 ± 4.0 §	4.0 ± 2.3 §	**2.7 ± 0.4**	(6)
cacc	I_{SS}	28.4 ± 5.5 §	4.4 ± 1.4	**25.7 ± 7.6** *§	(24)	41.4 ± 3.6 §¥	8.0 ± 1.8 ¥	**5.6 ± 1.1** *§¥	(3)
	I_i	16.9 ± 4.2 *	6.2 ± 1.6	**4.7 ± 1.5** *	(24)	17.7 ± 3.0 *¥	10.0 ± 2.6 ¥	**1.9 ± 0.3** ¥	(3)
	I_t	25.9 ± 5.0	17.1 ± 3.1 *	**1.7 ± 0.3** *	(20)	29.8 ± 1.2 ¥	23.8 ± 1.0 *¥	**1.2 ± 0.0**	(3)

Furthermore, the Boltzmann parameters obtained from the chord conductance curves before and after Cl^- substitution by NO_3^- in the extracellular medium (Figure 26, Table 23), evidence some changes to the properties of the active channels in the plasma membrane under difference anionic species. While in the wild type the difference is not visible in the plot (Figure 26A) it become apparent when looking at the fitting results in Table 23, with noticeable changes to Vh and Vs parameters, denoting a slightly different sensitivity to Cl^- and NO_3^-. In the *cacc* mutant, a comparable difference is also observed, but with a decrease of the Vh parameter instead, again suggesting that the CaCC gene has a different affinity to these anions and that both anions contribute in slight different ways to the overall conductivity and membrane potential sensitivity of the anion channels.

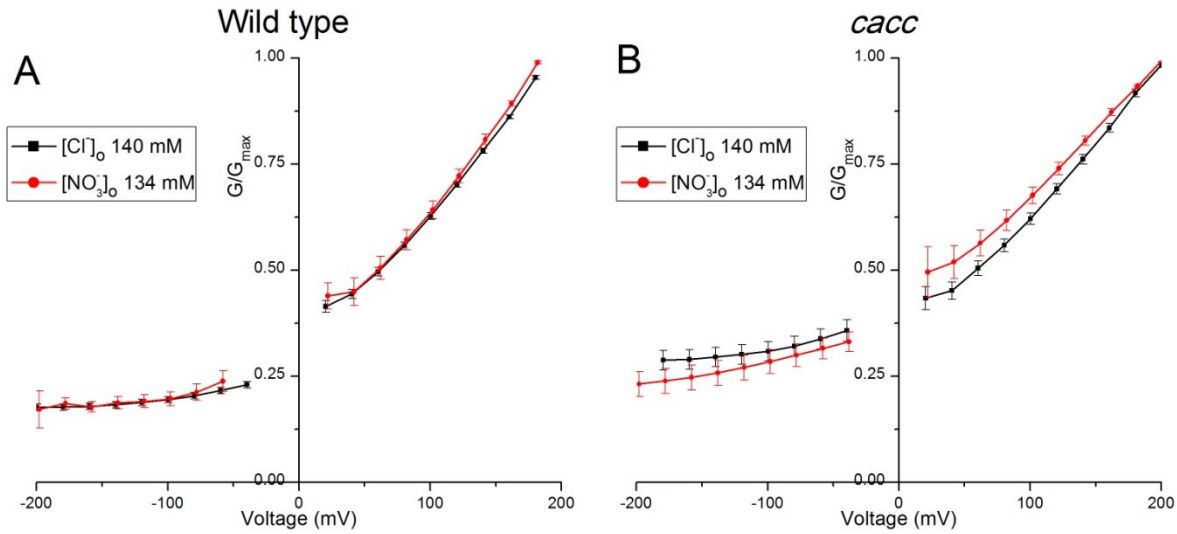

Figure 26 – Normalized average chord conductance curves of *Arabidopsis thaliana* wild type (A) and *cacc* mutant (B) steady state currents for external high [Cl^-] versus external high [NO_3^-] conditions.

Table 23 – Normalized chord conductance Boltzmann fits parameters for *Arabidopsis thaliana* wild type and *cacc* mutant steady state currents for external high [Cl^-] versus external high [NO_3^-] conditions. A1 and A0 are the minimal and maximum values of normalized conductance, V_h is the potential for the half-maximal chord conductance and indicates at which membrane potential the transition between the maximum and minimum states of conductance occurs, V_s is the slope of the G/G_{max} curve and a measure of the sensitivity of the currents to variations in membrane potential. Data is represented as mean ± SE.

	I_{SS}	A1 (kS)	A0 (kS)	V_h (mV)	V_s (mV^{-1})
wt	High $[Cl^-]_o$	0.16 ± 0.01	1.23 ± 0.09	114 ± 12	67 ± 7
	High $[NO_3^-]_o$	0.15 ± 0.01	1.56 ± 0.15	153 ± 17	79 ± 8
cacc	High $[Cl^-]_o$	0.29 ± 0.01	1.37 ± 0.08	158 ± 10	71 ± 5
	High $[NO_3^-]_o$	0.21 ± 0.01	1.29 ± 0.06	126 ± 8	81 ± 5

Role of internal pH on the anionic currents of *Arabidopsis* pollen

Having uncovered a significant effect of the external pH on the anionic currents and a phenotype on the *cacc* mutant background, the next obvious step was to access the effect of internal pH on the anionic currents. Given the knowledge that different internal pH domains in the growing pollen tube also denote different regions of anionic activity, this could potentially regulate different populations of anionic channels or modulate their activities differently.

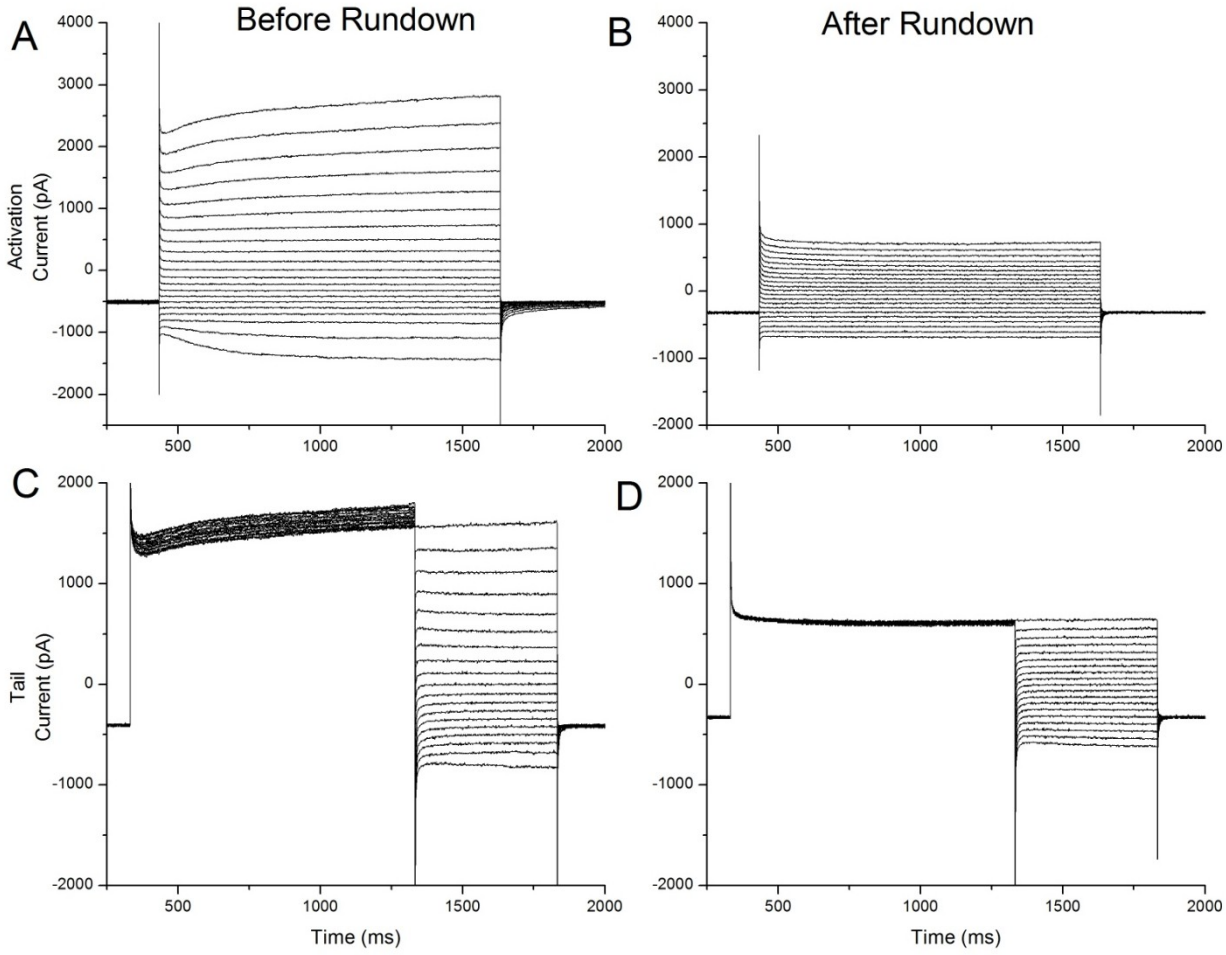

Figure 27 – Typical *Arabidopsis thaliana* wild type activation and tail currents, before and after rundown, under acidic internal pH condition, pH_i 6.8. (A-B) Activation currents, denoting outward rectification. Activation current undergoes rundown, as seen from panel A to B. (C-D) Tail currents, denoting a peak current after depolarization. Tail current also undergoes rundown, as seen from panel C to D.

To test the effect of different internal pH in pollen protoplasts a different pipette solution was used from the control conditions (P1/B1, table 2). We used the solution P2

(Table 2) with an acidic pH of 6.8, opposed to the control condition of 7.2, while keeping the bath solution unchanged (B1, with pH of 5.8). Using the same protocols as described previously, outward rectifying anionic currents were elicited using the usual voltage protocols. A example of the raw currents under acidic internal pH, before and after rundown, can be seen in Figure 27 for the wild type *Arabidopsis*, and in Figure 28 for the *cacc* mutant of *Arabidopsis thaliana*.

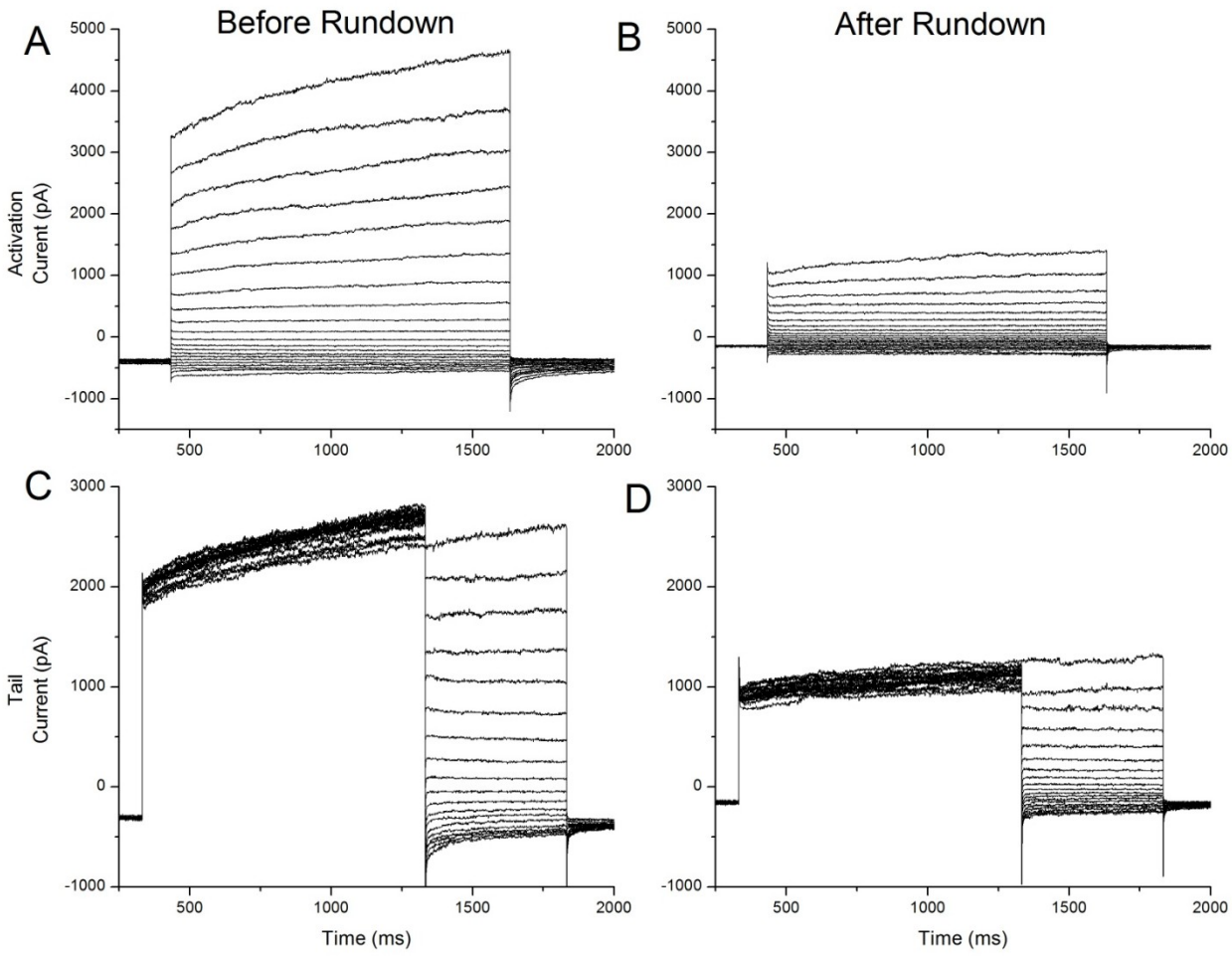

Figure 28 – Typical *Arabidopsis thaliana cacc* KO mutant activation and tail currents, before and after rundown, under acidic internal pH condition, pH_i 6.8. (A-B) Activation currents, denoting outward rectification. Activation current undergoes rundown, as seen from panel A to B. (C-D) Tail currents, denoting a peak current after depolarization. Tail current also undergoes rundown, as seen from panel C to D.

These experiments proved to be far more challenging than all the previous ones, given the difficulty to attain stable whole-cell seals under these different regimes. Even when stable seals were obtained, often they were lost after some time, not allowing a thorough characterization of the anionic currents. Even so, a handful of cells were able to sustain a stable seal for time enough to characterize their rundown. However, subsequent bath exchanges were not successful.

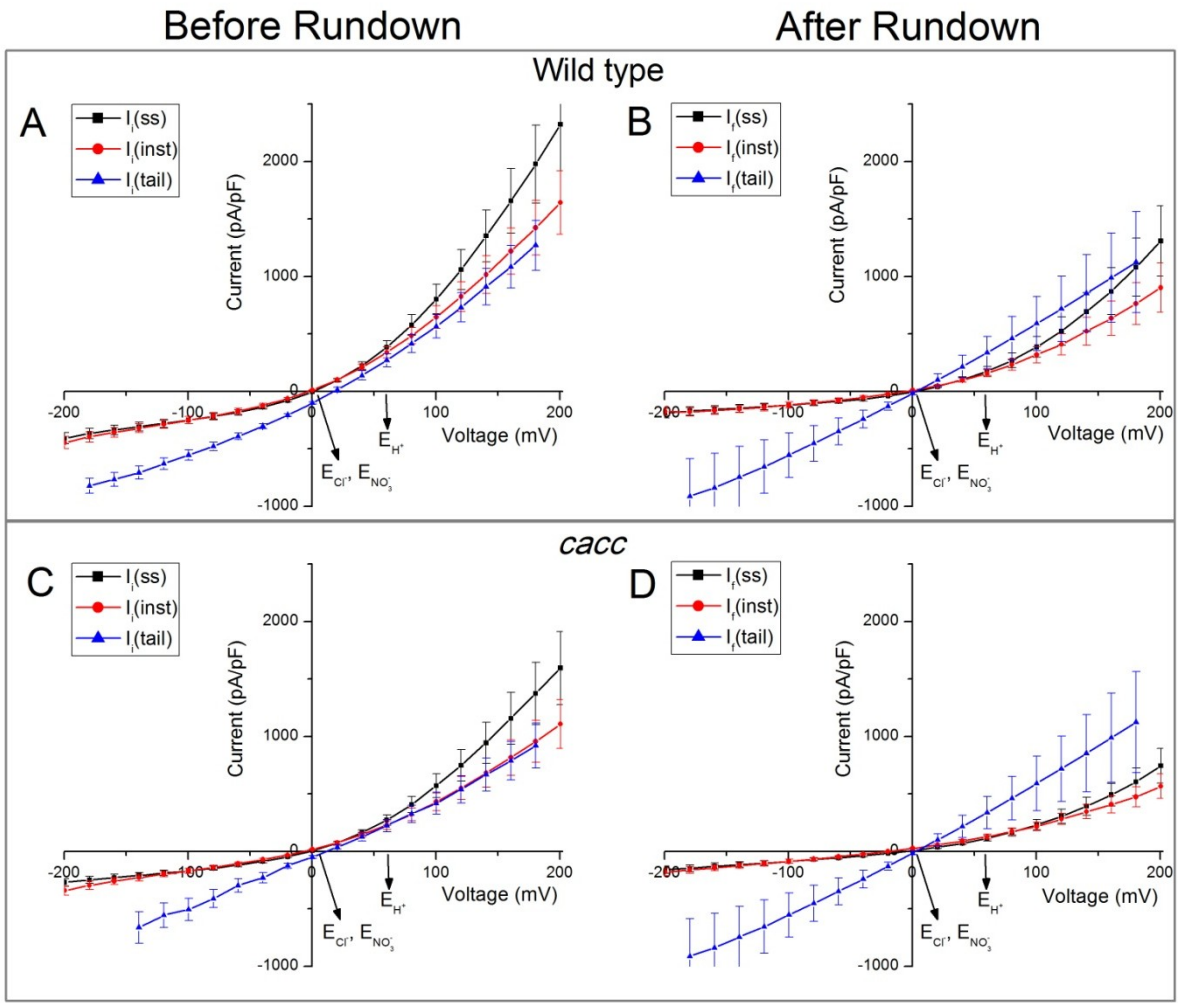

Figure 29 – Current-Potential (I-V) curves for all three current components measured under internal acidic pH condition, before (A,C) and after rundown (B,D), in *Arabidopsis thaliana* wild type (A-B) and *cacc* KO mutant (C-D). The black arrows (➔) mark the position for the calculated equilibrium potential for Cl- (E_{Cl}-), NO_3^- (E_{NO3}-) and H^+ (E_H+) for the condition tested.

Internal pH strongly modulates the anionic currents, but the effect is impaired in the cacc mutant

The average IV curves for all current components obtained during rundown under a different internal pH of 6.8, instead of the control pH of 7.2 can be seen in Figure 29 for both the wild type and the *cacc* mutant of *Arabidopsis thaliana*. In average, the currents under acidic internal pH are larger for the wild type protoplast then for the *cacc* mutant. This overall increase in current amplitudes can more easily be observed in Figure 30, where the wild type currents are always larger than the *cacc* mutant currents across all current components and at both positive and negative potentials, with the sole exception being the tail current after rundown elicited at negative potentials.

This effect on the currents amplitudes between wild type and *cacc* mutant by internal pH acidification is opposite of what was observed under control conditions (pH_i 7.2), where the mutant currents were consistently larger than the wild type, and can be more easily observed in Figure 31. It is easy to notice the effect of the two different internal pH on the anionic currents amplitudes, in both mutant and wild type, with respective effects to the different current components, and the effect of rundown to all of them.

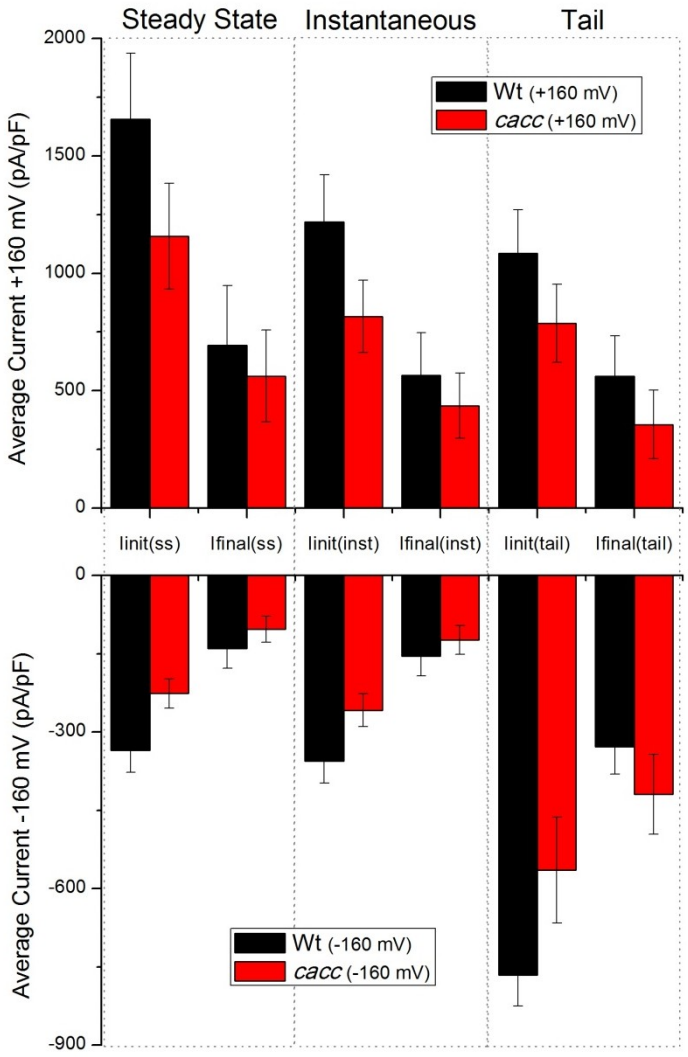

Figure 30 – *Arabidopsis thaliana* wild type and *cacc* mutant average current amplitude for the currents before and after rundown (I_{init} and I_{final}) at ±160 mV for all three current components under internal acidic pH condition.

Besides the effects on current amplitude, by acidification of the internal medium of the protoplast, the rundown properties are also affected (Table 24). Noticeably, the percentage of current lost by rundown is slightly increased for the wild type, compared to the control conditions, but not so for the *cacc* mutant. Still, as before, there is no statistical significant difference between the percentage of current lost during rundown

between wild type and mutant. So, despite the increase in initial currents, the percentage of current lost is essentially maintained, in both wild type and mutant, and under different internal pH as well. This would suggest that while internal pH is modulating the currents amplitude, the rundown process would not be affected by it, as it would affect the same number of channels in the end.

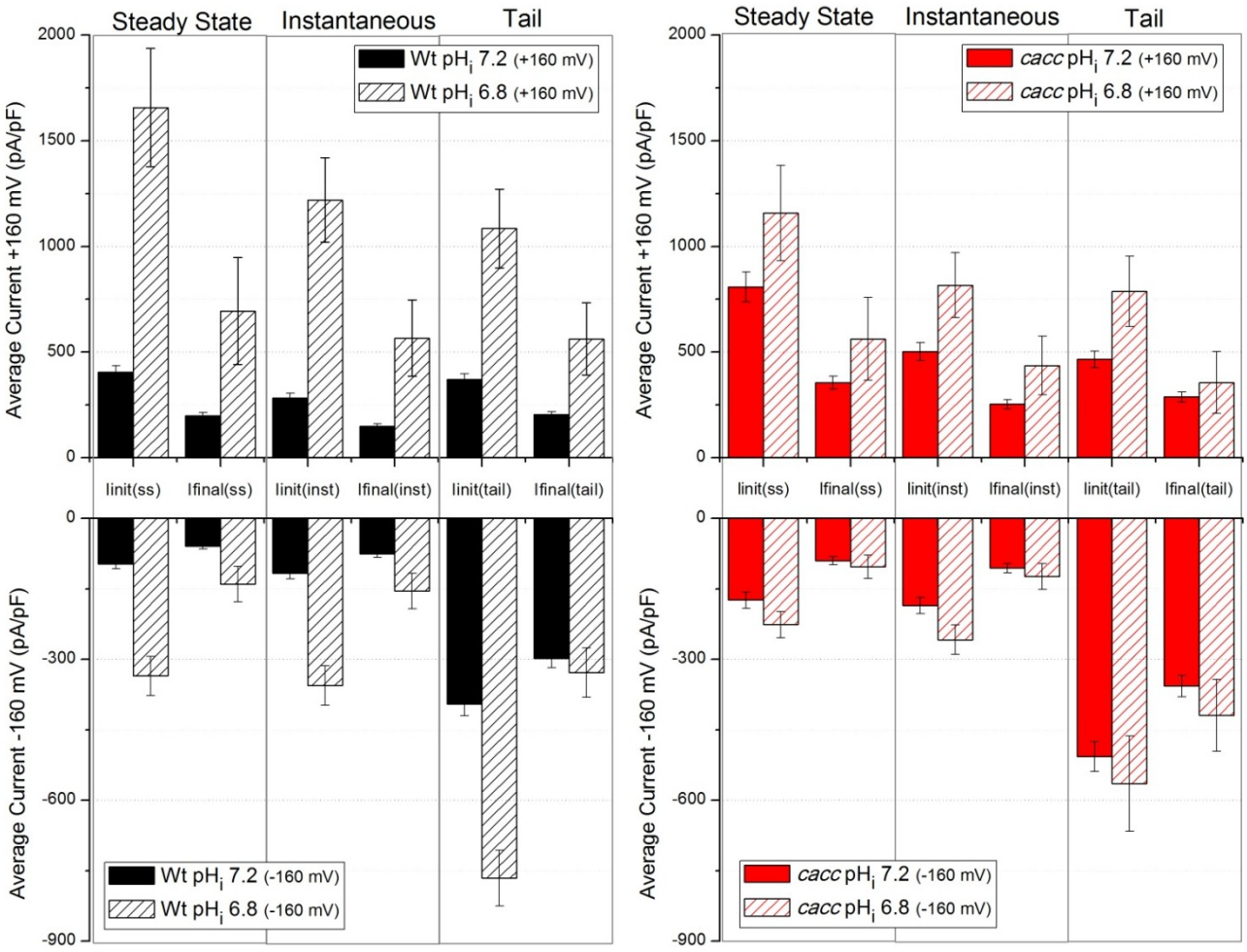

Figure 31 - Average current amplitude comparison between all three current components, before and after rundown, for *Arabidopsis thaliana* wild type and *cacc* mutant between the control condition (pH$_i$ 7.2) and internal acidic pH condition (pH$_i$ 6.8).

Looking at the average time it takes for rundown to be concluded under this condition, these values do not change significatively compared to the control condition. The average rundown time for wild type is of 83 ± 12 min, and for the *cacc* mutant is of 105 ± 15 min. In control conditions, these values were 80 ± 8 min and 134 ± 12 min, respectively for wild type and *cacc* mutant. Again, the rundown time is longer for the mutant, though faster under internal acidic pH. This would again confirm the idea that the absence of CaCC would lengthen the rundown period by having one less protein competing for the

unknown effector responsible for the rundown of currents. Furthermore, this result also validates the idea that the rundown process is not regulated by internal pH, as its length is not significatively changed.

Another interesting effect observed is that, in the wild type, the rundown of the currents elicited at positive or negative potentials are similar between them, as in the case of the control condition there was a clear reduction of percentage of rundown in the negative currents compared to the ones elicited at positive potentials.

Table 24 – *Arabidopsis thaliana* wild type and *cacc* mutant average normalized initial currents and percentage of current lost by rundown under acidic internal pH condition. I_{init} is the initial current density (pA/pF) measured at ±160 mV before rundown for each of the current components (steady state I_{ss}, instantaneous I_i and tail current I_t). RD% refers to the percentage of current lost during rundown, measured at ±160 mV. Data is represented as mean ± SE. *, refers to statistical significant differences between comparable items within the same table column, while ¥ refers to statistical significant differences between wild type and *cacc* mutant ($p < 0.05$).

pH_i 6.8		V_m (mV)	I_{init} (pA/pF)	n	RD %	n
wt	I_{ss}	+160	1657 ± 280 *	(6)	58 ± 9	(6)
		-160	-335 ± 42		58 ± 9	
	I_i	+160	1220 ± 199	(6)	53 ± 9	(6)
		-160	-356 ± 42		56 ± 9	
	I_t	+160	1085 ± 186 *	(6)	48 ± 8	(4)
		-160	-766 ± 59 *		57 ± 11	
cacc	I_{ss}	+160	1157 ± 226	(6)	51 ± 14	(6)
		-160	-226 ± 28 ¥		55 ± 12	
	I_i	+160	816 ± 154 ¥	(6)	46 ± 11	(6)
		-160	-258 ± 31 ¥		52 ± 13	
	I_t	+160	787 ± 167	(6)	55 ± 13	(5)
		-160	-565 ± 101 *¥		26 ± 25	

Channels conductance is modulated by internal pH, while keeping channel's rectification.

Looking at the slope conductance values for the anionic currents under acidic internal pH (Table 25), a few changes are observed. In the wild type the forward and backward slope conductance values for the steady state and the instantaneous currents differ significatively between the current before and the current after rundown, while their ratio is mostly unchanged by rundown. These differences are not observed in the mutant, though the average values of some of these parameters suggest that there might be a similar difference as well.

Table 25 – Slope conductances for *Arabidopsis thaliana* wild type and *cacc* mutant currents before and after rundown under an acidic internal pH condition. I_{init} is the initial current, and I_{final} is the final current before and after rundown for each of the current components (steady state I_{ss}, instantaneous I_i and tail current I_t). gF, gB and gF/gB refer to the forward conductance, backward conductance and their ratio (gF and gB are in nSiemmens). Data is represented as mean ± SE. *, refers to statistical significant differences between comparable items within the same table column, while § refers to statistical differences from the control pH values to other tested pH conditions ($p < 0.05$).

		I_{init}				I_{final}			
pH_i 6.8		gF (nS)	gB (nS)	gF/gB	n	gF (nS)	gB (nS)	gF/gB	n
wt	I_{SS}	88.7 ± 16.2 *§	11.4 ± 3.2 §	**11.3 ± 3.5** *	(6)	52.2 ± 16.8 §	3.7 ± 0.7 §	**17.0 ± 6.2**	(6)
	I_i	58.4 ± 9.8	§14.8 ± 3.6 §	**4.7 ± 1.2**	(6)	29.9 ± 9.6 §	5.0 ± 1.2 §	**13.0 ± 8.1**	(6)
	I_t	56.4 ± 11.7	29.4 ± 9.9 *	**2.9 ± 0.8**	(6)	46.9 ± 19.5	30.2 ± 11.5 *	**1.5 ± 0.1** *	(4)
cacc	I_{SS}	70.3 ± 11.5	13.6 ± 5.0	**10.8 ± 3.3** *	(6)	50.8 ± 16.2	10.3 ± 3.6 *	**9.2 ± 4.2** *	(6)
	I_i	49.3 ± 9.4	24.7 ± 8.4	**3.8 ± 1.3**	(6)	33.5 ± 10.9	17.9 ± 7.6	**3.1 ± 0.8** *	(6)
	I_t	49.7 ± 12.2	24.1 ± 18.2	**1.9 ± 0.9**	(6)	54.5 ± 18.8	42.1 ± 16.9 *	**1.4 ± 0.2** *	(5)

Another interesting aspect that goes in line with the increased anionic current amplitude is the increase in forward and backward slope conductance values, compared to those obtained under alkaline internal pH. This increase is not observed for the conductance ratio, as it would be expected since the currents keep similar rectification under both conditions, though with different current amplitudes. The exception being the instantaneous current after rundown in wild type, which in internal acidic pH has a much higher conductance ratio in wild type compared to the control condition. Overall, this would suggest that internal pH modulates the channels conductivity, while keeping the outward rectification, the balance between positive and negative currents amplitudes, unchanged.

Internal pH does not have a significant effect on the reversal potentials of the anionic currents except on the instantaneous current

By analyzing the reversal potentials for these currents (Table 26), the results are rather similar to what was obtained before with the control solutions. The notable exception is the reversal potential for the instantaneous current in wild type before rundown, which has a value closer to the equilibrium potential of Cl^- under internal acidic pH. Still, all of these parameters keep their relative differences to each other and undergo a slight shift during rundown as in the control condition, more notably the instantaneous reversal potential, in both wild type and mutant.

If anything, there appears to be a shift towards slightly more positive values in the wild type reversal potentials, while the values for the mutant remain unchanged between both

internal pH conditions. By acidifying the internal medium, we are in effect reducing the pH gradient across the membrane, which might explain the slight changes observed between these results and the control. In fact, the *cacc* mutant, which we shown before to have an impaired response to external pH, has no variation to its reversal potentials here. However, the wild type reversal potentials do show some suggestive shifts to their reversal potentials under this condition, which further supports the hypothesis that the CaCC gene may be acting as a H^+/anion co-transporter, where its effects are mainly observed by the instantaneous current component.

Table 26 – Reversal potentials for *Arabidopsis thaliana* wild type and *cacc* mutant currents before and after rundown under an acidic pH condition. I_{ss}, I_i and I_t stand for the steady state, the instantaneous and the tail current respectively. I_{init} is the initial current, and I_{final} is the final current before and after rundown for each of the current components. V_{rev} refers to the reversal potential (mV). Data is represented as mean ± SE. *, refers to statistical significant differences between comparable items within the same table column, while § refers to statistical differences between comparable items in the initial and final currents ($p < 0.05$).

		I_{init}		I_{final}	
pH_i 6.8		V_{rev} (mV)	n	V_{rev} (mV)	n
wt	I_{SS}	0.3 ± 0.7 *	(6)	-1.8 ± 2.3 *	(6)
	I_i	-6.3 ± 3.3 *	(6)	-17.4 ± 7.9 *	(6)
	I_t	36.2 ± 18.5 *	(6)	31.3 ± 32.9 *	(4)
cacc	I_{SS}	-2.5 ± 2.1 *	(6)	-4.3 ± 4.0 *	(6)
	I_i	-10.3 ± 4.6 *§	(6)	-26.1 ± 6.6 *§	(6)
	I_t	17.4 ± 6.9 *	(6)	39.5 ± 21.7 *	(5)

Anionic channels sensitivity to membrane potential is not greatly altered by internal pH

By plotting the chord conductance curves for the anionic currents under acidic internal pH for both wild type and *cacc* mutant (Figure 32) and by fitting these curves with a Boltzmann-type equation (Table 27) further information can be extracted from this data.

Of interest is the result that the slope factor (V_s) for the initial current, before rundown, is patently higher in the internal acidic pH condition, than in the control. This difference is also observed in the current after rundown but only in the wild type, although be it marginal. In the *cacc* mutant, this is only seen for the initial current, with the other two currents actually having lower or equal V_s values. Interestingly only the current after rundown shows different V_s between wild type and mutant. Alongside this the change in half-maximal chord conductance (V_h) for the current after rundown under acidic internal

pH condition is more striking compared to the control condition, with a large shift to more positive values in wild type. However, in the case of the mutant a less pronounced shift is observed instead, with a decrease in V_h in the initial currents as well, that is not observed in wild type.

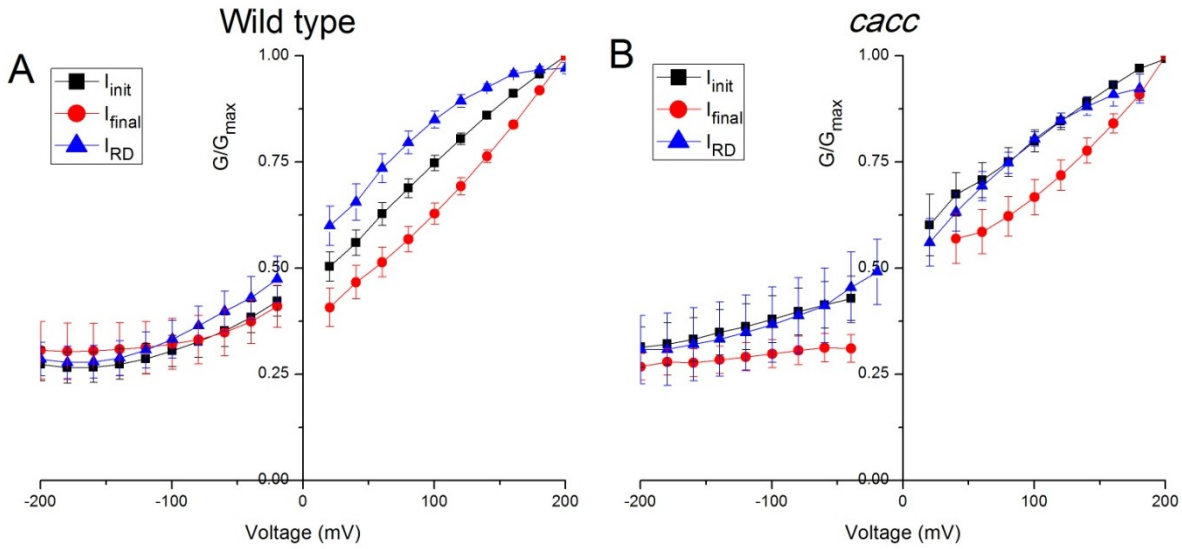

Figure 32 – Normalized average chord conductance curves for *Arabidopsis thaliana* wild type (A) and *cacc* mutant (B) steady state currents under internal acidic pH condition. I_{init} is the initial current, and I_{final} is the final current after rundown. I_{RD} is the current obtained by subtraction of the I_{final} from I_{init}, the current lost by rundown.

Table 27 – Normalized chord conductance Boltzmann fits parameters for *Arabidopsis thaliana* wild type and *cacc* mutant steady state rundown currents under internal acidic pH condition. A1 and A0 are the minimal and maximum values of normalized conductance, V_h is the potential for the half-maximal chord conductance and indicates at which membrane potential the transition between the maximum and minimum states of conductance occurs, V_s is the slope of the G/G_{max} curve and a measure of the sensitivity of the currents to variations in membrane potential. I_{init} is the initial current, and I_{final} is the final current after rundown. I_{RD} is the current obtained by subtraction of the I_{final} from I_{init}, the current lost by rundown. Data is represented as mean ± SE.

	I_{SS}	A1 (kS)	A0 (kS)	V_h (mV)	V_s (mV^{-1})
wt	I_{init}	0.23 ± 0.01	1.16 ± 0.01	85 ± 2	75 ± 2
	I_{final}	0.29 ± 0.01	1.54 ± 0.10	179 ± 12	78 ± 5
	I_{RD}	0.27 ± 0.01	1.01 ± 0.01	32 ± 2	52 ± 2
cacc	I_{init}	0.30 ± 0.01	1.09 ± 0.01	62 ± 3	70 ± 4
	I_{final}	0.26 ± 0.02	1.08 ± 0.09	103 ± 15	62 ± 11
	I_{RD}	0.31 ± 0.08	0.99 ± 0.10	44 ± 2	57 ± 3

Our results have shown that changes to the internal pH in pollen protoplasts have a profound impact to the anionic currents. A strong modulation by internal pH of the

anionic currents is patently observed, with striking differences between wild type and the *cacc* mutant as well. The results also support the hypothesis for the presence of a anionic-proton co-transporter mechanism, the CaCC gene, that may explain some of the finer aspects of the anionic currents, although more experiments would be needed to further confirm this. Overall, the anionic currents appear to be strongly modulated and regulated by both internal and external pH. Furthermore, part of this modulation seems to be impaired in the *cacc* mutant, which appears to behave as an H^+/anion co-transporter, as evidenced by the experimental data.

Competition assay of *cacc* mutant line

The pollen transcriptome of *Arabidopsis thaliana* has highlighted the presence of several putative anion channels in pollen grains (Pina et al., 2005; Borges et al., 2008). One such channel is the Anactomin1/TMEM16A homologue, a Ca^{2+}-activated Cl^- channel (CaCC) that is expressed in pollen but not in sperm cells. It is not highly expressed in pollen, and is found in other plant tissues as well. Nevertheless, its remarkably similar characteristics in terms of electrophysiological response to the previously reported anionic currents in pollen protoplasts made it a primary candidate to be tested.

Contrary to what is known in mammals, where there are 10 family members of this family, only one is present in *Arabidopsis* and it appears to be conserved across many other different plants, most of them with only one homologous gene as well.

In mammals, this gene family has a dual function. Some of its members act as bona-fide Ca^{2+}-activated Cl^- channels, while others have been shown to act as voltage-activated Cl^- channels, without any dependence on $[Ca^{2+}]$ and more surprisingly even, is that some of the remaining members have been shown to function as phospholipid scramblases.

Previous work in our lab has shown by PCR that the T-DNA insertion line for this gene was a true knockout (Gonçalves, P. unpublished). However, the homozygous mutant plants show no macroscopic phenotype or defects in pollen development, aside from the electrophysiological phenotype previously shown.

To further test the function of this gene regarding its possible role in fertilization, a pollen competition assay was performed using pollen from heterozygous mutant plants. However, no statistical significant differences were found for either the self-cross, the KO pollen on WT pistil or the reciprocal cross, all showing the expected segregation ratios of 3:1, 1:1 and 1:1 respectively (Figure 33).

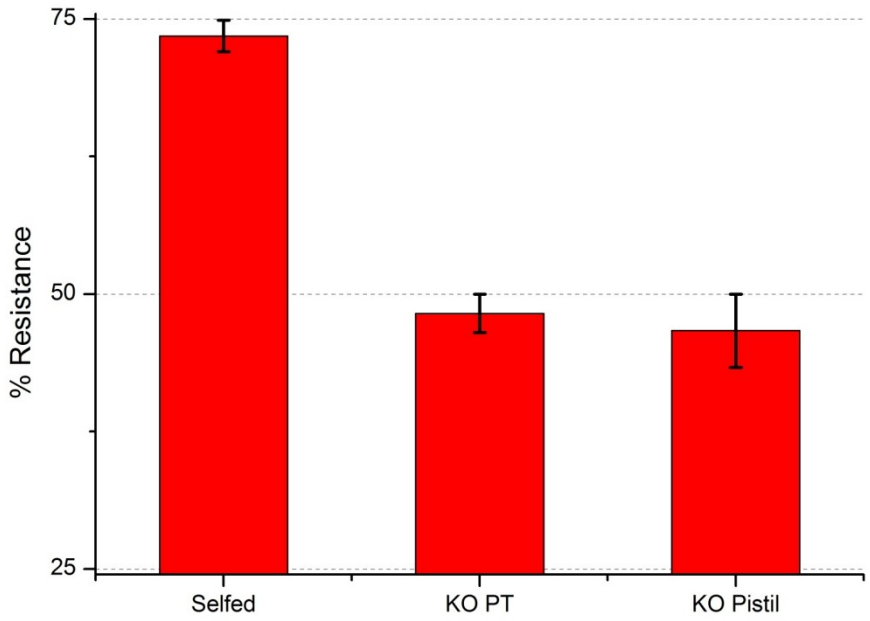

Figure 33 – Competition assays. Percentage of antibiotic resistance conferred by the T-DNA insertion for the CaCC gene, showing the percentage of resistant plants for selfed, KO pollen on wild type pistil (KO PT), and wild type pollen on KO pistil (KO Pistil). Dotted lines mark the segregation values of 3:1 (75%) and 1:1 (50%).

Nonetheless, all crosses evidenced a slight decrease of the expected segregation ratio which might indicate a small seed set phenotype too small to be detected under our sampling conditions (n = 814). Furthermore, taking in to account the specificity of the electrophysiological phenotype observed for this mutant line, it is likely, that its contribution to the overall function of the pollen tube be in fact small, or restricted to very specific conditions that may have not been induced in this test.

The role of external pH in the anionic currents of *Lilium longiflorum* pollen

The dependence of the anionic currents with pH was first tested in *Lilium longiflorum* pollen grain protoplasts, before switching to *Arabidopsis thaliana*. These results are here described, making a comparison between the two species. A full characterization of the properties of these anionic currents in *Lilium longiflorum* was not made, still the data obtained allowed to validate our data with the previously published results (Tavares et al., 2011). Still, the main purpose was to determine if extracellular pH changes in Lily pollen protoplasts anionic currents had any effect on their anionic currents.

These experiments were performed in conditions similar to those described for *Arabidopsis* under control conditions. The solutions used were similar to the ones used in *Arabidopsis* control condition (P1/B1, Table 2), with the exception of the osmolarity, which was reduced by 100 mOsm, for both the bath and the pipette solutions. For the different extracellular pH conditions solutions B5 and B6 were used, after complete rundown of the currents was attained as done previously. All recording conditions and protocols were equal to the ones used for *Arabidopsis*, with the only difference being the aforementioned osmolarity decrease in recording solutions and some changes to the protoplast production protocol, as mention accordingly in the Material and Methods.

Anionic currents in Lilium longiflorum pollen share properties with Arabidopsis anionic currents, but with distinguishable features

Under these control conditions, very similar to the ones used previously published (Tavares et al., 2011), we've obtained comparable currents to those reported. The average I-V curves for activation and tail currents elicited by the voltage protocols in use can be seen in Figure 34.

These currents share many properties with the *Arabidopsis* anionic currents, most importantly being strong outward rectifying currents, conducting in both directions and undergoing a rundown process that typically last for over an hour in both species.

All currents components undergo rundown, as can be seen in Table 28, lasting in average 90 min, quite similar to what was observed in *Arabidopsis*, which might suggest a common mechanism between the two species rundown process. The currents amplitude for *Lilium* is larger than in *Arabidopsis*. As for the percentage of current lost during rundown, the results are also different, with *Lilium*'s percentage of current lost during

rundown being substantially lower when compared to *Arabidopsis*. These differences are visible across all current components and particularly at the currents elicited by positive potentials.

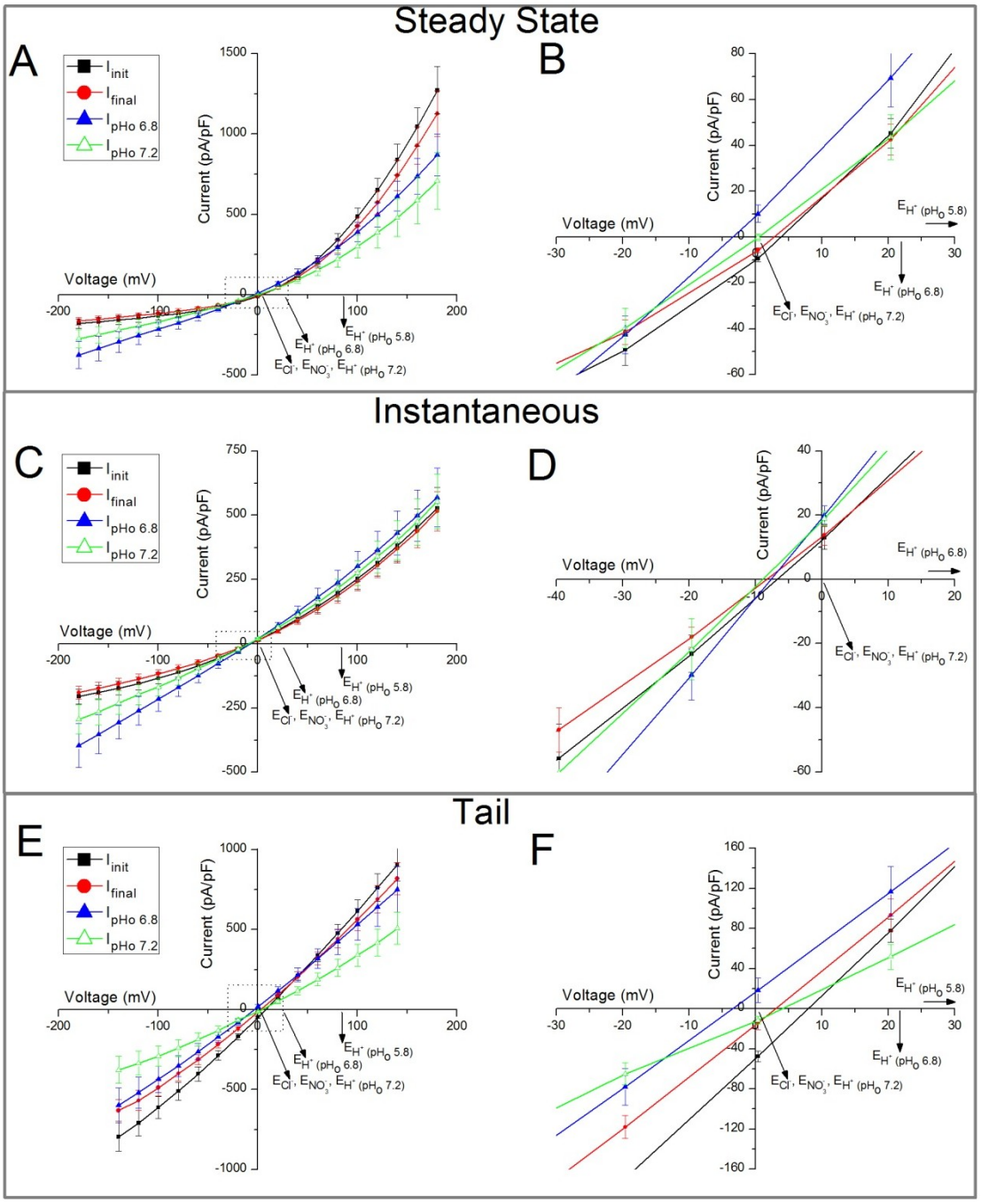

Figure 34 – Current-Potential (I-V) curves for all three current components in *Lilium longiflorum* wild type, before and after rundown, and after rundown under different extracellular pH conditions. (A) steady state currents, with detail near V_{rev} in panel B. (C) instantaneous currents, with detail near V_{rev} in panel D. (E) tail currents with detail near V_{rev} in panel F. The dotted box in plots A, C and E mark the region shown in detail in plots B, D and F respectively. The black arrows (➔) mark the position for the calculated equilibrium potential for Cl- (E_{Cl}-), NO_3^- (E_{NO3}-) and H^+ (E_H+) for the each different extracellular pH tested.

Anionic currents in Lilium longiflorum are regulated by external pH, but differently from Arabidopsis

Looking at the currents elicited under different external pH conditions (Figure 34, pH_o 6.8 and pH_o 7.2) it is observable the effect of external pH has on the anionic currents of *Lilium longiflorum* pollen protoplast. Noticeably with increasing alkalinization of the extracellular medium, the steady state anionic currents decrease in amplitude in the positive potential range, and increase in the negative potential range. This effect however is not conserved in all current components, since in the instantaneous and the tail positive currents the decrease in amplitude under bath alkalinization is not readily observed, or its effect is rather small. Furthermore, in the tail currents, in the negative potential range the opposite effect is observed, with a decrease in tail current amplitude with increasing external pH. This is in stark contrast with what is observed in *Arabidopsis*, where the effect of external pH changes is consistent across all current components, and involves an increase in currents amplitudes across all potentials with extracellular pH alkalinization. Still, it is clear that external pH does have a regulatory effect on the anionic currents in *Lilium longiflorum*, albeit a rather different effect when compared to *Arabidopsis*.

Table 28 – *Lilium longiflorum* wild type average normalized initial currents and percentage of current lost by rundown. I_{init} is the initial current density (pA/pF) measured at ±160 mV before rundown for each of the current components (steady state I_{ss}, instantaneous I_i and tail current I_t). RD% refers to the percentage of current lost during rundown, measured at ±160 mV. Data is represented as mean ± SE. *, refers to statistical significant differences between comparable items within the same table column ($p < 0.05$).

Lily	V_m (mV)		I_{init} (pA/pF)		n	RD %	n
wt	I_{ss}	+160	1045 ± 120		(8)	31 ± 7	(8)
		-160	-169 ± 29			29 ± 6	
	I_i	+160	454 ± 70	*	(8)	35 ± 7	(8)
		-160	-189 ± 28			31 ± 6	
	I_t	+140	906 ± 102		(8)	22 ± 6	(8)
		-140	-795 ± 90	*		26 ± 5	

Taking a look at the slope conductance of these curves (Table 29) we can see that the currents before and after rundown, share similar properties with *Arabidopsis*, with all slope conductance parameters being reduced during rundown, as would be expected to fit with the corresponding decrease in current amplitudes. The values that are significantly different are also in line with what is observed for the currents in *Arabidopsis* during rundown, with the forward conductance of the instantaneous current and the backward conductance of the tail current standing out for the others. Besides this, the conductance ratios are also different between themselves, though this is partially lost after rundown due to the lower ratio of the instantaneous current, but still, not very different from what

has been seen in *Arabidopsis*. Once again, suggesting that the rundown process may be due to the same factors.

As we look at the slope conductance value under different external pH conditions the major differences fall on the backward conductance for the external pH of 6.8, and by consequence, the ratio is also affected, showing a clear effect of the alkalinization of the extracellular medium on the conductance of the anionic currents, by mainly modulating the current in the negative potentials region. At a pH of 7.2, this effect seems to be altered, but some of the forward conductances do show substantial differences when compared to the current after rundown. All in all, the main point is that with increasing external pH there seems to be a progressive reduction of the rectification, that while in *Arabidopsis* it appear to be driven simultaneous by changes to both the forward and backward conductance, in *Lilium* it seems to be driven differentially by each. This further adds to the point that the regulation of the anionic currents by pH in *Lilium* is done differently than in *Arabidopsis*.

Table 29 – Slope conductances for *Lilium longiflorum* currents before and after rundown, and after rundown under different external pH conditions. I_{init} is the initial current, and I_{final} is the final current before and after rundown for each of the current components (steady state I_{ss}, instantaneous I_i and tail current I_t). gF, gB and gF/gB refer to the forward conductance, backward conductance and their ratio (gF and gB are in nSiemmens). Data is represented as mean ± SE. *, refers to statistical significant differences between comparable items within the same table column, while § refers to statistical differences from the control pH values to other tested pH conditions (p < 0.05).

			$I_{initial}$			I_{final}			pH_o 6.8			pH_o 7.2		
Lily			**g (nS)**	**gF/gS**	**n**	**g (nS)**	**gF/gS**	**n**	**g (nS)**	**gF/gS**	**n**	**g (nS)**	**gF/gS**	**n**
wt	I_{SS}	gF	70.0 ± 16.7	24.0 ± 4.6 *	(8)	**52.0 ± 13.0**	**19.8 ± 3.2 ***	**(8)**	43.5 ± 10.7	10.6 ± 3.7 *§	(6)	18.0 ± 8.6 §	4.3 ± 1.2 §	(3)
		gB	3.6 ± 1.0			**3.0 ± 0.8**			9.0 ± 3.2 §			4.3 ± 2.0		
	I_i	gF	20.2 ± 4.7 *	4.5 ± 1.2 *	(8)	**15.8 ± 3.8 ***	**3.7 ± 0.8**	**(8)**	16.6 ± 4.0 *	1.6 ± 0.2 §	(6)	12.3 ± 5.6	2.1 ± 0.5	(3)
		gB	6.4 ± 1.8			**5.3 ± 1.3**			11.3 ± 2.8 §			5.3 ± 2.2		
	I_t	gF	44.4 ± 11.2	1.8 ± 0.3 *	(8)	**35.4 ± 8.6**	**2.7 ± 0.8**	**(8)**	37.5 ± 7.7	1.4 ± 0.2 §	(5)	14.2 ± 5.1 §	2.3 ± 0.5	(3)
		gB	28.7 ± 8.7 *			**21.2 ± 7.5 ***			29.2 ± 7.5 *			6.4 ± 2.7 §		

Anionic currents reversal potential in Lilium longiflorum under different external pH evidence the absence of H^+/anion co-transport

Looking back at the reversal potentials of the currents (Table 30), we can observe the same type of shifts for the reversal potentials of the instantaneous and tail currents as we have observed for *Arabidopsis*. Such that the instantaneous reversal potential is shifted to more negative values and the tail reversal potential to more positive values, while the steady state reversal potentials stays closer to zero, the expected equilibrium potential. Nonetheless, these shifts are smaller in amplitude than those in *Arabidopsis*, particularly taking in to account the instantaneous and tail reversal potentials after rundown in

Arabidopsis. It seems that during rundown there is no significant change to the reversal potentials, while for *Arabidopsis*, at least for the instantaneous, and possibly for the tail reversal potentials, there is always a consistent shift to values far from the E_{Cl}-.

Table 30 – Reversal potentials for *Lilium longiflorum wild type* currents before and after rundown, and after rundown under different external pH conditions. I_{ss}, I_i and I_t stand for the steady state, the instantaneous and the tail current respectively. I_{init} is the initial current, and I_{final} is the final current before and after rundown for each of the current components. V_{rev} refers to the reversal potential (mV). Data is represented as mean ± SE. *, refers to statistical significant differences between comparable items within the same table column, while § refers to statistical differences between comparable items in the initial and final currents (p < 0.05).

		$I_{initial}$		I_{final}		pH_o 6.8		pH_o 7.2	
Lily		V_{rev} (mV)	n	V_{rev} (mV)	n	V_{rev} (mV)	n	V_{rev} (mV)	n
wt	I_{SS}	5.0 ± 1.0 *	(8)	**4.0 ± 1.4**	**(8)**	-3.9 ± 2.2 §	(6)	0.8 ± 1.3 §	(3)
	I_i	-11.0 ± 6.3 *	(8)	**-9.0 ± 4.4** *	**(8)**	-13.8 ± 4.1 *	(6)	-19.4 ± 14.8 *	(3)
	I_t	9.9 ± 2.2 *	(8)	**6.2 ± 2.7**	**(8)**	-1.7 ± 3.1 §	(5)	6.2 ± 4.4	(3)

The most striking difference however derives from the reversal potentials under different external pH in *Lilium longiflorum*, where it does not evidence a linear relationship with external pH as in *Arabidopsis*. While different external pH does seem to elicit some variations on the reversal potentials, particularly at pH_o 6.8, these changes are not retained in pH_o 7.2. Furthermore, the instantaneous reversal potential seems to go to more negative values with increasing external pH, quite the opposite of what is observed in *Arabidopsis*. Taken together, these results evidence that the proposed H^+/anion co-transporter present in *Arabidopsis* plasma membrane, must not be present in *Lilium longiflorum*. Suggesting that the effect of pH on the currents in *Lilium* should be only modulating the anion channels activity.

Therefore, the question remains as to why these different current components, namely the instantaneous current, have such a negative reversal potential compared to the other currents, since there are no permeable ions in solutions that could drive the reversal potential to such values, as mention before. Another interesting aspect is that the tail reversal potentials in *Lilium* seem much more closer related to the steady states reversal potentials, while in *Arabidopsis* they appear to mirror the effects of the instantaneous current instead.

Chord conductance evidence the similarities between rundown process between Lilium and Arabidopsis, and their differences on pH regulation

Finally, by analyzing the chord conductance of the anionic currents on Lily protoplasts (Figure 35) we can observe the same effect as in *Arabidopsis*. The currents before and after rundown change the Boltzmann parameters (Table 31). However, these changes are

in accordance to what was observed for *Arabidopsis*, with an increase in V_h and V_s for the current after rundown compared to the initial current. Once again, this reiterates that the rundown process in these two species appears to be similar.

Table 31 – Normalized chord conductance Boltzmann fits parameters for *Lilium longiflorum* wild type steady state rundown currents, and after rundown under different external pH conditions. A1 and A0 are the minimal and maximum values of normalized conductance, V_h is the potential for the half-maximal chord conductance and indicates at which membrane potential the transition between the maximum and minimum states of conductance occurs, V_s is the slope of the G/G_{max} curve and a measure of the sensitivity of the currents to variations in membrane potential. I_{init} is the initial current, and I_{final} is the final current after rundown. Data is represented as mean ± SE.

Lily	I_{SS}	A1 (kS)	A0 (kS)	V_h (mV)	V_s (mV^{-1})
wt	I_{init}	0.13 ± 0.01	1.30 ± 0.08	107 ± 9	69 ± 6
	I_{final}	0.13 ± 0.01	1.67 ± 0.17	155 ± 17	83 ± 7
	$I_{pHo\ 6.8}$	0.28 ± 0.04	1.29 ± 0.13	100 ± 18	90 ± 17
	$I_{pHo\ 7.2}$	0.49 ± 0.01	1.07 ± 0.06	109 ± 12	55 ± 7

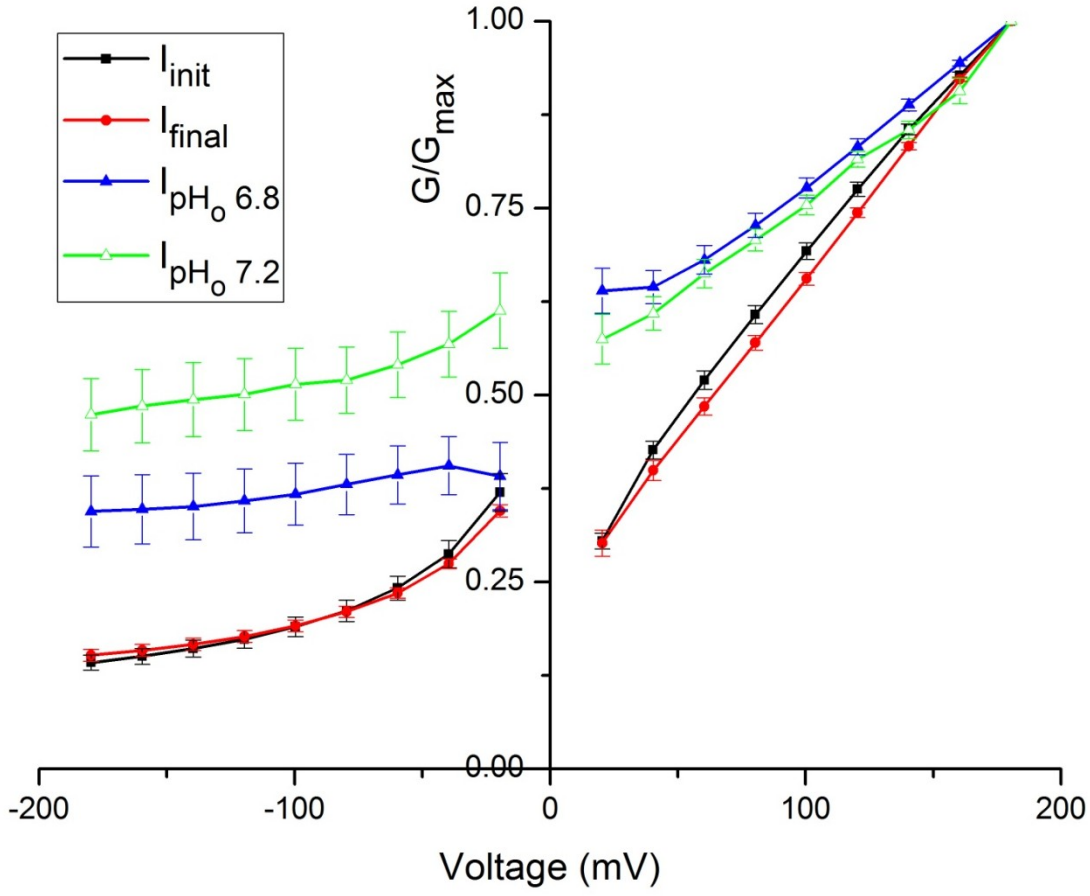

Figure 35 – Normalized average chord conductance curves of *Lilium longiflorum* wild type steady states currents before and after rundown, and after rundown under two different extracellular pH conditions.

On the other hand, the chord conductance curves for the currents elicited with different external pH show a similar effect to what was observed in *Arabidopsis*, with an increase in A0, which coordinates with the increasing negative currents under external alkalinization. Looking at the fit parameters however, we also observe that the Vh parameter decreases, as in the case of *Arabidopsis* with increasing external pH. However, in *Lilium*, the slope factor also appears to decrease under these conditions, which is the opposite of what was observed for the *Arabidopsis* currents. Once more, this confirms the fact that despite external pH regulating both species anionic currents, the mechanism by which it does so, appears to be different between species.

Overall, these experiments have highlighted the conserved role of pH in regulating anionic currents in pollen. However, the effect pH has in each species anionic currents appears to be distinct, which might reflect the different nature of anionic channels present in each species pollen plasma membrane, as it would appear, that in *Lilium*, there is no H^+/anion co-transporter activity for instance. Since both species also have different environments to operate, it is to be expected that the regulation of these currents to be also particular for each of them.

Results - Part II

Spatial and temporal patterns of the extracellular ionic fluxes of *Nicotiana tabacum*

The specific properties of the anionic currents here presented in this thesis, evidence the complexity of regulation and behaviors of this specific type of ionic transport in pollen. While the relationship between anions and pH was also shown, they are part of a larger network of interactions that involves other ionic transports and are closely linked to pollen tube growth. By using the vibrating probe (an ion-specific self-referencing technique), it has been possible to extensively map different ions, such as H^+, Ca^{2+}, K^+ and Cl^-/anions along different sites of growing pollen tubes. These studies have shown a distinct and polarized distribution of each ionic flux (Figure 36). Each ion has a specific spatial pattern distribution. This in turn generates a global ionic current, taking in to account all the measurable ionic fluxes, that is also polarized and as a strict spatial pattern.

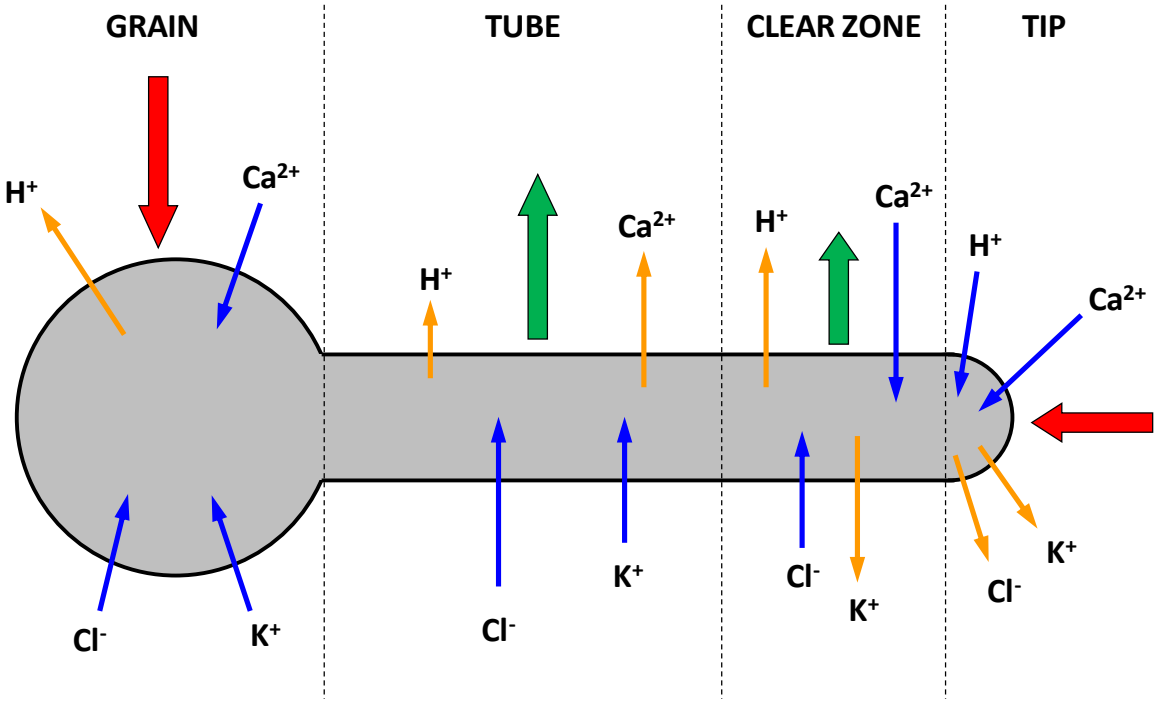

Figure 36 – Overall ion flux distribution and net ionic current on pollen tubes. Blue arrows refer to ion influx, yellow arrows to ion efflux. The red and green arrows refer to the net ionic current.

These ionic currents are essentially dominated by either Cl^- at the tube tip or by K^+ at the pollen grain, where their flux magnitude far surpasses that of the other ions.

Understanding the role of the anion currents previously measured in the context of the growing of the pollen tube, requires us to understand how all these different fluxes are interconnected.

In some species and under certain conditions, the tip-focused fluxes often exhibit oscillatory behaviors, with a similar period to that of the apical growth, further reinforcing the link between these ionic fluxes and growth. It should be noted that all these fluxes have been shown to be essential for pollen tube growth, since disruption of any of these ionic fluxes impairs pollen tube fitness, disrupting the internal gradients, stopping growth and causing premature pollen tube burst or growth malformations and development. Furthermore all ionic fluxes show periods of oscillation similar to growth, although with distinct phase delays (Holdaway-Clarke et al., 1997; Messerli et al., 1999; Feijó et al., 2001; Zonia et al., 2002; Holdaway-Clarke & Hepler, 2003). On the other hand, non-oscillatory ionic fluxes have been measured from the grain and along the tube shank (Feijó et al., 1999; Moreno et al., 2007).

Many of these studies were performed in growing pollen tube of *Lilium longiflorum*, having been extensively characterized. Here we present an approach to a different species, *Nicotiana tabacum*, and a comparison between their fluxes. This species was chosen as a middle point between *Lilium* and *Arabidopsis*, in terms of pollen grain and tube size, and for the fact of also being a eudicot, as *Arabidopsis*. *Arabidopsis* pollen was not tested due to its small grain and pollen tube size.

Dynamic efficiency of the Vibrating Probe

For this characterization, a *de novo* assessment of the vibrating probe calibration and dynamic efficiency was undertaken, as described in the Materials and Methods section. By using different artificial sources the relative dynamic efficiency of the vibrating probe was mapped for each of the ions used, taking in to account different properties of the pipette size, LIX column, pipette opening size, vibrating excursion and frequency. From these tests, a profile of relative efficiency could be made that allowed to correct the flux measurements taking in to account the properties of the vibrating probe sensibility to different concentrations (Figure 37).

Previous reports on these ionic probes efficiency had stipulated fix values for their efficiency. Still, based on our results it's clear that these probes have highly variable sensitivity depending on the concentrations they are measuring, and for an in depth quantitative analysis of extracellular ionic fluxes it is important to take this in to consideration to correct the measured values. Still, under certain ranges of gradients, our data still coincides with the published efficiency values, particularly when taking in to

account the usual range of potential that these probes are measuring in the case of the pollen tube. The published values were of 80% for H^+, 50% to Ca^{2+}, 70% for K^+ and there was no reported value for the Cl^- probe. With our data these values, within the same ranges, fall in the order of 79 ± 2%, 59 ± 4%, 57 ± 4% and 43 ± 6% respectively for H^+, Ca^{2+}, K^+ and Cl^-.

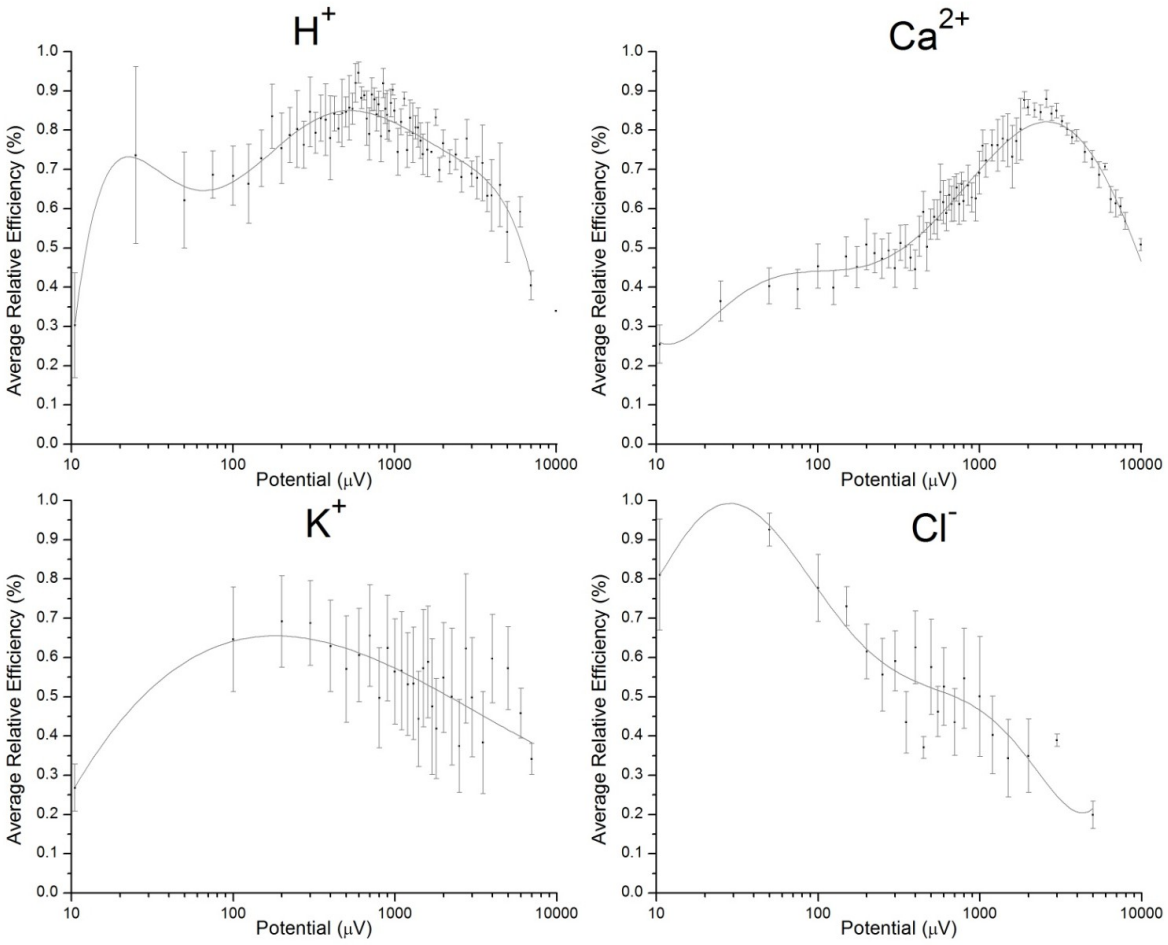

Figure 37 – Average relative efficiency for the vibrating probe for different ions in terms of measured potential difference. Black lines are a high level polynomial fit.

Nicotiana tabacum extracellular ion fluxes

With this done, we then proceeded to measure the ionic fluxes in growing pollen tubes of *Nicotiana tabacum*. Sample traces for each of the ions tested can be seen in Figure 38, measured near the tip of healthy growing pollen tubes, and denoting the presence of oscillatory influxes of H^+ and Ca^{2+} ions and efflux of K^+ and Cl^- ions, comparable to what has been observed for other species. A reference measurement was also performed for

each measurement at a region of the Petri dish devoid of pollen tubes or grains, as a control and is shown in the traces too. The H^+ and Ca^{2+} probe has a very good noise to signal ratio, making every measurement much more stable and simple then the other two ions that are much more difficult to obtain stable probes.

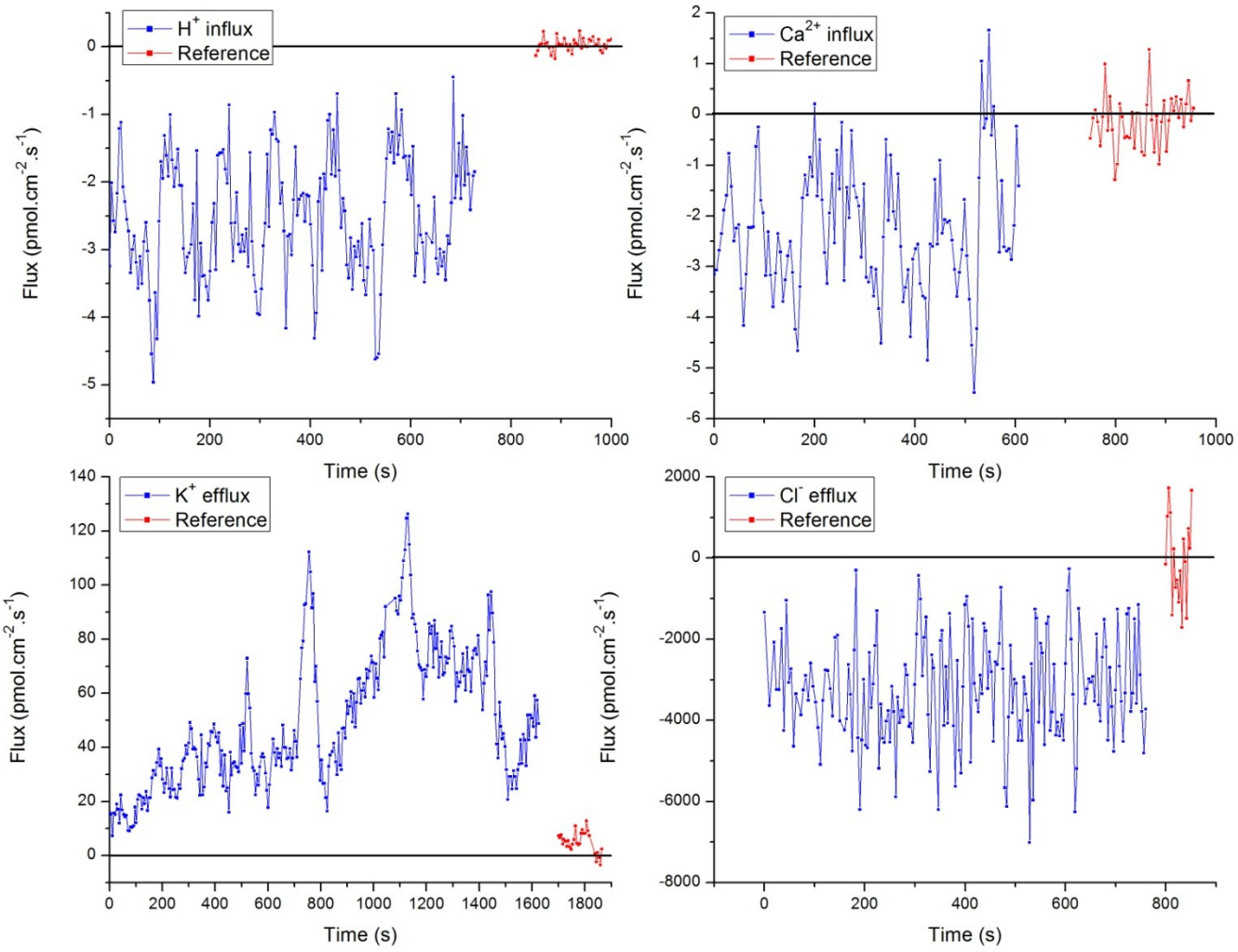

Figure 38 – Sample traces for each of the major extracellular fluxes in growing pollen tube of *Nicotiana tabacum* measured at the tip of a growing pollen tube, along with a reference measurement for each of the ions tested.

Comparing to the better studied *Lilium* pollen, the *Nicotiana* ionic fluxes show a few noticeable differences, with some retained features as well. The spatial distribution and net flux direction of all the different ionic extracellular fluxes is retained across species. Their flux amplitudes however, are clearly different. There seems to be a conserved mechanism regarding the ionic fluxes between species that emphasis H^+ and Ca^{2+} influx at the tip of the pollen tube with efflux of K^+ and Cl^- ions. Of particular interest in the tip is the presence of a large efflux of Cl^- that far exceeds the amplitude of all the other ions measured at the tip. Furthermore, taking in to account the global ionic currents generated

by these net fluxes, two distinct domains are present, creating two electric dipoles, a small one between tip and the tube, and another between the grain and the tube.

Despite the smaller pollen tube size of *Nicotiana*, its ionic fluxes are in average larger than the ones measured in *Lilium* (Table 32). These fluxes demonstrate plenty of variability between replicates, which can also correlate with length and growth speed of pollen tubes, but in average, their fluxes, are within the minimum and maximum values shown.

Table 32 – Comparison between tip ionic fluxes and main oscillation periods from growing pollen tubes of *Nicotiana tabacum* and *Lilium longiflorum*.

		Fluxes (pmol.cm-2.s-1)		Oscillation Period (s)	
		Min	Max	Primary	Secondary
N. tabacum	H^+	-1	-15	125	88
	Ca^{2+}	-1	-30	123	86
	K^+	25	400	225	123
	Cl^-	-1000	-5000	140	76
L. longiflorum	H^+	-1	-10	31	67
	Ca^{2+}	-7	-90	30	67
	K^+	30	200	29	59
	Cl^-	-200	-4000	15	10

Furthermore, the fluxes measured at the pollen tip normally oscillated, as mentioned before, while in other regions no oscillations are detected in ion fluxes. While the periodicity of these oscillations is not always regular, displaying a wealth of behaviors, it is common to have two main period components that dominate each series. By applying both Fourier and Wavelet analysis, using the advantages of both different analysis techniques to complement each other, these oscillations were analyzed. As can be seen in table 32, the main periodicity of flux oscillation in both species varies substantially. Nonetheless, within the same species, the periodicity of each ionic flux remains constant. The exception being Cl^- in *Lilium* and K^+ in *Nicotiana*, whose periodicity appears to be altered, halved in *Lilium* and doubled in *Nicotiana*, respectively.

Spatial and temporal distributions of extracellular ion fluxes and their oscillatory components

At the clear zone, and as we progress towards the tube shank, all fluxes inverted their net flow direction, which might be simply an indication of the difference in membrane potential between the tip and the rest of the pollen tube. This transition is here shown for both H^+ and Ca^{2+} ions, due to the good signal-to-noise ratio of these probes. By using an altered protocol for the vibrating probe that consisted in measuring multiple points along the pollen tube shank, in one single measurement it was possible to make a more detailed map of their fluxes spatial distribution along the length of the growing pollen tube. This was also used to measure different points surrounding the pollen tube tip, instead of the traditional position right at the apex. By design a protocol that allowed to measure in a quart of a circle, it allowed us to get measurements at different points, from the tip until the sub-apical region. This approach allowed us to interpolate the neighboring measurements and make a more complete map of the spatial variations of these two ionic fluxes (Figure 39).

With this type of measurement, the obvious trade back is losing temporal resolution and potentially increasing the vibration in the medium, which could result in the dissipation of local gradients. Taking this in to account, the number of excursion for successive measurements was adjusted, so that no effect on the local gradients could be detected from a single measurement or this multiple measurement. The strong advantage of this approach is allowing for a greater spatial resolution that is not normally used in pollen tubes.

For instances, more accurate measurement of the actual point of the flux inversion can be made, being estimated to occur between 20 to 30 µm away from the tube tip for both studied ions. However, the most important result from this approach is the ability to have a near continuum profile of the extracellular fluxes in a growing pollen tube, instead of just discrete measurements at specific key points. This allows the understanding of how these net fluxes change across the different membrane domains, how quickly, and how they can relate to each other.

One surprising result was that the H^+ flux measured at the tip of the pollen tube is not actually the maximum point of influx for H^+ in the growing pollen tube of *Nicotiana tabacum*. The maximum point of influx is actually shifted from the tip by an angle of 67.5º. In fact, the H^+ flux then suddenly drops with the approaching sub-apical region, due to the strong presence of the H^+-ATPase in that region, as can be seen by the strong efflux after 30 µm from the tip. This does not occur with the Ca^{2+} fluxes. Their region of maximum

influx is indeed located right at the front of the tube pollen tip, and this influx gradually decreases up to the 20 µm region away from the tip when it then reverts to a net efflux.

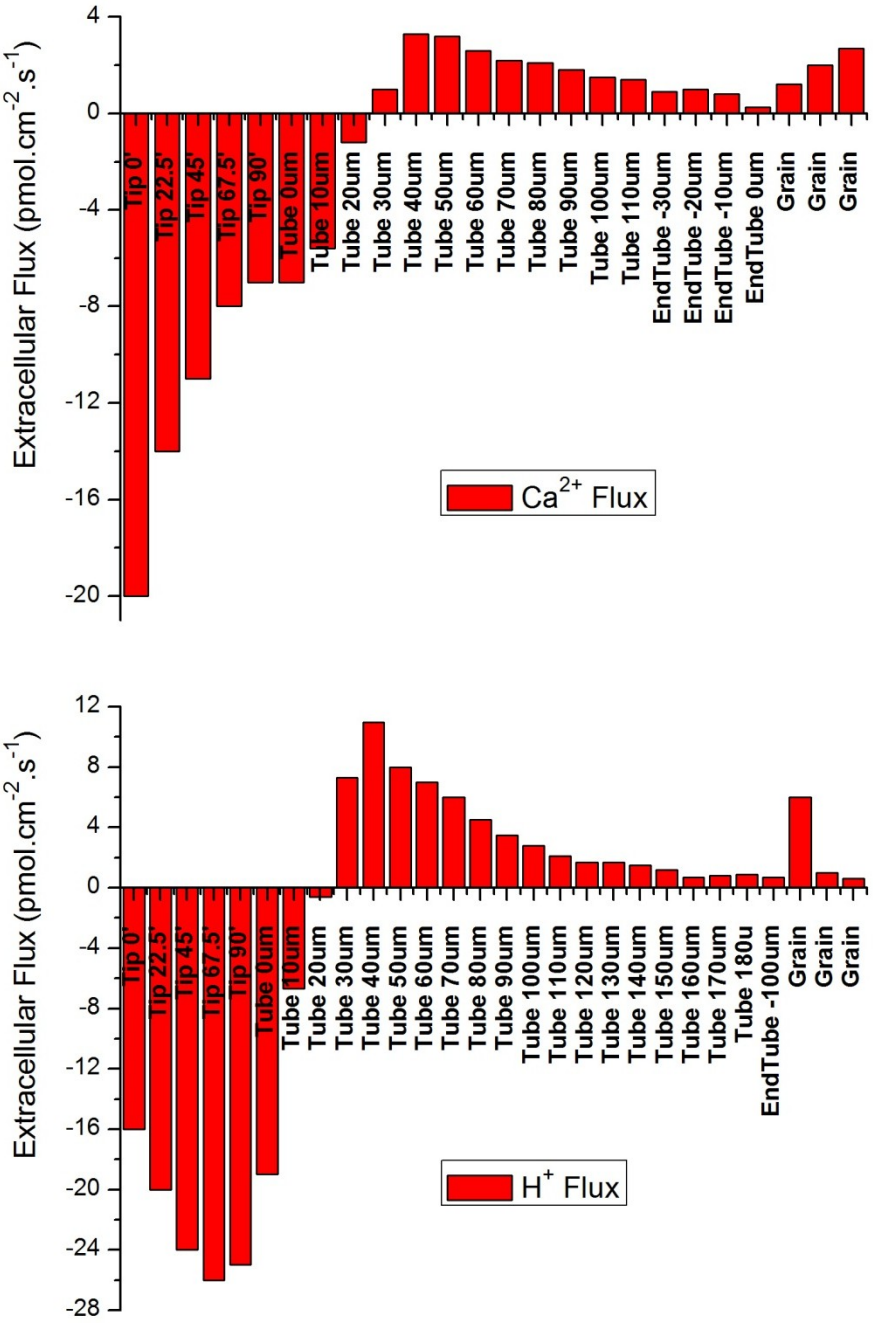

Figure 39 – Detailed map of extracellular fluxes of Ca^{2+} and H^{+} in *Nicotiana tabacum* growing pollen tubes. The different measurements at the tip were done around at the tip, with the position at 0º at the front of the growing pollen tube, and the others gradually going to the side of the tip. The following measurements were made alongside the pollen tube shank, measured in relation to the distance to the tip.

Another important information that can be analyzed with this type of approach is the frequency of different fluxes at different positions. It is commonly assumed that only at the tip of the pollen tube do the ionic fluxes oscillate, as this has been evidenced by multiple reports. However, nothing is know about where exactly and how do these ionic fluxes stop oscillating away from the tip. Are they localized solely at the tip, or also at the start of the shank? Are they still measurable after the flux inversion region, or only before? While our data cannot answer these questions yet, it can some shed light to the complexity of these phenomena and provide a method to address this in the future.

By analyzing measurements from the same pollen tube at two different points on the tip - one at the apex and another at a 90º angle, both still under influx regime of H^+ - we have been able to identify differences in the periodicity of the oscillations in those fluxes (Figure 40). Our data shows that one of the main periodic components of the oscillations is lost at 90º angle from the tip. Similar results were also obtained for the Ca^{2+} extracellular oscillations in the same conditions, also evidencing the loss of one oscillation component at 90º position away from the tip.

Taken as a whole, these experiments have evidenced that each specific species has a specific signature in terms of ionic fluxes and their oscillations at the tip that may reflect different regulatory mechanism and roles for each ion in pollen tube growth, and may be evidence of different channels present in the plasma membrane of pollen. These are all likely to be an indication of the different adaptation mechanism each species has to undergo for a successfully fertilization.

Overall, we have post forward a novel optimized efficiency measurements for the commonly used vibrating probes and have presented an overall perspective on the ruling ionic fluxes in a new species, *Nicotiana tabacum*. The main result is the persistence of same spatial distribution between the different fluxes that appears to be preserved between species, while their flux magnitudes and oscillatory regimes change. We propose that this spatial distribution is crucial for the maintenance of polarized growth, while the specificity of flux oscillation and intensity are fine-tuned for each individual species to better adjust to each different specific environments they should encounter in their path to fertilization.

Finally, we have also been able to map extensively two of these ionic fluxes along the growing pollen tube, from tip to grain. This approach has revealed further details that had not been address so far. For once, the distribution of ionic fluxes is not entirely focused on the tip, at least in the case of H^+, with its local maximum influx region being shifted towards the side of the tip. This is an intriguing result, as this region is highly active in endocytosis, while the tip is mainly engaged in exocytosis, and these differences may be

linked. Furthermore, the frequency components of the flux oscillations are not preserved across the influx region of H^+ and Ca^{2+} on the tip, with differences between the different regions. The exact nature of these differences should be addressed, as they are likely to reflect significant different mechanism underlying them.

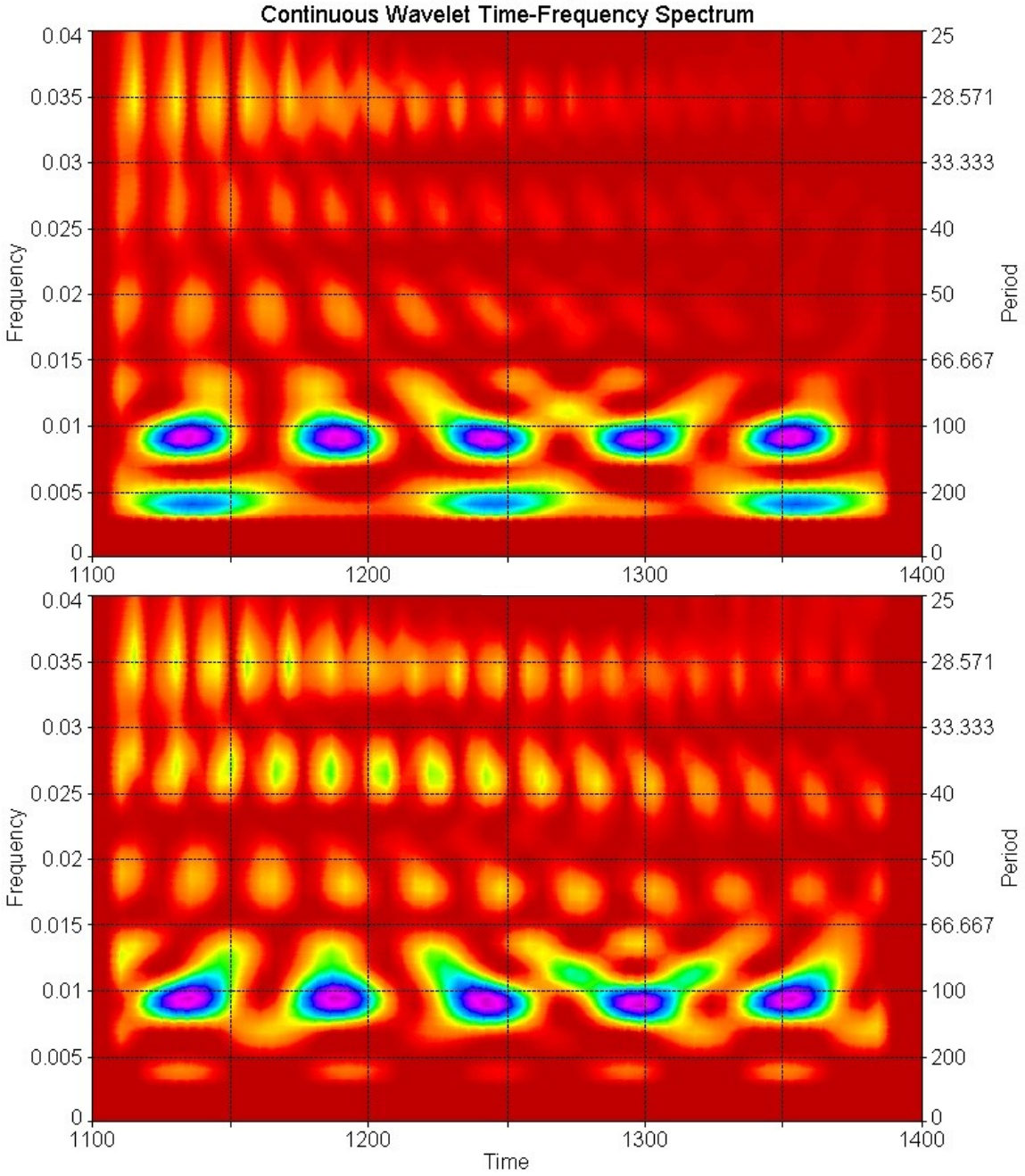

Figure 40 – Continuous wavelet analysis of H^+ extracellular fluxes at the tip of a growing pollen tube of *Nicotiana tabacum* measured at two different positions, one at the apex (top spectrum) and at 90º from the tip, near the start of the sub-apical domain (bottom spectrum).

Discussion

The anionic currents of *Arabidopsis thaliana* pollen grain protoplasts have been previously described (Tavares, 2011). A pioneer work in identifying the anionic currents in the plasma membrane of *Arabidopsis* pollen protoplasts, this paper also paved the way for the molecular characterization of the anion channels present in pollen that are responsible for these currents.

In this thesis, the basic characterization of the anionic currents is expanded, by focusing and comparing the results obtained via the instantaneous component of the activation currents with the steady state currents, and looking closer at the tail currents. This analysis was used across all experiments performed.

The anionic currents response to pH is completely novel in this context, while the experiments with different [Cl^-] and [NO_3^-] had been partially done before, but again further expanded in their scope. Furthermore, a full electrophysiological characterization of a CaCC gene mutant line is presented. This work provides, for the first time to our knowledge, the identification of a putative Cl^- transporter in the plasma membrane of *Arabidopsis* pollen with a clear electrophysiologic phenotype.

From the initial work done in our lab the existence of anionic currents in pollen grain protoplasts of *Lilium longiflorum* (Tavares, 2011; Tavares et al., 2011) and *Arabidopsis thaliana* (Tavares, 2011) was demonstrated. These previous works showed an $[Ca^{2+}]_i$ regulation of the anionic currents in both species. Different current populations were identified based on their electrophysiological properties and by pharmacology. The three populations identified were all anionic currents. Of this population, one was lost during a lengthy rundown process, while the other two persisted after rundown. The two components that remained after rundown were further distinguished by pharmacology, where one of them was inhibited by the application of NPPB while the other was not.

Despite having successfully identified these anionic currents and confirming them to be anionic in nature, as well as regulated by intracellular [Ca^{2+}], there were still a few parameters and experimental results that deviated from the expected values if assuming that only anions were being transported. Two of those results were the fact that the observed reversal potential shift with decreasing extracellular [Cl^-] failed to reach the calculated Nernst equilibrium values, which could be explained partially by the NO_3^- contribution, but there was also the fact that the instantaneous and tail currents (which

were not extensively characterized on that initial approach) often shifted to unexpected values far away from the calculated equilibrium potentials.

It was based on these observations that the initial hypothesis for this thesis was made. The hypothesis being that pH or H^+ could somehow regulate the observed anionic currents in pollen grains plasma membrane, and that the observed differences would arise from H^+ transport and/or pH regulation. This hypothesis was based in line with recent reports highlighting the importance of H^+ as a novel second messenger (Prolo & Goodman, 2008), along with several reports that have demonstrated that previously putative anionic channels in plants are actually H^+/Cl^- transporters (Accardi & Miller, 2004; Scheel et al., 2005; Pusch et al., 2006). This, together with the knowledge that pH can regulate the activity of numerous other channels (Johannes et al., 1998; Carpaneto et al., 2005; Colcombet et al., 2005; Picollo et al., 2010; Orhan et al., 2011; Ortiz-Ramirez et al., 2011), and the well established presence of distinct domains of H^+ influx and efflux in the growing pollen tube plasma membrane along with distinct intracellular pH domains (Feijó et al., 1999; Certal et al., 2008), served to consolidate our hypothesis.

This hypothesis was first tested on *Lilium longiflorum* pollen, due to easiness of use and availability. Lily pollen is also much easier to patch then the smaller *Arabidopsis* pollen, and although there are subtle differences and regulation between the two species, they both evidence similar global behaviors in terms of anionic currents. After the preliminary results evidenced a strong effect to external pH, the work shifted towards *Arabidopsis* to confirm similar response and to integrate these results with the characterization of mutant lines of putative anionic channels that were being generated in our lab at the time.

One such aspect that bonds together all these current components is the process of current rundown that is observed in all of them, with nearly identical magnitudes between them. This process of rundown has also been described to occur for many other types of currents across many different cell systems (Marty & Neher, 1995), including anionic channels in plants (Becq, 1996; Binder et al., 2003; Tavares et al., 2011). While the nature of this process is so far unknown, it has been shown before to be $[Ca^{2+}]_i$ dependent in *Lilium longiflorum* pollen grain protoplast (Tavares et al., 2011), where the duration and magnitude of the rundown process was shown to increase under higher $[Ca^{2+}]_i$. While under our experimental conditions in *Arabidopsis thaliana*, when the effect of internal pH was tested, no significant effect to the rundown process was observed.

It is likely that the instantaneous and tail currents reflect finer aspects of the anionic currents that are not observed in steady state. Sudden changes in membrane potential can induce transient fluxes to counter-balance. For instance, in the tail current, sudden

changes in plasma membrane depolarization induce a large increase in the anionic currents amplitude, particularly at the expected physiological range for the plasma membrane potential. These effects are obviously expressed in the currents slope conductance, reflecting their increased or decreased conductance and consequently changes to their current rectification.

However, one of the most easily observable differences between the three current components is their reversal potential. They differ substantially from the expected equilibrium potentials for the permeable ions in solutions, namely that of Cl^-, the main permeable ion in our solutions. While the steady state current reversal potential remains close to the expected values, both transient currents - instantaneous and tail currents - shift away from that reference value, which raised the question as to what exactly is being transported besides anions in those currents.

Under control conditions, the instantaneous current reversal potential is systematically more negative then the steady state, while the tail current reversal potential is shifted to more positive values. After rundown, this difference tended to be slightly more accentuated. The plausible explanation for these differences would reside in the other permeable ions in solution. However, by design, the solutions in use have few other permeable ions present. Moreover, those that are present, are at very low concentrations or their conductivity blocked by the presence of specific blockers, as is the case of Ca^{2+}, for instance. One notable exception is the unavoidable presence of H^+ in solution.

In fact, H^+ transport could account for the tail currents potential reversal shift alone, as the expected shift for a passive H^+ current, under our control conditions, would be a shift to more positive values. This H^+ leak current would be driven by depolarization, and quickly dissipated within milliseconds, and could reflect gating properties of the anionic channels, as in those instances before the protein conforms to the new membrane potential a passive current of H^+ could leak through, leading to the observable shift in the reversal potential of the tail currents.

However, this passive flux of H^+ cannot explain the shift in the instantaneous current reversal potential, as it would suggest that H^+ would be flowing against their electrochemical gradient. However, the presence of the H^+-ATPase in the plasma membrane of pollen tubes (Certal et al., 2008), known for the maintenance of an alkaline band in growing pollen tubes by actively pumping H^+ out of the pollen tube against their gradient, could account for that (Chapman, 1978; Glitsch & Tappe, 1995). It is plausible that under hyperpolarization conditions, that would mimic the typical conditions in which the H^+-ATPase is expected to be active in the sub-apical and shank regions of the pollen tube (as opposed to the depolarized pollen tip, where the pump is not present at all), a

transient shift could be driven by the H^+ pump resulting in the observed shift in reversal potential, opposite of what would be expected for passive H^+ transport.

When the extracellular pH changes, several changes are observed in the anionic currents, across the three different components of the currents. With increasing pH all current components increase their magnitude and start progressively losing their outward rectification. While these changes are not identical between the three components, all evidence the same trends of amplitude increase and balancing the forward and backward conductance, this is achieved mainly by a greater increase of the backward conductance, compared to the forward. Interestingly, by lowering the external pH a similar effect is also observed, and not a reduction of the currents' amplitudes, suggesting a biphasic effect of pH on the regulation of the anionic currents, with a current amplitude low somewhere between 5.8 and 6.2. This could also suggest a change in conformation of the anionic transporters under acidic external pH, as has been described before for other anionic channels in plants (Matsuda et al., 2010), where their co-transport activity becomes uncoupled at acidic external pH conditions. Furthermore, all the observed effects were reversible, which implies that the plasma membrane and channel proteins were not denaturated in the process.

Since the differences observed between these currents could be driven by H^+ transport, it is interesting to observe that the three current components become similar between themselves at higher external pH, by abolishing the pH gradient across the plasma membrane, according to the results from their conductances and current amplitudes.

This is even more easily observed looking at their reversal potentials, where upon bath alkalinization all reversal potentials get closer to zero, the equilibrium potential for Cl^- and the new equilibrium potential for H^+. This is a strong evidence for the existence of H^+/anion co-transport in the plasma membrane of *Arabidopsis* pollen, and confirms the hypothesis that H^+ are indeed responsible for the observable differences detected on the anionic currents.

Still, it should be noted that the majority of effects of this co-transport system is only observable transiently in the anionic currents, as its effect on the steady state currents is mostly negligible. Nonetheless, under specific conditions, these effects can have a larger impact in the pollen tube, as it can be seen in the *cacc* mutant, where the absence of this gene renders the anionic currents in the pollen plasma membrane insensitive to external pH changes, which could have detrimental effects on pollen tube fitness under specific pH conditions.

When looking at the mutant line of the At1g73030 gene, a TMEM16A homologue, identified as a Ca^{2+}-activated Chloride Channel (CaCC), while there's no discernible macroscopic phenotype in this homozygous mutant line, a clear electrophysiological phenotype arises, especially when the pH conditions are changed. There are also differences under control conditions, as evidenced by the data here presented, showing an overall increase in current amplitude and a longer period of rundown.

The most remarkable feature of this mutant line though is it absence of response to external pH, where currents mostly keep their parameters unchanged under different external pH, without changes to amplitude, conductances, rectification or reversal potentials. These results indicate that by mutating this gene, the anionic currents response to external pH was essentially abolished, which would suggest that this response would be mediated primarily by this anionic co-transporter.

The *cacc* mutant line's anionic currents are not H^+ dependent and are not modulated by external pH. The observed increase in currents amplitude for the initial currents, is possible because the CaCC may be acting as an anionic co-transporter, transporting anions against their ionic gradient, thus, its absence would support larger overall observable currents. Plus, the observed longer rundown periods could indicate that the CaCC could be competing for the same unknown effector that is responsible for the rundown of the currents, as in its absence, it would take longer for this effector to be depleted.

Given the important role of external pH on the anionic currents, it was expected to find that internal pH had an equally important role in regulating the anionic currents. The conditions tested, mimic to some extend the two major intracellular domains in terms of pH likely to be present inside a pollen tube, an acidic tip and an alkaline shank. Our results evidence a large increase in anionic current under more acidic internal pH conditions (pH_{in} 6.8), in line with what had been observed in extracellular ionic fluxes in the growing tube, with massive anionic fluxes at the acidic tip (Feijó et al., 1999; Zonia et al., 2002). What is interesting is that the *cacc* mutant does not have the same type of response as in the wild type. Despite a slight increase in current amplitude in the mutant, it fails to reach the same levels that it achieves in the wild type. What our data seems to suggest is that under internal acidic conditions, the CaCC gene may actually be transporting anions along their gradient, thus contributing to the observed increase in anionic current, which in the *cacc* mutant, results in a reduced current amplitude, contrarily to what's observed under control conditions (pH_{in} 7.2).

Besides the effect in current amplitude, internal pH does not seem to directly affect the rundown process, with the same percentage of current lost during rundown under both conditions. Nonetheless, internal pH seems to be modulating the channels conductance,

and there is a slight shift in terms of reversal potentials, that further support the idea that the CaCC is co-transporting H^+ along the plasma membrane. Taken as a whole, this demonstrates the complex role of pH in regulating the anionic currents and the CaCC gene, with a wide array of effects.

The regulation by pH of the currents is patent, but is not the only modulator of these currents, as evidenced by the experiments with changing external [Cl^-]. While many of the parameters do change accordingly, as one would expect for changes to the main permeable ion concentration, most of the currents at the physiological range of membrane potential evidence a strong regulation of their activity by external [Cl^-], which has been observed for other anion channels as well (Garrill et al., 1994; Skerrett & Tyerman, 1994; Schmidt & Schroeder, 1994; Thomine et al., 1997). This could be part of a feedback loop to activate or deactivate the anionic channels, depending on the external conditions, even a way to modulate the channels activities depending on their localization on the pollen membrane. For instances, at the pollen tube tip, the anionic efflux would generate a local increase in anionic concentration, that would in turn potentiate the activation of the anionic currents. This could be part of the growth and ionic fluxes oscillations previously reported in some growing pollen tubes (Michard et al., 2009).

In the *cacc* mutant, there is no observable difference in response to external [Cl^-] changes compared to wild type, further reinforcing that this protein's role primarily linked to pH, rather than [Cl^-] when it comes to regulation. Still, an interesting effect could be observed here, pointing out to an apparent saturation of the anionic currents with increasing external [Cl^-], with halted changes in amplitude, conductances and reversal potentials. This being shown in the *cacc* background, evidences that the remaining putative anionic channels might be predominantly other facilitated transport proteins, rather than just ionic channels.

While the response to [Cl^-] changes is similar between wild type and *cacc* mutant, the same is not true for [NO_3^-] changes. In the wild type, the anionic currents do not seem to distinguish from either Cl^- or NO_3^-, transporting both under similar conditions, as is evidence by the relative permeability between the two anions, that falls very close to be 1, with just a slight preference towards NO_3^- over Cl^-. However, in the *cacc* mutant background, the currents under high external [NO_3^-] are severely reduced, up to a third of their equivalent amplitudes under high external [Cl^-] in the mutant. In fact, this result would at first glance suggest that the substitution of Cl^- by NO_3^- in the bath medium would mimic the previous experiments of external [Cl^-] reduction. However, no changes were observed to the reversal potential in this anionic substitution, and more importantly, the anionic currents amplitudes in the *cacc* mutant under high external [NO_3^-] are equal to the

ones obtained under similar conditions for the wild type. These results suggest that both ions are still being transported across the membrane and both contributing to the equilibrium potential, thus keeping it at stable value. Furthermore, it presents evidence that the CaCC gene is not acting as an unspecific anionic co-transporter, but as a specific H^+/Cl^- co-transporter.

Finally, looking back at the results from *Lilium longiflorum*, plenty of differences arise with *Arabidopsis*, despite both evidencing outward rectifying anionic currents. Both species have strong anionic currents that undergo rundown with comparable lengths, which is surprising given the difference in volume from both protoplasts. Still, despite the rundown length being the same, the percentual drop in currents is strikingly different between the two species. This indicates that the nature of the channels present in both plasma membrane's must also be different, with the channels present in *Lilium longiflorum* being less dependent on the unknown effector responsible for the rundown of currents than those of *Arabidopsis*.

Regarding the external pH response of *Lilium* anionic currents, quite a few changes are also observed. Noticeably the effect of external pH is not consistently observed across all current components, opposed to what has been seen in *Arabidopsis*, where all current components always show the same tendency. Still, the overall effect appears to be of an increase in current amplitude at negative potentials, and a decrease under positive potentials, which again differs from *Arabidopsis*. Nonetheless, it is obvious that external pH has an effect on the anionic currents of *Lilium longiflorum*, with different effects to the different current components, and with a broader range of effects localized in the physiological potentials.

Another important difference is the reversal potentials of the currents in *Lilium*, which present much less pronounced shifts than in *Arabidopsis*. What's more, there does not appear to be a H^+ driven adjustment of the reversal potentials with increasing external pH, as was observed in *Arabidopsis*. This is evidence that the proposed co-transport for *Arabidopsis* should not be present in the plasma membrane of *Lilium* pollen.

All in all, pH seems to have a conserved role in regulating anionic currents in pollen plasma membrane, in both eudicots and monocots plants, though the finer aspects of this regulation changes substantially between the two studied species, such as the presence of a H^+/anion co-transport system in *Arabidopsis* and its absence in *Lilium*. This was also observed when the extracellular fluxes of *Nicotiana tabacum* were measured and compared with the ones from *Lilium longiflorum*, evidencing conserved mechanisms, namely in the spatial distribution of the extracellular fluxes for all the ions, but also revealing a degree of variability between these same fluxes, in terms of intensity and

oscillatory periodicity. That again, might be an indication of the specific adaptation each pollen tube requires for successful fertilization in each species.

On a final note, the absence of a macroscopic phenotype from the *cacc* mutant line, and the lack of a statistical significance on seed set phenotype in the competition assays, reveals that this specific gene plays only a small role on the overall pollen development. The most likely scenario is that its function might be limited to a very specific set of conditions, and otherwise its function could be accomplished by other similar channels or transporters.

We have shown in this work that the anionic currents in pollen protoplasts are highly regulated by pH, both internal and external. Furthermore, a co-transport system was also identified, transporting both H^+ and Cl^-. This transporter was identified molecularly, being the first positive identification of an anionic transporter in pollen plasma membrane. Besides the regulatory role of pH, it was also shown that extracellular $[Cl^-]$ concentrations have a regulatory effect on the anionic currents, which along with the previous results from other works that evidenced that $[Ca^{2+}]_{in}$ also regulates these currents, gives rise to a rather complex regulatory network. Our data also suggests that other anionic facilitated transport mechanism may be active in the plasma membrane of pollens as well.

The question remains as to the molecular identity of all the other anionic channels/transporters, as some of the most likely candidates have not given satisfactory results. In the case of the CaCC gene, its phenotype was rather selective to a precise set of conditions; it is likely that the same may happen for many of the others unidentified genes, thus adding to the difficulty of identifying them. Given their central role in pollen tube growth and intricate regulatory network of these currents, it is plausible to assume that strong compensatory mechanism should be in play to counteract any missing component, shadowing any possible mutant phenotype. Alongside that, it seems our knowledge of anion channels in general is still blooming, with recent discoveries highlighting rather complex and unexpected behaviors for otherwise presumably simple channels (Baukrowitz et al., 1994; Miller, 2006; von der Fecht-Bartenbach et al., 2007; Silva & Gerós, 2009; Conde et al., 2010). All this taken in to account, could be reason enough to understand why their identification in pollen has been particularly elusive. We hope that our work opens the door to further discoveries and to extend our understanding of the mechanisms underlying pollen tube growth and development.

Another useful approach would be the use of the vibrating probe technique to complement the patch clamp experiments, taking advantage of both techniques specific strengths. Our results obtained with *Nicotiana tabacum* served mainly as a proof of principle of the power of this electrophysiological technique in measuring and detecting

phenomena that would be impossible to measure under patch clamp conditions. They also revealed complex patterns that had not been shown so far, evidencing conserved spatial patterns of flux distribution between different species, and specific differences that distinguish them significatively. Improving the quality of the ionic probes for anions would be extremely useful for this study in particular, to be able to map in greater detail the different domains for anionic extracellular fluxes. Even more important would be the ability to port these experiments to *Arabidopsis thaliana* and to take full advantage of all the molecular tools available. To be able to map the extracellular fluxes differences in the *cacc* mutant background with the wild type, for both anions and H^+, would provide further insight on the role of this gene in particular. This surely is one direction to extend our understanding of the anionic transport in pollen tubes and to help unravel the missing identity of the other channels present in the pollen plasma membrane.

Bibliography

Accardi A, Miller C. **2004**. Secondary active transport mediated by a prokaryotic homologue of ClC Cl- channels. *Nature* **427**: 803–7.

De Angeli A, Monachello D, Ephritikhine G, Frachisse J-M, Thomine S, Gambale F, Barbier-Brygoo H. **2006**. The nitrate/proton antiporter AtCLCa mediates nitrate accumulation in plant vacuoles. *Nature* **442**: 939–42.

Armstrong CM, Hille B. **1998**. Voltage-gated ion channels and electrical excitability. *Neuron* **20**: 371–80.

Artigas P, Gadsby DC. **2003**. Na+/K+-pump ligands modulate gating of palytoxin-induced ion channels. *Proceedings of the National Academy of Sciences of the United States of America* **100**: 501–5.

Axon Instruments. **1993**. *The Axon Guide*. Axon Instruments, Lda.

Baukrowitz T, Hwang TC, Nairn AC, Gadsby DC. **1994**. Coupling of CFTR Cl-channel gating to an ATP hydrolysis cycle. *Neuron* **12**: 473–482.

Becker JD, Feijó JA. **2007**. How many genes are needed to make a pollen tube? Lessons from transcriptomics. *Annals of botany* **100**: 1117–23.

Becker D, Geiger D, Dunkel M, Roller A, Bertl A, Latz A, Carpaneto A, Dietrich P, Roelfsema MRG, Voelker C, et al. 2004. AtTPK4, and Arabidopsis tandem-pore K+ channel, poised to control the pollen membrane voltage in a pH- and Ca2+-dependent manner. *Sciences-New York* **101**: 15621–15626.

Becq F. **1996**. Ionic channel rundown in excised membrane patches. *Biochimica et biophysica acta* **1286**: 53–63.

Berkefeld H, Fakler B, Schulte U. **2010**. Ca2+-Activated K+ Channels: From Protein Complexes to Function. *Physiological Reviews*: 1437–1459.

Binder K, Wegner LH, Heidecker M, Zimmermann U. **2003**. Gating of Cl- currents in protoplasts from the marine alga Valonia utricularis depends on the transmembrane Cl-gradient and is affected by enzymatic cell wall degradation. *The Journal of membrane biology* **191**: 165–78.

Boavida LC, Becker JD, Feijó JA. **2005**. The making of gametes in higher plants. *The International journal of developmental biology* **49**: 595–614.

Boavida LC, Vieira AM, Becker JD, Feijó JA. **2005**. Gametophyte interaction and sexual reproduction: how plants make a zygote. *The International journal of developmental biology* **49**: 615–32.

Borges FS, Gomes G, Gardner R, Moreno N, McCormick S, Feijó JA, Becker JD. **2008**. Comparative transcriptomics of Arabidopsis sperm cells. *Plant physiology* **148**: 1168–81.

Breygina MA, Matveeva NP, Ermakov IP. **2009**. The role of Cl− in pollen germination and tube growth. *Russian Journal of Developmental Biology* **39**: 157–164.

Breygina MA, Smirnova A V, Maslennikov M V, Matveeva NP, Yermakov IP. **2010**. Effects of anion channel blockers NPPB and DIDS on tobacco pollen tube growth and its mitochondria state. *Cell and Tissue Biology* **4**: 289–296.

Breygina MA, Smirnova A V, Matveeva NP, Yermakov IP, Yermako. **2009**. Membrane potential changes during pollen germination and tube growth. *Tsitologyia* **51**: 815–823.

Caputo A, Caci E, Ferrera L, Pedemonte N, Barsanti C, Sondo E, Pfeffer U, Ravazzolo R, Zegarra-Moran O, Galietta LJ V. **2008**. TMEM16A, a membrane protein associated with calcium-dependent chloride channel activity. *Science (New York, N.Y.)* **322**: 590–4.

Carew M a, Yang X, Schultz C, Shears SB. **2000**. Myo-Inositol 3,4,5,6-Tetrakisphosphate Inhibits an Apical Calcium-Activated Chloride Conductance in Polarized Monolayers of a Cystic Fibrosis Cell Line. *The Journal of biological chemistry* **275**: 26906–13.

Carpaneto A, Geiger D, Bamberg E, Sauer N, Fromm J, Hedrich R. **2005**. Phloem-localized, proton-coupled sucrose carrier ZmSUT1 mediates sucrose efflux under the control of the sucrose gradient and the proton motive force. *The Journal of biological chemistry* **280**: 21437–43.

Certal AC, Almeida RB, Carvalho LM, Wong E, Moreno N, Michard E, Carneiro J, Rodriguéz-Léon J, Wu H-M, Cheung AY, et al. 2008. Exclusion of a proton ATPase from the apical membrane is associated with cell polarity and tip growth in Nicotiana tabacum pollen tubes. *The Plant Cell* **20**: 614–634.

Chapman JB. **1978**. The reverse potential for an electrogenic sodium pump - a method for determining the free energy of ATP breakdown? *Journal of General Physiology* **72**: 403–408.

Chen Z-H, Hills A, Lim CK, Blatt MR. **2010**. Dynamic regulation of guard cell anion channels by cytosolic free Ca2+ concentration and protein phosphorylation. *The Plant journal : for cell and molecular biology* **61**: 816–25.

Colcombet J, Lelièvre F, Thomine S, Barbier-Brygoo H, Frachisse J-M. **2005**. Distinct pH regulation of slow and rapid anion channels at the plasma membrane of Arabidopsis thaliana hypocotyl cells. *Journal of experimental botany* **56**: 1897–903.

Colmenero-Flores JM, Martínez G, Gamba G, Vázquez N, Iglesias DJ, Brumós J, Talón M. **2007**. Identification and functional characterization of cation-chloride cotransporters in plants. *The Plant journal : for cell and molecular biology* **50**: 278–92.

Conde A, Diallinas G, Chaumont F, Chaves M, Gerós H. **2010**. Transporters, channels, or simple diffusion? Dogmas, atypical roles and complexity in transport systems. *The international journal of biochemistry & cell biology* **42**: 857–68.

Dean RB, Curtis HJ, Cole KS. **1940**. Impedance of biomolecular films. *Science (New York, N.Y.)* **91**: 50–51.

Durrett TP, Gassmann W, Rogers EE. **2007**. The FRD3-mediated efflux of citrate into the root vasculature is necessary for efficient iron translocation. *Plant physiology* **144**: 197–205.

Dutta R, Robinson KR. **2004**. Identification and Characterization of Stretch-Activated Ion Channels in Pollen Protoplasts. *Plant Physiology* **135**: 1398–1406.

Fairman WA, Vandenberg RJ, Arriza JL, Kavanaugh MP, Amara SG. **1995**. An excitatory amino-acid transporter with properties of a ligand-gated chloride channel. *Nature* **375**: 599–603.

Fan L-M, Wang YF, Wang H, Wu WH. **2001**. In vitro Arabidopsis pollen germination and characterization of the inward potassium currents in Arabidopsis pollen grain protoplasts. *Journal of experimental botany* **52**: 1603–14.

Fan L-M, Wang YF, Wu WH. **2003**. Outward K+ channels in Brassica chinensis pollen protoplasts are regulated by external and internal pH. *Protoplasma* **220**: 143–52.

Fan L-M, Wu W-H, Yang H-Y. **1999**. Identification and Characterization of the Inward K+ Channel in the Plasma Membrane of Brassica Pollen Protoplasts. *Plant Cell Physiol.* **40**: 859–865.

Von der Fecht-Bartenbach J, Bogner M, Krebs M, Stierhof Y-D, Schumacher K, Ludewig U. **2007**. Function of the anion transporter AtCLC-d in the trans-Golgi network. *The Plant journal : for cell and molecular biology* **50**: 466–74.

Feijó JA, Costa SS, Prado AM, Becker JD, Certal AC. **2004**. Signalling by tips. *Current opinion in plant biology* **7**: 589–98.

Feijó JA, Sainhas J, Hackett GR, Kunkel JG, Hepler PK. **1999**. Growing pollen tubes possess a constitutive alkaline band in the clear zone and a growth-dependent acidic tip. *The Journal of cell biology* **144**: 483–96.

Feijó JA, Sainhas J, Holdaway-Clarke TL, Cordeiro S, Kunkel JG, Hepler PK. **2001**. Cellular oscillations and the regulation of growth: the pollen tube paradigm. *BioEssays : news and reviews in molecular, cellular and developmental biology* **23**: 86–94.

Frietsch S, Wang Y-F, Sladek C, Poulsen LR, Romanowsky SM, Schroeder JI, Harper JF. **2007**. A cyclic nucleotide-gated channel is essential for polarized tip growth of pollen. *Proceedings of the National Academy of Sciences of the United States of America* **104**: 14531–6.

Garrill A, Tyerman SD, Findlay GP. **1994**. Ion channels in the plasma membrane of protoplasts from the halophytic angiosperm Zostera muelleri. *The Journal of membrane biology* **142**: 381–393.

Geiger D, Maierhofer T, Al-Rasheid K a S, Scherzer S, Mumm P, Liese A, Ache P, Wellmann C, Marten I, Grill E, et al. 2011. Stomatal closure by fast abscisic acid signaling is mediated by the guard cell anion channel SLAH3 and the receptor RCAR1. *Science* **4**.

Geiger D, Scherzer S, Mumm P, Marten I, Ache P, Matschi S, Liese a, Wellmann C, Al-Rasheid K a S, Grill E, et al. 2010. Guard cell anion channel SLAC1 is regulated by CDPK protein kinases with distinct Ca2+ affinities. *Proceedings of the National Academy of Sciences of the United States of America* **107**: 8023–8.

Gilliham M, Sullivan W, Tester M, Tyerman SD. **2006**. Simultaneous flux and current measurement from single plant protoplasts reveals a strong link between K+ fluxes and current, but no link between Ca2+ fluxes and current. *The Plant Journal* **46**: 134–44.

Glitsch H, Tappe A. **1995**. Change of Na+ pump current reversal potential in sheep cardiac Purkinje cells with a varying free energy of ATP hydrolysis. *Journal of Physiology* **484**: 605–616.

Griessner M, Obermeyer G. **2003**. Characterization of whole-cell K+ currents across the plasma membrane of pollen grain and tube protoplasts of Lilium longiflorum. *The Journal of membrane biology* **193**: 99–108.

Gu Y, Fu Y, Dowd P, Li S, Vernoud V, Gilroy S, Yang Z. **2005**. A Rho family GTPase controls actin dynamics and tip growth via two counteracting downstream pathways in pollen tubes. *Journal of Cell Biology* **169**: 127–138.

Gutermuth T, Lassig R, Portes M-T, Maierhofer T, Romeis T, Borst J-W, Hedrich R, Feijó J a, Konrad KR. **2013**. Pollen tube growth regulation by free anions depends on the interaction between the anion channel SLAH3 and calcium-dependent protein kinases CPK2 and CPK20. *The Plant cell* **25**: 4525–43.

Halliwell J V, Plant TD, Robbins J, Standen NB. **1994**. Voltage clamp techniques. In: Ogden DC, ed. Microelectrode Techniques, the Plymouth workshop handbook. Cambridge: Company of Biologist, 17–35.

Hamill OP, Marty A, Neher E, Sakmann B, Sigworth FJ. **1981**. Improved Patch-Clamp Techniques for High-Resolution Current Recording from Cells and Cell-Free Membrane Patches. *Pflügers Archiv* **391**: 85–100.

Helling D, Possart A, Cottier S, Klahre U, Kost B. **2006**. Pollen tube tip growth depends on plasma membrane polarization mediated by tobacco PLC3 activity and endocytic membrane recycling. *The Plant cell* **18**: 3519–3534.

Hepler PK, Kunkel JG, Rounds CM, Winship LJ. **2012**. Calcium entry into pollen tubes. *Trends in Plant Science* **17**: 32–38.

Hepler PK, Lovy-Wheeler Al, Mckenna ST, Kunkel JG. **2006**. Ions and Pollen Tube Growth. *Plant Cell Monographs* **3**: 47–69.

Hepler PK, Vidali L, Cheung AY. **2001**. Polarized cell growth in higher plants. *Annual review of cell and developmental biology* **17**: 159–187.

Hille B. **1992**. *Ionic Channels of Excitable Membranes*. Sunderland, Massachusetts: Sinauer Associates Inc.

Hodgkin AL, Huxley AF, Katz B. **1952**. Measurement of current-voltage relations in the membrane of the giant axon of Loligo. *Journal of Physics* **116**: 424–448.

Holdaway-Clarke TL, Feijó JA, Hackett GR, Kunkel JG, Hepler PK. **1997**. Pollen Tube Growth and the Intracellular Cytosolic Calcium Gradient Oscillate in Phase while Extracellular Calcium Influx Is Delayed. *The Plant cell* **9**: 1999–2010.

Holdaway-Clarke TL, Hepler PK. **2003**. Control of pollen tube growth: role of ion gradients and fluxes. *New Phytologist* **159**: 539–563.

Hwang J, Gu Y, Lee Y-JJ, Yang Z. **2005**. Oscillatory ROP GTPase Activation Leads the Oscillatory Polarized Growth of Pollen Tubes (C Waterman-Storer, Ed.). *Molecular Biology of the Cell* **16**: 5385–5399.

Jaffe LF, Levy S. **1987**. Calcium gradients measured with a vibrating calcium-selective electrode. *Proc IEEE/EMBS Conf* **9**: 779–781.

Jaffe LF, Nuccitelli R. **1974**. An ultrasensitive vibrating probe for measuring steady extracellular currents. *The Journal of Cell Biology* **63**: 614–628.

Jaffe LA, Weisenseel MH, Jaffe LF. **1975**. Calcium accumulations within the growing tips of pollen tube. *The Journal of Cell Biology* **67**: 488–492.

Jentsch TJ, Neagoe I, Scheel O. **2005**. CLC chloride channels and transporters. *Current opinion in neurobiology* **15**: 319–25.

Johannes E, Crofts a, Sanders D. **1998**. Control of Cl- efflux in chara corallina by cytosolic pH, free ca2+, and phosphorylation indicates a role of plasma membrane anion channels in cytosolic pH regulation. *Plant physiology* **118**: 173–81.

Kochian L V, Shaff JE, Kühtreiber WM, Jaffe LF, Lucas WJ. **1992**. Use of an extracellular, ion-selective, vibrating microelectrode system for the quantification of K+, H+, and Ca2+ fluxes in maize roots and maize suspension cells. *Planta* **188**: 601–610.

Kühtreiber W, Jaffe LF. **1990**. Detection of Extracellular Calcium Gradients with a Calcium-specific Vibrating Electrode. *The Journal of Cell Biology* **110**: 1565–1573.

Kunkel JG, Cordeiro S, Xu YJ, Shipley AM, Feijó JA. **2006**. The use of non-invasive ion-selective microelectrode techniques for the study of plant development. In: Volkov, ed. Plant Electrophysiology - Theory and Methods.109–138.

López-Bucio J, de La Vega OM, Guevara-García a, Herrera-Estrella L. **2000**. Enhanced phosphorus uptake in transgenic tobacco plants that overproduce citrate. *Nature biotechnology* **18**: 450–3.

Lu Y, Chanroj S, Zulkifli L, Johnson M a., Uozumi N, Cheung AY, Sze H. **2011**. Pollen Tubes Lacking a Pair of K+ Transporters Fail to Target Ovules in Arabidopsis. *the Plant Cell Online* **23**: 81–93.

Malhó R, Feijó JA, Pais MSS. **1992**. Effect of electrical fields and external ionic currents on pollen-tube orientation. *Sexual Plant Reproduction* **5**: 57–63.

Malhó R, Liu Q, Monteiro D, Rato C, Camacho L, Dinis a. **2006**. Signalling pathways in pollen germination and tube growth. *Protoplasma* **228**: 21–30.

Marmont G. **1949**. Studies on the axon membrane; a new method. *Journal of cellular physiology* **34**: 351–382.

Martinoia E, Maeshima M, Neuhaus HE. **2007**. Vacuolar transporters and their essential role in plant metabolism. *Journal of experimental botany* **58**: 83–102.

Martinoia E, Meyer S, De Angeli A, Nagy R. **2012**. Vacuolar Transporters in Their Physiological Context. *Annual review of plant biology*: 183–213.

Marty A, Neher E. **1995**. Tight-Seal Whole-Cell Recording. In: Sakmann B, Neher E, eds. Single-Channel Recording. New York: Springer US, 31–52.

Mascarenhas JP. **1993**. Molecular Mechanisms of Pollen Tube Growth and Differentiation. *The Plant cell* **5**: 1303–1314.

Matsuda JJ, Filali MS, Collins MM, Volk K a, Lamb FS. **2010**. The ClC-3 Cl-/H+ antiporter becomes uncoupled at low extracellular pH. *The Journal of biological chemistry* **285**: 2569–79.

Matveeva NP, Andreyuk DS, Voitsekh OO, Ermakov IP. **2003**. Regulatory Changes in the Intracellular pH and Cl- Efflux at Early Stages of Pollen Grain Germination in vitro. *Russian Journal of Plant Physiology* **50**: 318–323.

Matveyeva NP, Andreyuk DS, Yermakov IP. **2003**. Transport of Cl – across the Plasma Membrane during Pollen Grain Germination in Tobacco. *Biochemistry (Moscow)* **68**: 1247–1251.

Messerli MA, Danuser G, Robinson KR. **1999**. Pulsatile influxes of H+, K+ and Ca2+ lag growth pulses of Lilium longiflorum pollen tubes. *Journal of cell science* **112 (Pt 1**: 1497–509.

Messerli MA, Robinson KR. **1997**. Tip localized Ca2+ pulses are coincident with peak pulsatile growth rates in pollen tubes of Lilium longiflorum. *Journal of cell science* **110 (Pt 1**: 1269–78.

Messerli MA, Smith PJS, Lewis RC, Robinson KR. **2004**. Chloride fluxes in lily pollen tubes: a critical reevaluation. *The Plant journal : for cell and molecular biology* **40**: 799–812.

Meyer S, Mumm P, Imes D, Endler A, Weder B, Al-Rasheid K a S, Geiger D, Marten I, Martinoia E, Hedrich R. **2010**. AtALMT12 represents an R-type anion channel required for stomatal movement in Arabidopsis guard cells. *The Plant journal : for cell and molecular biology*: 1054–1062.

Michard E, Alves F, Feijó JA. **2009**. The role of ion fluxes in polarized cell growth and morphogenesis: the pollen tube as an experimental paradigm. *The International journal of developmental biology* **53**: 1609–22.

Michard E, Dias PN, Feijó JA. **2008**. Tobacco pollen tubes as cellular models for ion dynamics: improved spatial and temporal resolution of extracellular flux and free cytosolic concentration of calcium and protons using pHluorin and YC3.1 CaMeleon. *Sexual Plant Reproduction* **21**: 169–181.

Michard E, Lima PT, Borges FS, Silva AC, Portes MT, Carvalho JE, Gilliham M, Liu L-HL-H, Obermeyer G, Feijó JA. **2011**. Glutamate receptor-like genes form Ca2+ channels in pollen tubes and are regulated by pistil D-serine. *Science* **332**: 434–7.

Miller C. **2006**. ClC chloride channels viewed through a transporter lens. *Nature* **440**: 484–9.

Moreno N, Colaço R, Feijó JA. **2007**. The Pollen Tube Oscillator: Integrating Biophysics and Biochemistry into Cellular Growth and Morphogenesis. In: Mancuso S, Shabala S, eds. Rhythms in Plants: Phenomenoly, Mechanisms, and Adaptive Significance. Heidelberg, 39–62.

Mouline K, Véry A-A, Gaymard F, Boucherez J, Pilot G, Devic M, Bouchez D, Thibaud J-B, Sentenac H. **2002**. Pollen tube development and competitive ability are impaired by disruption of a Shaker K+ channel in Arabidopsis. *Genes & Development* **16**: 339–350.

Obermeyer G, Blatt MR. **1995**. Electrical properties of intact pollen grains of Lilium longiflorum : characteristics of the non-germinatingpollen grain. *Journal of Experimental Botany* **46**: 803–813.

Obermeyer G, Kolb HA. **1993**. K+ channels in the plasma membrane of Lily pollen protoplasts. *Botanica Acta* **106**: 26.31.

Orhan G, Fahlke C, Alekov AK. **2011**. Anion- and proton-dependent Gating of ClC-4 anion/proton transporter under uncoupling conditions. *Biophysical journal* **100**: 1233–41.

Ortiz-Ramirez C, Mora SI, Trejo J, Pantoja O. **2011**. PvAMT1;1, a highly selective ammonium transporter that functions as an H+/NH4+ symporter. *The Journal of biological chemistry* **286**: 31113–31122.

Parton RM, Fischer-Parton S, Trewavas AJ, Watahiki MK. **2003**. Pollen tubes exhibit regular periodic membrane trafficking events in the absence of apical extension. *Journal of cell science* **116**: 2707–2719.

Picollo A, Malvezzi M, Accardi A. **2010**. Proton block of the CLC-5 Cl-/H+ exchanger. *The Journal of general physiology* **135**: 653–9.

Pina C, Pinto F, Feijó JA, Becker JD. **2005**. Gene Family Analysis of the Arabidopsis Pollen Transcriptome Reveals Biological Implications for Cell Growth , Division Control , and Gene Expression Regulation. *Plant Physiology* **138**: 744–756.

Piñeros MA, Kochian L V. **2001**. A patch-clamp study on the physiology of aluminum toxicity and aluminum tolerance in maize. Identification and characterization of Al(3+)-induced anion channels. *Plant physiology* **125**: 292–305.

Prolo LM, Goodman MB. **2008**. Keeping it regular with protons. *Nature* **452**: 6–7.

Pusch M, Zifarelli G, Murgia a R, Picollo a, Babini E. **2006**. Channel or transporter? The CLC saga continues. *Experimental physiology* **91**: 149–52.

Qu H-Y, Shang Z-L, Zhang S-L, Liu L-M, Wu J-Y. **2007**. Identification of hyperpolarization-activated calcium channels in apical pollen tubes of Pyrus pyrifolia. *New phytologist* **174**: 524–36.

Ramos AC, Lima PT, Dias PN, Kasuya MCM, Feijó JA. **2009**. A pH signaling mechanism involved in the spatial distribution of calcium and anion fluxes in ectomycorrhizal roots. *The New phytologist* **181**: 448–62.

Rato C, Monteiro D, Hepler PK, Malhó R. **2004**. Calmodulin activity and cAMP signalling modulate growth and apical secretion in pollen tubes. *Plant Journal* **38**: 887–897.

Roy S, Holdaway-Clarke T, Hackett G, Kunkel J, Lord E, Hepler P. **1999**. Uncoupling secretion and tip growth in lily pollen tubes: evidence for the role of calcium in exocytosis. *The Plant journal : for cell and molecular biology* **19**: 379–86.

Ryan PR, Raman H, Gupta S, Horst WJ, Delhaize E. **2009**. A second mechanism for aluminum resistance in wheat relies on the constitutive efflux of citrate from roots. *Plant physiology* **149**: 340–51.

Ryan RM, Vandenberg RJ. **2002**. Distinct conformational states mediate the transport and anion channel properties of the glutamate transporter EAAT-1. *Journal of Biological Chemistry* **277**: 13494–13500.

Sakmann B, Neher E. **1984**. Patch clamp techniques for studying ionic channels in excitable membranes. *Annual review of physiology* **46**: 455–72.

Scheel O, Zdebik A a, Lourdel S, Jentsch TJ. **2005**. Voltage-dependent electrogenic chloride/proton exchange by endosomal CLC proteins. *Nature* **436**: 424–7.

Schiøtt M, Romanowsky SM, Baekgaard L, Jakobsen MK, Palmgren MG, Harper JF. **2004**. A plant plasma membrane Ca2+ pump is required for normal pollen tube growth and fertilization. *Proceedings of the National Academy of Sciences of the United States of America* **101**: 9502–7.

Schmidt C, Schroeder JI. **1994**. Anion Selectivity of Slow Anion Channels in the Plasma Membrane of Guard Cells (Large Nitrate Permeability). *Plant physiology* **106**: 383–391.

Schroeder BC, Cheng T, Jan YN, Jan LY. **2008**. Expression cloning of TMEM16A as a calcium-activated chloride channel subunit. *Cell* **134**: 1019–29.

Shang Z, Ma L, Zhang H, He R, Wang X, Cui S, Sun D. **2005**. Ca2+ influx into lily pollen grains through a hyperpolarization-activated Ca2+-permeable channel which can be regulated by extracellular CaM. *Plant & cell physiology* **46**: 598–608.

Shipley AM, Feijó JA. **1999**. The use of the vibrating technique to study steady extracellular currents during pollen germination and tube growth. In: Cresti M, Moscatelli A, eds. Fertilisation in Higher Plants: molecular and cytological aspects. Berlin, Heidelberg: Springer-Verlag, 235–250.

Siegel RS, Xue S, Murata Y, Yang Y, Nishimura N, Wang A, Schroeder JI. **2009**. Calcium elevation-dependent and attenuated resting calcium-dependent abscisic acid induction of stomatal closure and abscisic acid-induced enhancement of calcium sensitivities of S-type anion and inward-rectifying K channels in Arabidopsis guard cells. *The Plant journal : for cell and molecular biology* **59**: 207–20.

Silva P, Gerós H. **2009**. Regulation by salt of vacuolar H+-ATPase and H+-pyrophosphatase activities and Na+/H+ exchange. *Plant signaling & behavior* **4**: 718–726.

Skerrett M, Tyerman SD. **1994**. A channel that allows inwardly directed fluxes of anions in protoplasts derived from wheat roots. *Planta* **192**.

Slotboom DJ, Konings WN, Lolkema JS. **2001**. Glutamate transporters combine transporter- and channel-like features. *Trends in Biochemical Sciences* **26**: 534–539.

Smith PJ, Sanger RH, Jaffe LF. **1994**. The vibrating Ca2+ electrode: a new technique for detecting plasma membrane regions of Ca2+ influx and efflux. *Methods Cell Biol* **40**: 115–134.

Song L-F, Zou J, Zhang W, Wu W-H, Wang Y. **2009**. Ion transporters involved in pollen germination and pollen tube tip-growth. *Plant signaling & behavior* **4**: 1193–5.

Sze H, Padmanaban S, Cellier F, Honys D, Cheng N-H, Bock KW, Conéjéro G, Li X, Twell D, Ward JM, et al. 2004. Expression Patterns of a Novel AtCHX Gene Family Highlight Potential Roles in Osmotic Adjustment and K+ Homeostasis in Pollen Development. *Plant Physiology* **136**: 2532–2547.

Tanaka I, Kitazume C, Ito M. **1987**. The isolation and culture of Lily pollen protoplasts. *Plant Science* **50**: 205–211.

Tavares B. **2011**. Anionic Currents in Pollen Grain Protoplasts from Arabidopsis thaliana and Lilium longiflorum. *Repositório da Universidade de Lisboa - Teses de Doutoramento*: 1–142.

Tavares B, Dias PN, Domingos P, Moura TF, Feijó JA, Bicho A. **2011**. Calcium-regulated anion channels in the plasma membrane of Lilium longiflorum pollen protoplasts. *New phytologist* **192**: 45–60.

Taylor LP, Hepler PK. **1997**. Pollen Germination and Tube Growth. *Annual review of plant physiology and plant molecular biology* **48**: 461–491.

Thomine S, Guern J, Barbier-Brygoo H. **1997**. Membrane Biology Voltage-Dependent Anion Channel of Arabidopsis Hypocotyls: Nucleotide Regulation and Pharmacological Properties. *The Journal of Membrane Biology* **159**: 71–82.

Tsay YF, Schroeder JI, Feldmann KA, Crawford NM. **1993**. The herbicide sensitivity gene CHL1 of Arabidopsis encodes a nitrate-inducible nitrate transporter. *Cell* **72**: 705–713.

Wang Y-F, Fan L-M, Zhang W-Z, Zhang W, Wu W-H. **2004**. Ca2+-Permeable Channels in the Plasma Membrane of Arabidopsis Pollen Are Regulated by Actin Microfilaments. *Plant Physiology* **136**: 3892–3904.

Wang Y, Zhang W-Z, Song L-F, Zou J-J, Su Z, Wu W-H. **2008**. Transcriptome analyses show changes in gene expression to accompany pollen germination and tube growth in Arabidopsis. *Plant physiology* **148**: 1201–11.

Weisenseel MH, Jaffe LF. **1976**. The Major Growth Current Through Lily Pollen Tubes Enters as K+ and Leaves as H+. *Planta* **133**: 1–7.

Weisenseel MH, Nuccitelli R, Jaffe LF. **1975**. Large electrical currents traverse growing pollen tubes. *The Journal of cell biology* **66**: 556–67.

Wu Y, Xu X, Li S, Liu T, Ma L, Shang Z. **2007**. Heterotrimeric G-protein participation in Arabidopsis pollen germination through modulation of a plasmamembrane hyperpolarization-activated Ca2+-permeable channel. *New phytologist* **176**: 550–9.

Yamaguchi T, Aharon GS, Sottosanto JB, Blumwald E. **2005**. Vacuolar Na+/H+ antiporter cation selectivity is regulated by calmodulin from within the vacuole in a Ca2+- and pH-dependent manner. *Proceedings of the National Academy of Sciences of the United States of America* **102**: 16107–16112.

Yang YD, Cho H, Koo JY, Tak MH, Cho Y, Shim W-S, Park SP, Lee J, Lee B, Kim B-M, et al. 2008. TMEM16A confers receptor-activated calcium-dependent chloride conductance. *Nature* **455**: 1210–1215.

Yoon GM, Dowd PE, Gilroy S, McCubbin AG. **2006**. Calcium-dependent protein kinase isoforms in Petunia have distinct functions in pollen tube growth, including regulating polarity. *The Plant cell* **18**: 867–878.

Zdebik A a, Zifarelli G, Bergsdorf E-Y, Soliani P, Scheel O, Jentsch TJ, Pusch M. **2008**. Determinants of anion-proton coupling in mammalian endosomal CLC proteins. *The Journal of biological chemistry* **283**: 4219–27.

Zifarelli G, Murgia AR, Soliani P, Pusch M. **2008**. Intracellular proton regulation of ClC-0. *The Journal of general physiology* **132**: 185–98.

Zifarelli G, Pusch M. **2010**. CLC transport proteins in plants. *FEBS letters* **584**: 2122–7.

Zonia L, Cordeiro S, Feijó JA. **2001**. Ion dynamics and hydrodynamics in the regulation of pollen tube growth. *Sexual Plant Reproduction* **14**: 111–116.

Zonia L, Cordeiro S, Tupý J, Feijó JA. **2002**. Oscillatory Chloride Efflux at the Pollen Tube Apex Has a Role in Growth and Cell Volume Regulation and Is Targeted by Inositol 3,4,5,6-Tetrakisphosphate. *The Plant Cell* **14**: 2233–2249.

Zonia L, Munnik T. **2004**. Osmotically Induced Cell Swelling versus Cell Shrinking Elicits Specific Changes in Phospholipid Signals in Tobacco Pollen Tubes. *Plant Physiology* **134**: 813–823.